Università degli Studi di Padova

Dipartimento di Ingegneria Industriale DII

Corso di Laurea Magistrale in Ingegneria Aerospaziale

Preliminary assessment of turbomachinery configurations for an intercooled-recuperated microturbine electric generator

Relatore:

Ing. Francesco Barato

Laureanda:

Giulia Lana

Matricola: 2020208

ANNO ACCADEMICO 2022/2023

Abstract

To address the growing interest in more sustainable air transport, the present work reports the preliminary design of a microturbine generator to power the electric motors that propel a small aircraft with a thrust power of 100 kW.
To get a good assessment of the performance of the gas turbine unit, this project aims to develop a method to estimate the efficiencies of compressors and turbines based on non-dimensional parameters and to integrate it into the analysis of the performance of the whole unit.
After some evaluation, an intercooled-recuperated gas turbine engine setup was shown to be the most beneficial in terms of weight, efficiency, and fuel consumption. Since this configuration requires two compressors, the effects on the efficiency of mounting the two compressors on the same shaft or two different ones are assessed here. As the latter option is revealed to be the most advantageous in terms of isentropic efficiency, at least two turbines are needed. If two radial turbines are employed, either one or both has to generate the net power; the latter option is demonstrated to be the most efficient.
The alternative of using a radial free turbine to drive the generator, with the other two turbines only used for driving their respective compressor, is also evaluated; however, this performs worse than the alternative with two turbines and two generators, and is, therefore, discarded.
A simple procedure to evaluate the performances of the gas turbine unit and its turbomachinery components is detailed here.

Sommario

Per rispondere al crescente interesse per un trasporto aereo più sostenibile, il presente lavoro riporta la progettazione preliminare di un generatore a micro-turbina per alimentare i motori elettrici che azionano un piccolo velivolo con una potenza di spinta di 100 kW.
Per ottenere una buona valutazione delle prestazioni dell'unità, questo progetto mira a sviluppare un metodo per stimare i rendimenti di compressori e turbine basato su parametri non dimensionali e di integrarlo nell'analisi delle prestazioni dell'intera unità.
Dopo alcune valutazioni, una configurazione del motore a turbina con intercooler e recuperatore si è dimostrata essere la più vantaggiosa in termini di peso, rendimento e consumo di carburante. Dato che questa configurazione richiede due compressori, vengono qui valutati gli effetti sul rendimento del montaggio dei due compressori sullo stesso albero o su due diversi. Poiché quest'ultima opzione si rivela essere la più vantaggiosa in termini di rendimento isoentropico, è necessario usare almeno due turbine. Se vengono impiegate due turbine radiali, la potenza netta può essere generata da una delle due o da entrambe; quest'ultima opzione si è dimostrata essere la più efficiente.
Si è valutata anche l'opzione alternativa di utilizzare una *free turbine* radiale per l'azionamento del generatore, con le altre due turbine utilizzate solo per l'azionamento del rispettivo compressore; tuttavia, questa configurazione ha un funzionamento peggiore dell'alternativa con due turbine e due generatori, ed è, quindi, scartata.
Una semplice procedura per valutare le prestazioni dell'unità turbina a gas e delle sue turbomacchine è qui descritta nel dettaglio.

Acknowledgements

Before proceeding, I would like to take a moment to thank all of the people who made it possible for me to reach this goal.
My first heartfelt acknowledgment goes to my professor and thesis supervisor F. Barato, who had already shown his helpfulness on occasions before this thesis and has helped through all the highs and lows of the making of this project.
A special thank you goes to my parents who supported me physically, emotionally, and financially, and are the reason why I was able to accomplish what I did. I also thank my partner and my friends for believing in me even when I didn't, and for being by my side through thick and thin.
An honorable mention goes to my colleagues, especially the guys with whom I took part in the Erasmus Programme and the people from the THRUST student project. While it saddens me to distance myself from THRUST right before our rocket becomes reality, I'm proud of all of us and I know you will all go far.

Contents

1 Introduction

In a little over a century, the aviation industry has gone from learning to fly, to learning to fly faster, learning to fly further, learning to fly heavier planes, and now to having 100,000 plus commercial flights occurring around the world every day[19].
The number of flights performed globally has increased steadily since the early 2000s and reached 38.9 million in 2019. In Europe, according to EASA[11], the number of flights at EU27+EFTA airports increased by 15% between 2005 and 2019, from 8.1 million to 9.3 million, while passenger kilometers almost doubled (+90%). However, it is worth mentioning that the COVID-19 pandemic made this number decline to 5.1 million in Europe and 16.9 million globally.
The consequence of this growth is that the CO_2 emissions of all flights departing from EU27+EFTA airports reached 147 million tonnes in 2019, which was 34% more than in 2005. Globally, the aviation industry produces around 2.1% of all human-induced carbon dioxide emissions[2]; in the EU, this percentage goes up to 3.8%[9].
Even though these percentages do not seem very high, to combat climate change, several governments are taking legislative measures to reduce CO_2 emissions; in France, a measure announced in *la Loi Climate* of 2021 and validated by the European Commission on December 2, 2022, bans all short-haul flights inside the country (i.e. all flights between locations where there is a train alternative that takes less than 2.5 hours)[21]. In the US, the Environmental Protection Agency (EPA) passed a rule to require aircraft manufacturers to use fuel-efficient engines that release less carbon dioxide[8].
This data highlights the necessity of technological innovation to move towards a more sustainable flight.

1.1 Where are the electric planes?

Despite the initial widespread skepticism, it has become clear that electric cars are bound to replace traditional internal combustion vehicles. The Tesla Model Y is the best-selling car of 2022 in Europe, and demand for EVs is at an all-time high, despite being more expensive than their gas counterparts[20].

Figure 1.1: Tesla Model Y (Image by Greg GjerdingenCC BY-SA 4.0)

The question arises spontaneously, why are ground vehicles gradually being replaced by EVs, but the same process does not seem to take place for aircraft? Bill Gates, in his book *How to Avoid a Climate Disaster: The Solutions We Have and the Breakthroughs We Need*, puts it as follows[16]:

> Not long ago, my friend Warren Buffett and I were talking about how the world might decarbonize airplanes. Warren asked, "Why can't we run a jumbo jet on batteries?" He already knew that when a jet takes off, the fuel it's carrying accounts for 20 to 40 percent of its weight. So when I told him this startling fact — that you'd need 35 times more batteries by weight to get the same energy as jet fuel — he understood immediately. The more power you need, the heavier your plane gets. At some point, it's so heavy that it can't get off the ground. Warren smiled, nodded, and just said, "Ah."

Surprisingly, electric flight dates back to 1883, when Gaston Tissandier flew the first electrically powered airship. The following year, Charles Renard and Arthur Krebs, a couple of french army officers, gave a hydrogen-filled dirigible, *La France*, massive batteries and an 8-horsepower electric motor that enabled it to do something that no balloon had ever done before: return to its lunch site at the end of a flight [26][15] [28].

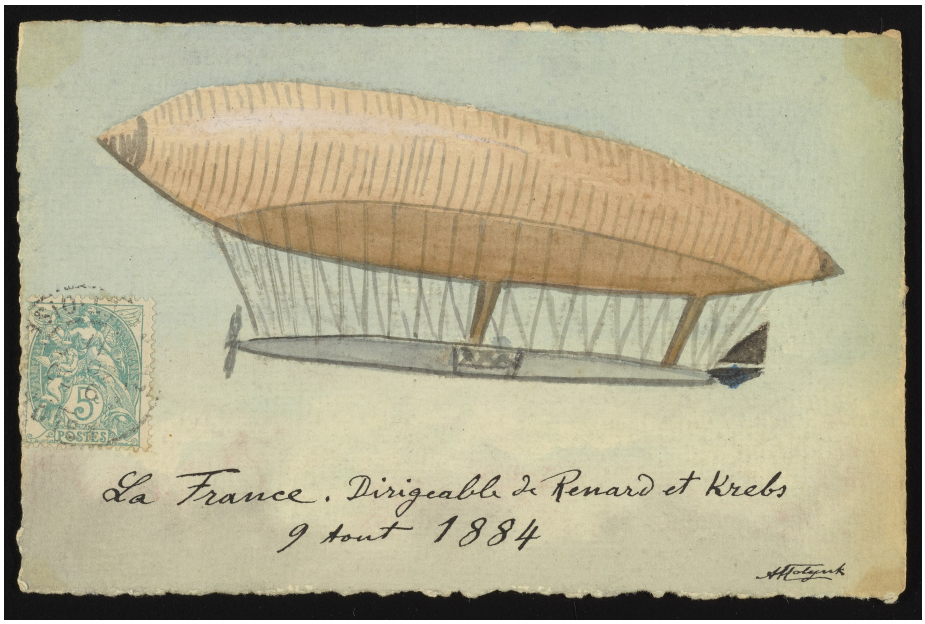

Figure 1.2: Artist's rendition of *La France* (Courtesy of Science History Institute)

Without counting devices that receive power from the ground, such as the Austro-Hungarian Petróczy-Kármán-Žurovec PKZ-1 electric-powered helicopter in 1917, which was tethered to the ground[17], electric flight had a resurgence in the late 1970s and, to this day, many companies are designing electrically-powered aircraft models, and for good reasons. Outside of the evident environmental factor, there are other advantages to electric propulsion over gas turbines, such as[32]:

- Noise: even though it still has to drive a rotor, propeller, or fan, which produces noise, an electric motor is quieter than a fuel engine. Also, electric motors enable distributed propulsion systems with multiple smaller and quieter rotors or fans.
- Efficiency: electric drivetrains can be more than 90% efficient, compared with 55% for today's large turbofans and 35% for small turboprops. It is no coincidence that the electrification of aircraft propulsion is beginning with the modification of regional aircraft powered by turboprops such as the Pratt and Whitney PT6.
- Scalability: whether one or two large motors are used, or many small motors in a distributed electric propulsion architecture, performance is about the same, which is not the case with turbines.

Distributed propulsion systems are not only beneficial for noise reduction but are also substantially smaller and lighter than jet engines of comparable power;

therefore, it is possible to place them in different, and more favorable locations than being suspended below the wing. An example is the NASA X-57 Maxwell, which is an electric aircraft modified from a Tecnam P2006T with 14 electric motors driving propellers mounted on the wing leading edges. All 14 electric motors are used during takeoff and landing, while only the outer two are used during the cruise. Another advantage of distributed propulsion systems like this is that the additional airflow over the wing generates greater lift, allowing for a narrower wing. The increased lift also allows for shorter runways[6][31][14].

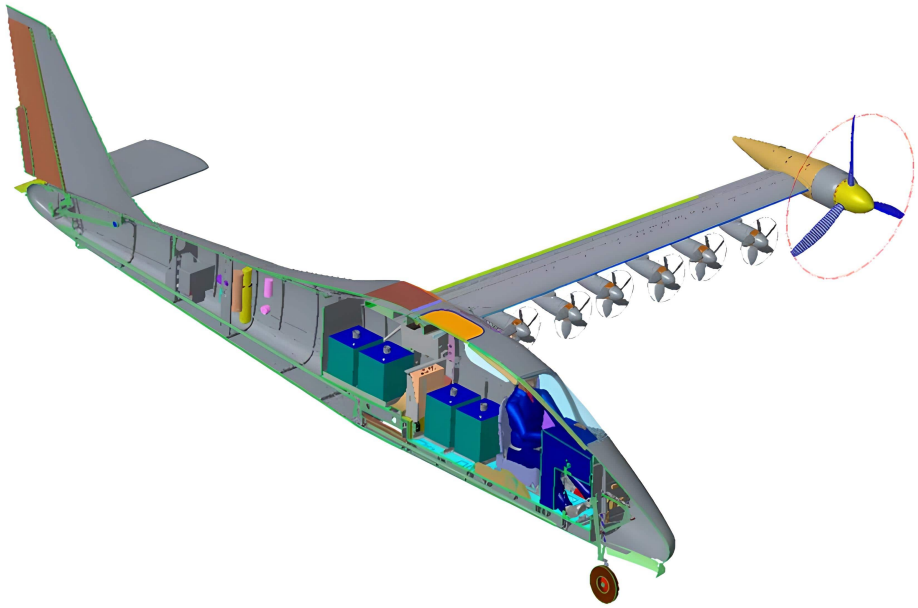

Figure 1.3: Model of the final mod 4 of the X-57 with centerline cut, showing battery system, high aspect ratio wing, electric motors, and traction power bus (Courtesy of NASA)

The electric motors are produced by Joby Aviation, a Californian company developing electrical vertical takeoff and landing (eVTOL) aircraft that it intends to operate as an air taxi service (see Figure 1.4), as this is a sector that some people believe will become popular in the near future and is becoming viable due to technological advancement[5].

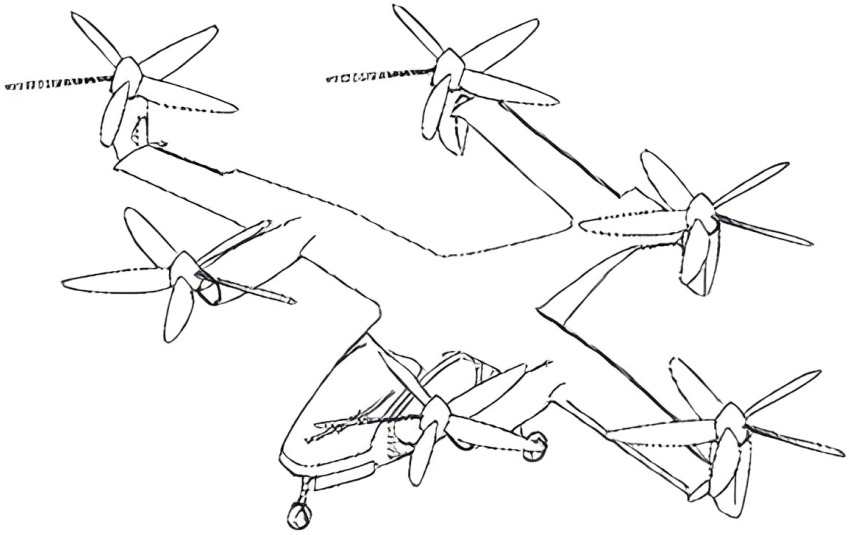

Figure 1.4: Schematic illustrations of a top view of a variation of the aircraft in a hover configuration. Source

All that being said, the biggest challenge in electrifying propulsion is energy storage. The gravimetric energy density (or specific energy) is defined as the ratio between the energy stored in a battery and its weight and it is usually expressed in Wh/kg (while the volumetric energy density is the ratio between the energy and the volume of a battery and is expressed in Wh/l). To understand how specific energy is defined, it is necessary to describe what an electric vehicle battery looks like.
Today's EVs use lithium-ion batteries and are made of the following components [24]:

- Battery Cell: Basic unit of a lithium-ion battery that exerts electric energy by charging and discharging. Made by inserting cathode, anode, separator, and electrolyte into a rectangular aluminum case.
  In an EV battery there are several cells mounted, and to safely and efficiently manage those cells, they are installed in form of modules and packs. Simply put, a cluster of cells makes up a module and a cluster of modules makes up a pack.

- Battery Module: A battery assembly put into a frame by combining a fixed number of cells to protect the cells from external shocks, heat, or vibration.

- Battery Pack: Final shape of the battery system installed to an electric vehicle. It is composed of modules and various control/protection systems

including a BMS (Battery Management System), a cooling system, etc.

The battery density of an EV is usually defined as either referring to the cell or to the pack. With that in mind, the energy density of Tesla's batteries with 2170 cells, which are used in their long-range vehicles because they provide the highest energy density (as opposed to 4680 cells), have an estimated pack level energy density of 150 Wh/kg, which corresponds to 265 Wh/kg at the cell level, as reported by Panasonic[12].
According to Colin McKerrancher, who is the Head of Advanced Transport at BloombergNEF[13], battery density at the cell level has almost tripled since 2010, which is the reason why the Tesla Model S, which came to market in 2012 with 402 km of range, can now reach up to 628 km of range in its long-range variant.
When it comes to predictions for the future, according to Saft Research Director Patrick Bernard, lithium-sulfur (Li-S) batteries based on solid-state electrolytes will allow an increase in gravimetric energy density of about 30% at the cell level[4].

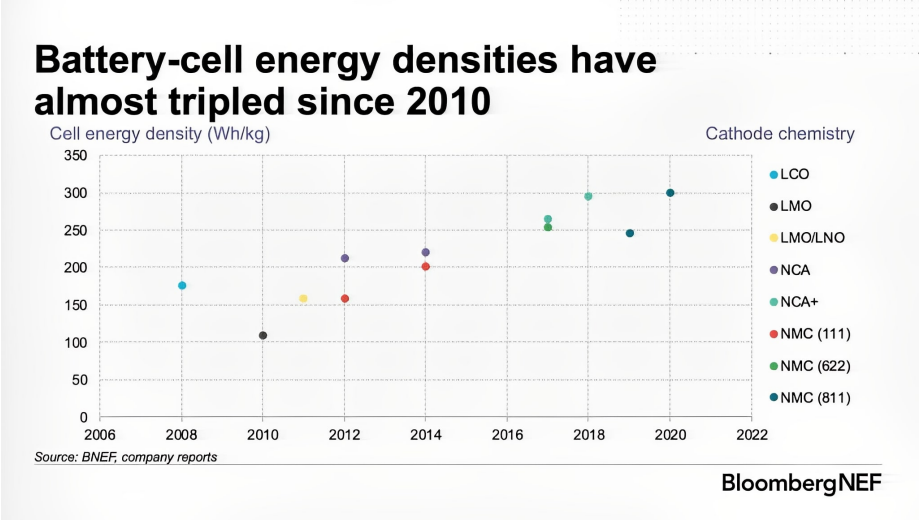

Figure 1.5: Screen capture from BloombergNEF presentation.

While this all sounds impressive, the current energy density of batteries is nowhere near the one of jet fuel, which is about 12,000 Wh/kg; this corresponds to about 45 times the energy density of Tesla's 2170 cells. While reducing weight is not as crucial in the automotive industry, it is critical in aviation.
The other hurdle to overcome is certification. Designing a new aircraft from the ground up to accommodate the shortfalls in battery technology means that it would take considerably longer to get it certified, which is the reason why companies prefer to retrofit old devices to get them certified quicker. In fact,

the world's first all-electric two-seater plane was from the Slovenian company Pipistrel, which retrofitted a glider in 2007 by putting an electric motor in it. The problem with retrofitting is that engineers are limited by the weight that the structure was originally built for[1].

Figure 1.6: The Pipistrel Velis Electro s/n 003 sitting at Ajdovscina airport after roll out from the assembly line. Source CC BY-SA 4.0

This is why, to this day, fully electric aircraft propulsion is limited to relatively small vehicles for short-range applications.

1.2 Hybrid electric propulsion

While a significant shift in energy storage technology is needed for fully electric aircraft, in the meantime, there are alternative ways to diminish the environmental impact of flying and retain some of the advantages of electric propulsion. Hybrid-electric aircraft combine fuel with electric propulsion. There are two alternatives[29]:

1. Designs with batteries: the batteries supply extra power in specific circumstances; for instance, they provide clean take-off and landing to reduce emissions near airports.

2. Designs without batteries: the electric propulsion system is driven by a small gas turbine generator, thereby improving the efficiency and reducing the fuel needed.

Hybrid systems can also be categorized in the following way[18]:

1. Series configuration: in a series hybrid configuration, the propeller (or fan/rotor) is driven only by the electric motor, which gets power from the combustion engine. The electrical power can be used to power the electric motor directly or can be stored in the battery by a charging process. This is the simplest configuration and is the most easily extended to distributed electric powertrains. Hence, it is widely accepted as the alternative propulsion system to hybridize multi-rotor aircraft and large-scale airplanes.

The benefit of series hybrid configurations is that the engine is completely decoupled from the propeller and its output power is not related to the power demand of the powertrain; therefore, the engine can run at its optimal operating state during different working conditions. The fuel efficiency of the engine can remain high and its lifespan can be lengthened. Moreover, the series architecture has the definite advantage of flexibility for locating the internal combustion engine and generator due to the mechanical decoupling.

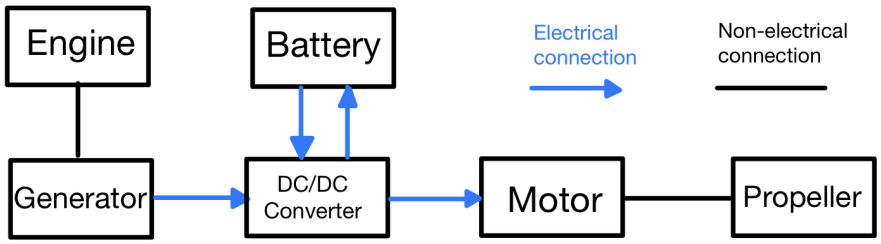

Figure 1.7: Example of series hybrid configuration

2. Parallel configuration: in a parallel hybrid configuration, the internal combustion engine and the electric motor are both connected to the propeller and contribute to the propulsion energy either simultaneously or individually. Also, the engine can simultaneously drive the propeller and motor/generator, thereby charging the battery pack.
   The advantage over the series configuration is that a smaller engine and a smaller electric motor can be used to get the same performance. However, the rotational speed of the propeller is not always the optimal speed of the engine, thus operating at the optimum region of the engine cannot be guaranteed.

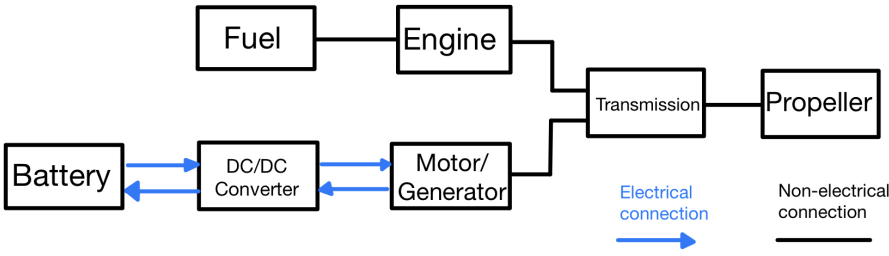

Figure 1.8: Example of parallel hybrid configuration

3. Series-parallel configuration: in a series-parallel configuration, also known

as *power-split* configuration, the propeller, engine, motor, and generator are connected to a planetary gear. While this structure makes power distribution more flexible and allows the engine and motor to operate in their most efficient region, it also requires the most complicated clutch/gearing mechanism and energy management. Because of its complexity, it is the least popular configuration concerning aircraft applications.

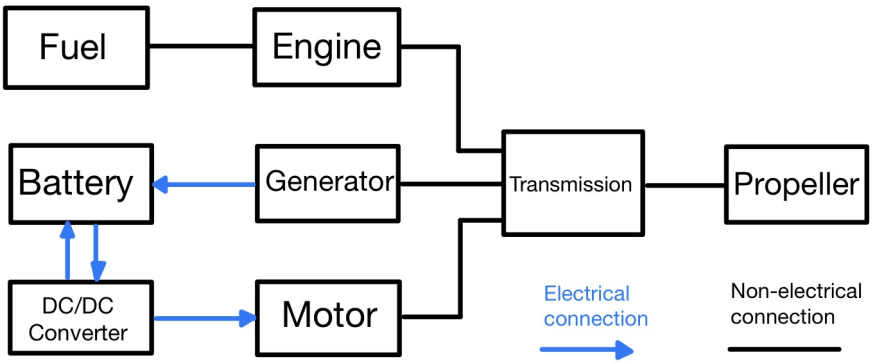

Figure 1.9: Example of series-parallel hybrid configuration

For its simplicity and flexibility, a series configuration will be studied in this work. Since the design will be optimized for cruise conditions, the battery pack will provide the extra power needed during take-off and climb.
In the system developed here, a gas microturbine[1] generates power which gets converted into electricity by a generator. An electric motor then uses the electrical power to drive the fan.
In section 2, an overview of the system is presented, together with the system requirements, and the starting point of the analysis. In section 3 and 4, the preliminary design procedures based on non-dimensional analysis for compressors and turbines, respectively, are examined. Finally, in section 5, the final results of the thermodynamic cycle that satisfy the requirements of section 2 are shown.
All calculations and plots are carried out on Matlab®.

[1]The word *microturbine* refers to devices that produce between 100 and 500 kW of net power

2 System definition

This work is the continuation of a previous project[23]. The original author used a scaled-up version (1:1.3) of the 2014 Airbus E-Fan[2] as a reference for the preliminary design calculations of the turbine generator. The reference specifications are described in Table1.

Figure 2.1: E-fan 1.0 SourceCC BY-SA 4.0

Number of fans n_{fan}	2
Wing span b	12.3 m
Chord c	1.1 m
Fan diameter d_{fan}	0.754 m
Oswald's factor e	0.65
Max Lift/Drag E_{max}	16

Table 1: Reference plane specifications

The requirements for this preliminary design are the following:

- Flight altitude: $h = 5000\,m$
- Time of flight: $t = 5\,h$

[2]This is just to have a starting point for the computations, the methods described in this work are not dependent on the reference aircraft

- Thrust power: $P_W = Thrust \cdot V_{cruise} = 100\,kW$

and the following parameters are assumed:

- Core engine weight (compressors+combustion chamber+turbines+shaft): 30 kg
- Fuel: biomethane
  - Fuel calorific value: $H_u = 50\,MJ/kg$
- Turbine inlet temperature (first stage): $T_{04} = 1503\,K$
- Fraction of pressure drop from the exit nozzle $\delta p_n = 0.006$

Where biomethane is the result of removing carbon dioxide, hydrogen sulfide, and water from biogas, which reduces greenhouse gas emissions[27].
From the requirements and the reference specifications, it is possible to compute with a simple analysis of aerodynamic forces the cruise speed, Mach number, and thrust:

$$V_{cruise} = 87.185\,m/s$$

$$M_a = 0.272$$

$$Thrust = 1147\,N$$

For the cycle analysis, the following efficiency values are assumed:

- Air intake isentropic efficiency: $\eta_d = 0.98$
- Pressure drop in the combustion chamber: $f_c = 0.98$
- Combustion efficiency; $\nu_c = 0.98$
- Exit nozzle isentropic efficiency: $\eta_n = 0.98$
- Conversion efficiency from the engine to the fan: $\eta_{fan} = 0.9025$
  Which is the product of the efficiencies of:
  - electrical generator: 0.95
  - motor: 0.95

Useful definitions

- Net power: power created by the gas turbine unit which is used to drive the electrical generator. It is the difference between the power generated by the turbine(s) and the one consumed by the compressors:

$$P_N = P_t - (P_{c,LPC} + P_{c,HPC})$$

where

  - P_t: power generated by the turbine(s) (all stages combined)
  - $P_{c,LPC}$: power consumed by the low-pressure compressor
  - $P_{c,HPC}$: power consumed by the high-pressure compressor

- Thermal efficiency: it is the energy transformation efficiency within the engine. In this work, two definitions are used: one that encompasses the whole system and one that only references the engine unit.

  - At the system level: It is defined as the ratio between the power imparted to the airflow (which includes both the contribution from the fans and the engine) P_J and the rate of energy supplied by the fuel.

$$\varepsilon_t^{sys} = \frac{P_J}{\dot{m}_{fuel} H_u} \tag{2.0.1}$$

  - At the unit level: It is defined as the ratio between the sum of the net power and the power imparted to the airflow through the nozzle, and the rate of energy supplied by the fuel.

$$\varepsilon_t^{unit} = \frac{P_N + P_{nozzle}}{\dot{m}_{fuel} H_u} \tag{2.0.2}$$

where P_J is defined as

$$P_J = n_{fan} P_{fan} + P_{nozzle} \tag{2.0.3}$$

in which

  - P_{fan}: power imparted to the airflow by the fan

$$P_{fan} = \frac{1}{2}\dot{m}_{fan}(V_{out}^2 - V_{cruise}^2)$$

    where

    * $\dot{m}_{fan}$: air mass flow passing through the fan
    * V_{out}: velocity of the air leaving the fan

  - P_{nozzle}: power imparted to the airflow by the nozzle

$$P_{nozzle} = \frac{1}{2}(1+f)\dot{m}V_{exit}^2 - \frac{1}{2}\dot{m}V_{cruise}^2$$

    where

    - $\dot{m}$: air mass flow passing through the engine
    - f: ratio between fuel mass flow $\dot{m}_{fuel}$ and $\dot{m}$
    - V_{exit}: velocity of the hot gases at the nozzle exit

- Propulsive efficiency: it is the conversion of the kinetic energy of air when it passes through the engine into propulsive power. It is defined as the ratio between the thrust power P_W and the power imparted to the airflow P_J

$$\varepsilon_p = \frac{P_W}{P_J} \tag{2.0.4}$$

  where the thrust power P_W is equal to

$$P_W = Thrust \cdot V_{cruise}$$

- Overall efficiency: it is the product of the propulsive and thermal efficiencies (where the thermal efficiency is the one of the whole system).

$$\varepsilon_o = \varepsilon_t^{sys} \varepsilon_p \tag{2.0.5}$$

- Specific Power: it is the ratio between P_J and the air mass flow.

$$SP = \frac{P_J}{\dot{m}} \tag{2.0.6}$$

- Specific Fuel Consumption: it is the ratio between the fuel mass flow and P_J.

$$SFC = \frac{\dot{m}_{fuel}}{P_J} \tag{2.0.7}$$

The relations between the different definitions of power are the following:

- between the P_N and P_{fan}

$$P_{fan} = \eta_{fan} \frac{P_N}{n_{fan}}$$

- between P_W and P_J

$$P_W = \varepsilon_p P_J$$

- between P_N and P_W

$$P_W = \varepsilon_p (\eta_{fan} P_N + P_{nozzle})$$

According to the results of the previous work, it is preferable to have a thermodynamic cycle with an intercooler and recuperator to get lower total weight, less fuel consumed, and higher overall efficiency. This setup makes it possible to keep the pressure ratio low, which allows for the use of radial compressors and turbines. Radial machines are convenient because, compared to axial ones, they are smaller, cheaper, and can reach a higher pressure ratio per stage. Also, by using ceramic components for the first turbine stage, it is possible to reach the high turbine inlet temperature cited before without using a cooling system.
The heat exchangers specifications are the following:

- **Intercooler**:
  - Pressure drop across the intercooler: $\delta p_{ic} = 0.03$
  - Intercooler efficiency: 0.6
  - Heat transfer coefficient: $U_{ic} = 150\, W/(m^2 K)$
  - Intercooler wall thickness: $h_{ic} = 0.001\, m$
  - Material: Aluminum
    - Density: $\rho_{Al} = 2700 kg/m^3$
- **Recuperator**:
  - Pressure drop across the recuperator: $\delta p_{rc} = 0.04$
  - Recuperator efficiency: 0.9
  - Heat transfer coefficient: $U_{rc} = 121\, W/(m^2 K)$
  - Material: ceramic
    - Density: $\rho_{ceramic} = 3300\, kg/m^3$

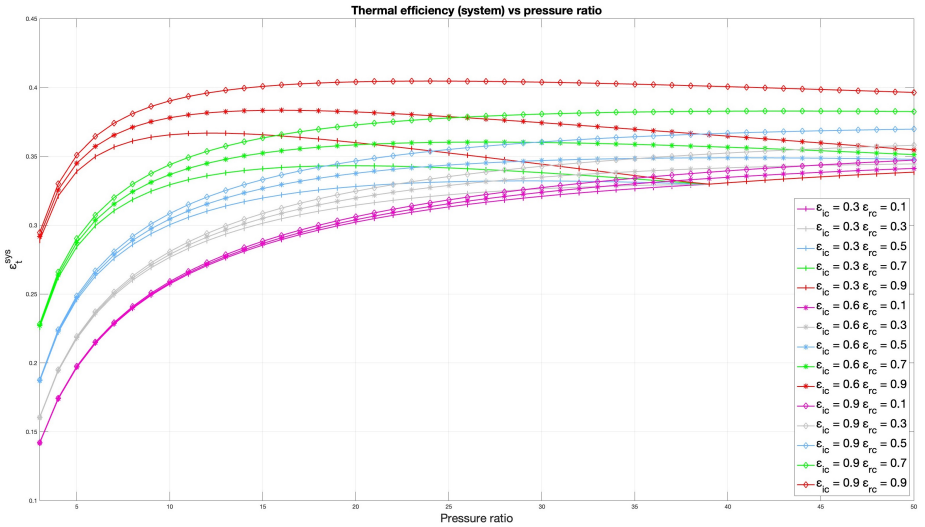

Figure 2.2: Thermal efficiency (of the whole system) versus pressure ratio and heat exchangers efficiency

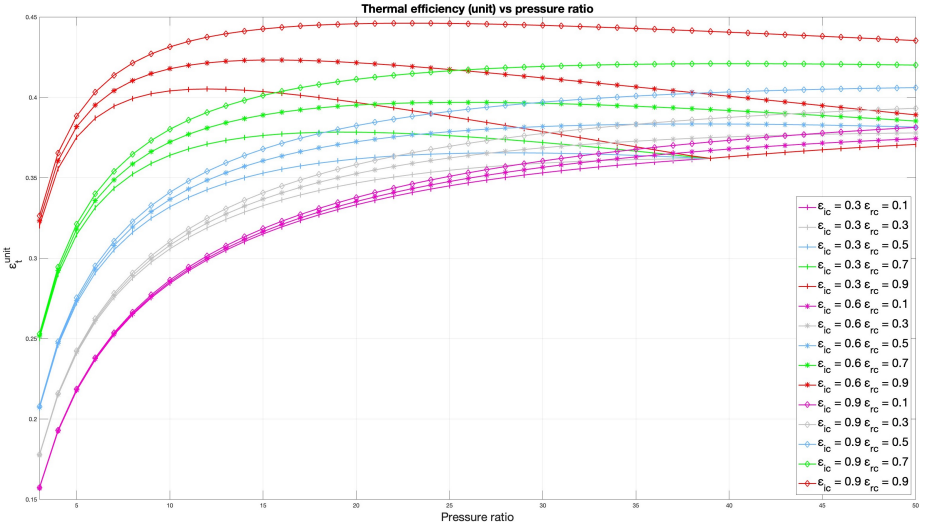

Figure 2.3: Thermal efficiency (of the engine unit) versus pressure ratio and heat exchangers efficiency

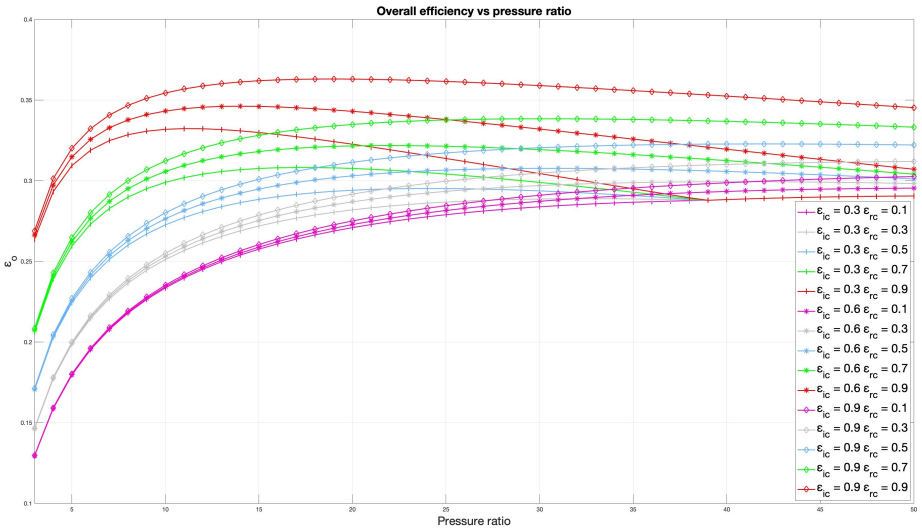

Figure 2.4: Overall efficiency versus pressure ratio and heat exchangers efficiency

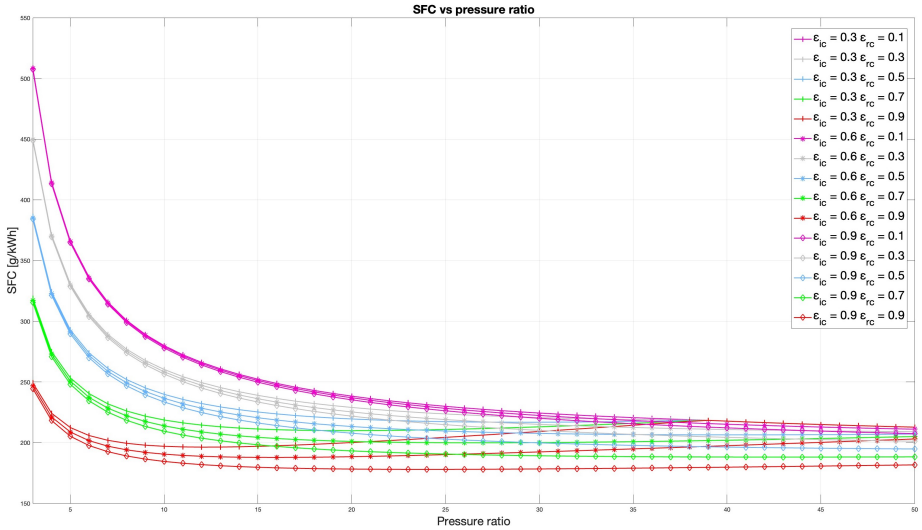

Figure 2.5: Specific fuel consumption versus pressure ratio and heat exchangers efficiency

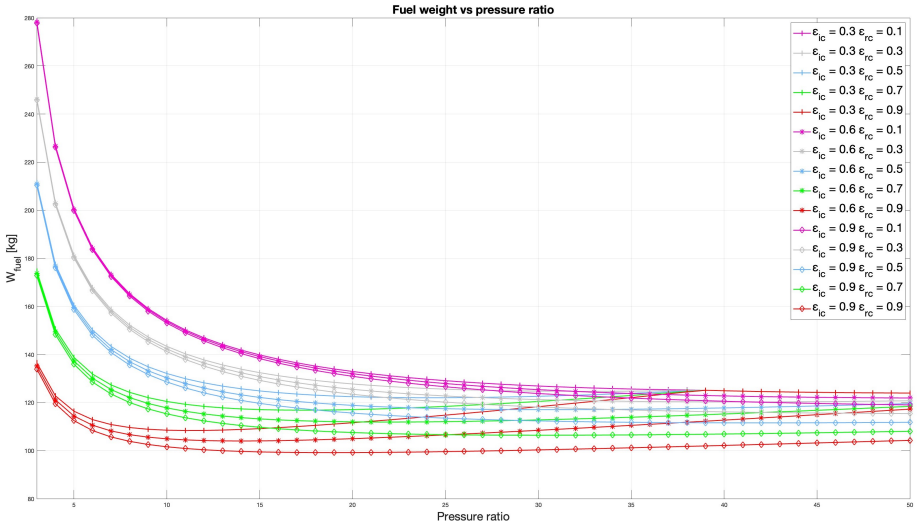

Figure 2.6: Fuel weight versus pressure ratio and heat exchangers efficiency

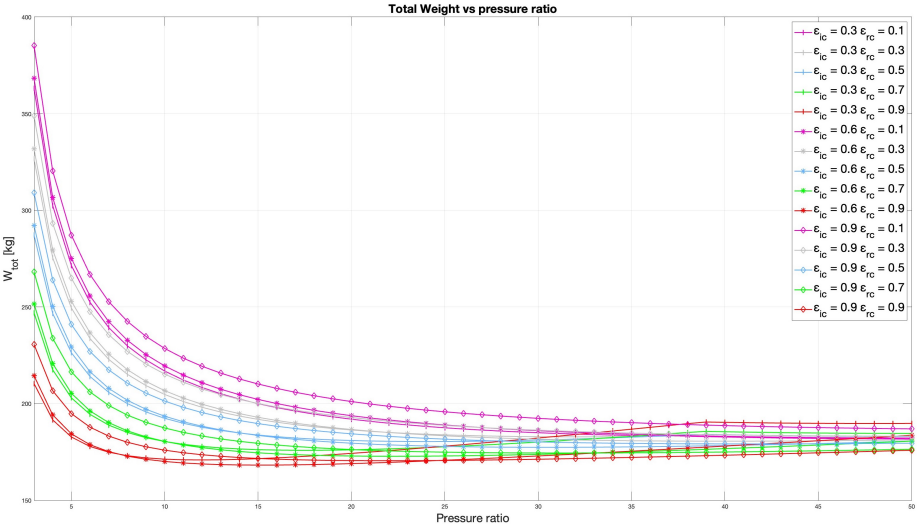

Figure 2.7: Total weight versus pressure ratio and heat exchangers efficiency

As can be seen from Figures 2.2, 2.3, 2.4, 2.5, and 2.6, the reason why a recuperator with high efficiency was chosen but a lower efficiency was selected for the intercooler is that the recuperator efficiency has a more significant impact than the intercooler one. Therefore, while it is reasonable to splurge on a heavier and more expensive recuperator, it is convenient to use a less efficient intercooler to save on weight and costs (see Figure 2.7).

As it is the focus of this project, the procedures to evaluate compressors and turbine efficiencies will be expressed in detail in sections 3 and 4. Also, the air mass flow must be computed appropriately to satisfy the requirement of having 100 kW of thrust power and this will be expanded upon in section 5. For now, these are the values that will be assumed:

- Air mass flow: $\dot{m} = 0.2892\, kg/s$
- Low-pressure compressor polytropic efficiency: $\eta_{p,LPC} = 0.8385$
- High-pressure compressor polytropic efficiency: $\eta_{p,LPC} = 0.8287$
- Turbines polytropic efficiency (all stages combined): $\eta_{p,t} = 0.8937$

The initial cycle analysis results are shown in the following images.

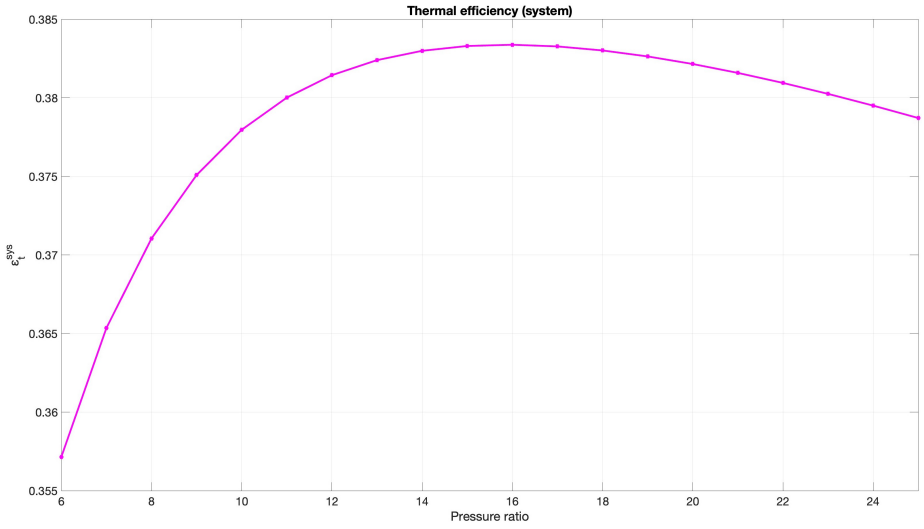

Figure 2.8: Thermal efficiency (of the whole system) versus pressure ratio

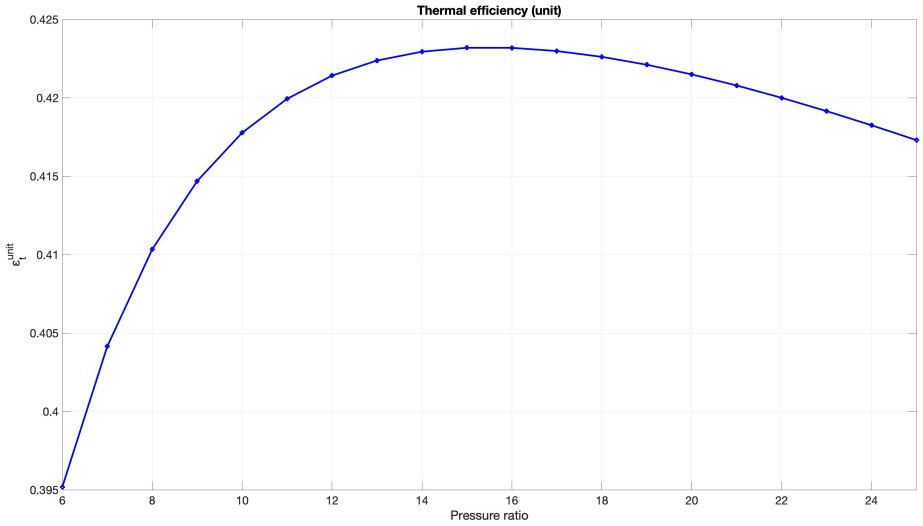

Figure 2.9: Thermal efficiency (of the engine unit) versus pressure ratio

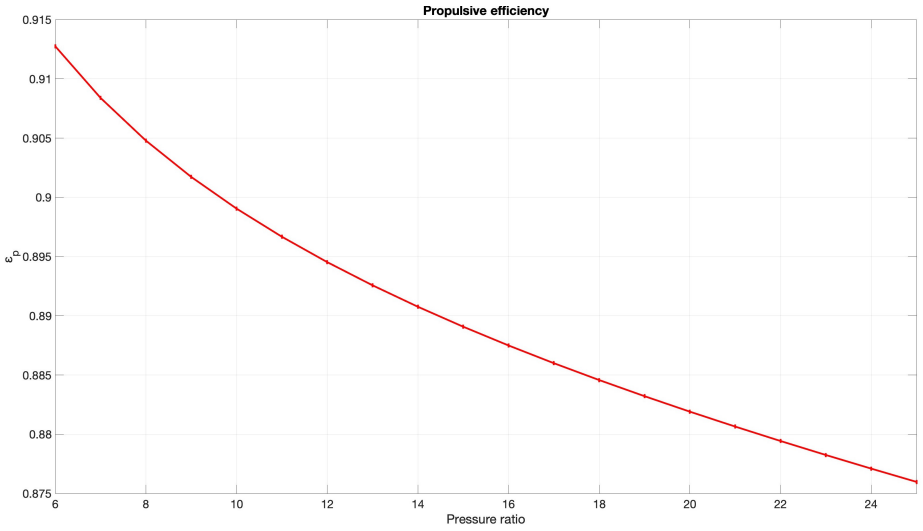

Figure 2.10: Propulsive efficiency versus pressure ratio

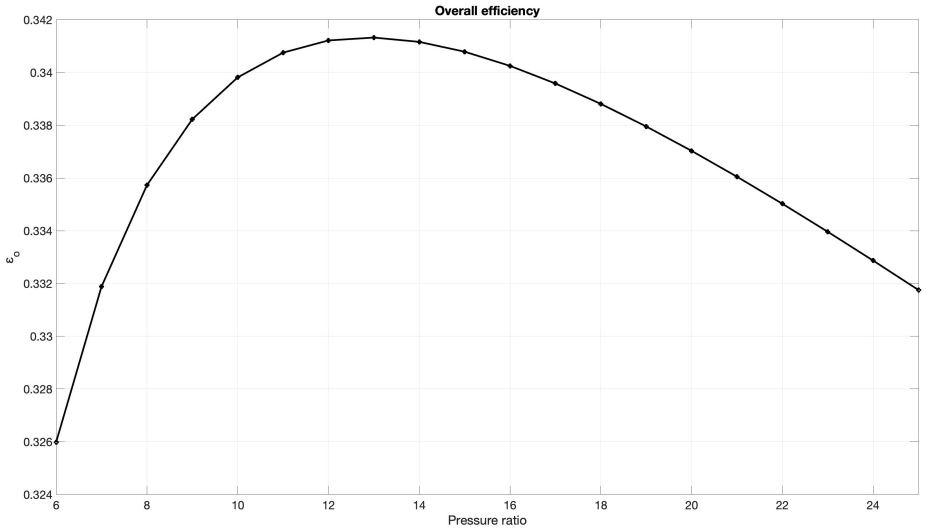

Figure 2.11: Overall efficiency versus pressure ratio

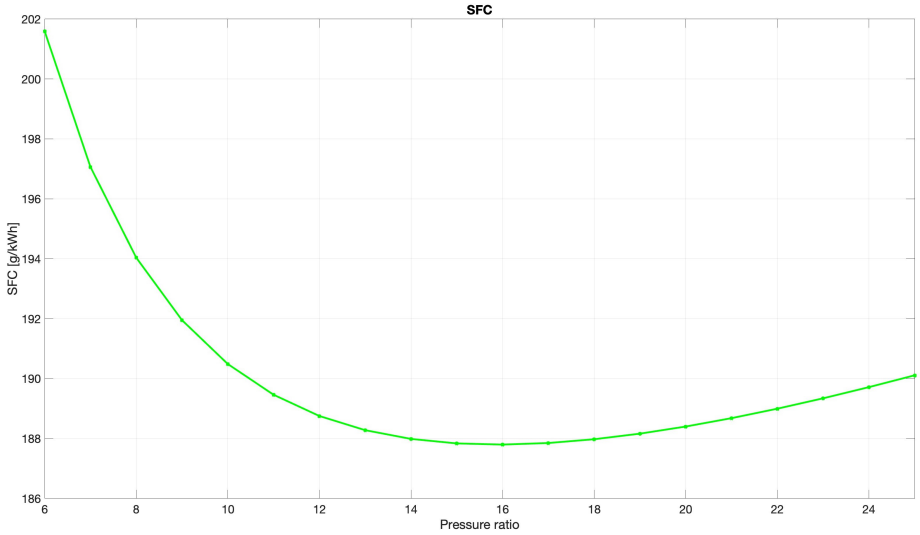

Figure 2.12: Specific fuel consumption versus pressure ratio

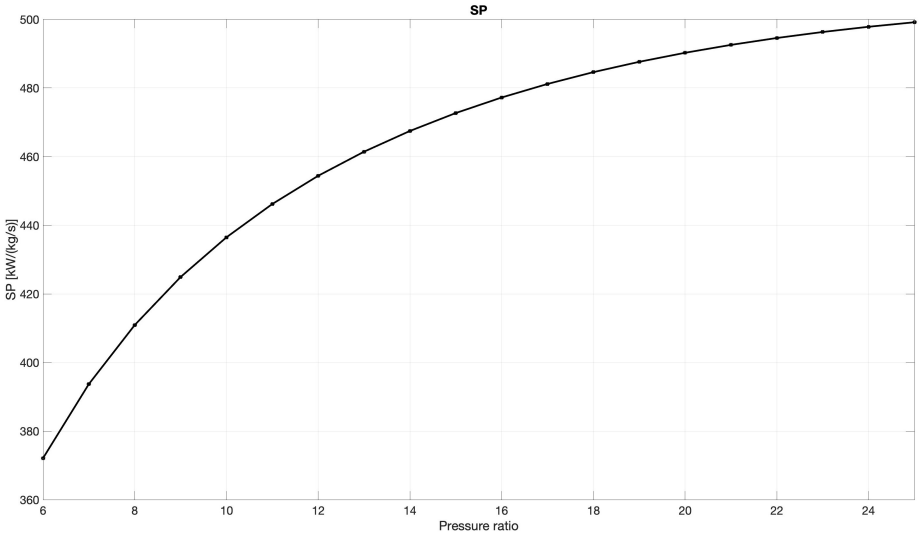

Figure 2.13: Specific power versus pressure ratio

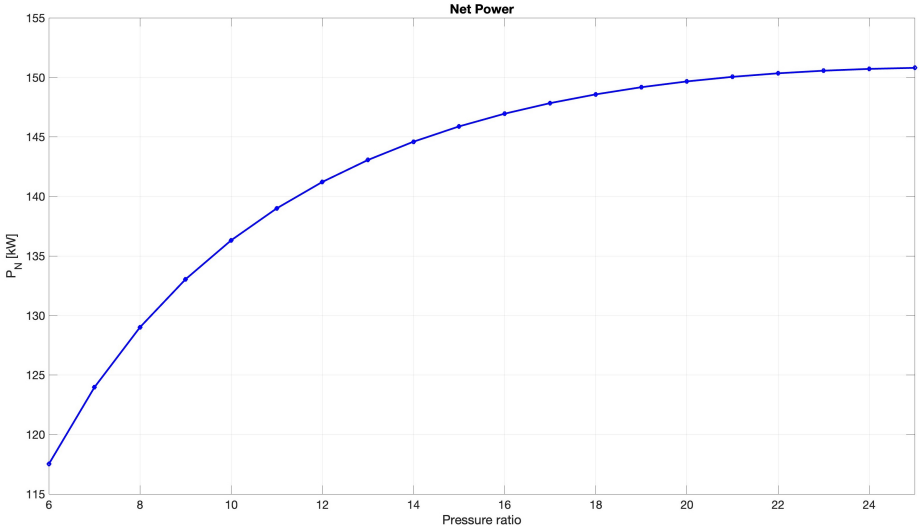

Figure 2.14: Net power versus pressure ratio

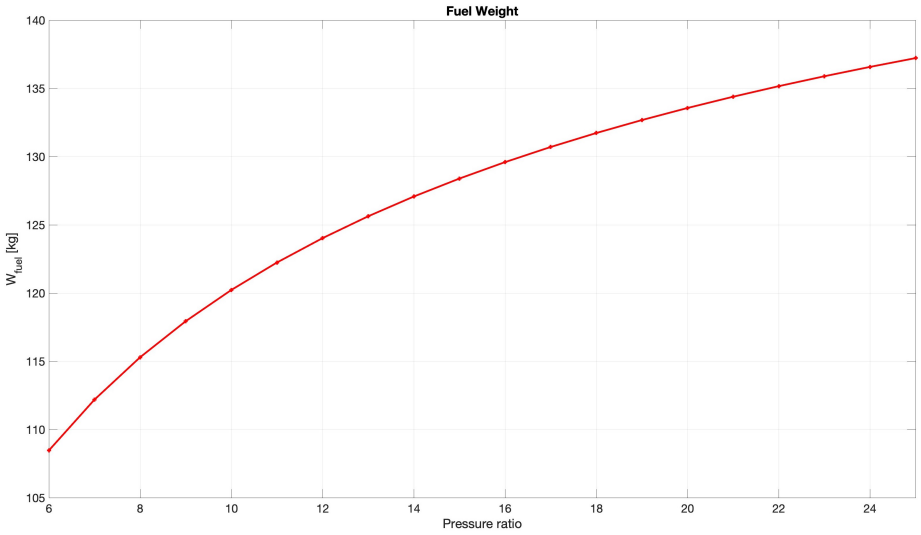

Figure 2.15: Fuel weight versus pressure ratio

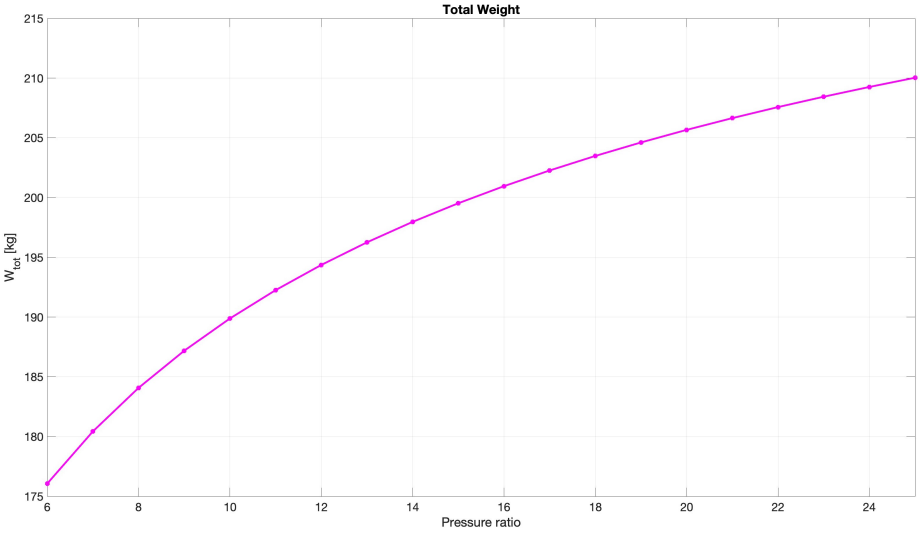

Figure 2.16: Total weight versus pressure ratio

The maximum overall efficiency (which is obtained at the same pressure ratio for which the fuel mass is minimized) is reached at a pressure ratio of $\pi_c = 13$, which will be used as the starting point in the following sections. The corresponding T-s diagram is shown in Figure 2.17 and Table 2 shows the initial cycle results.

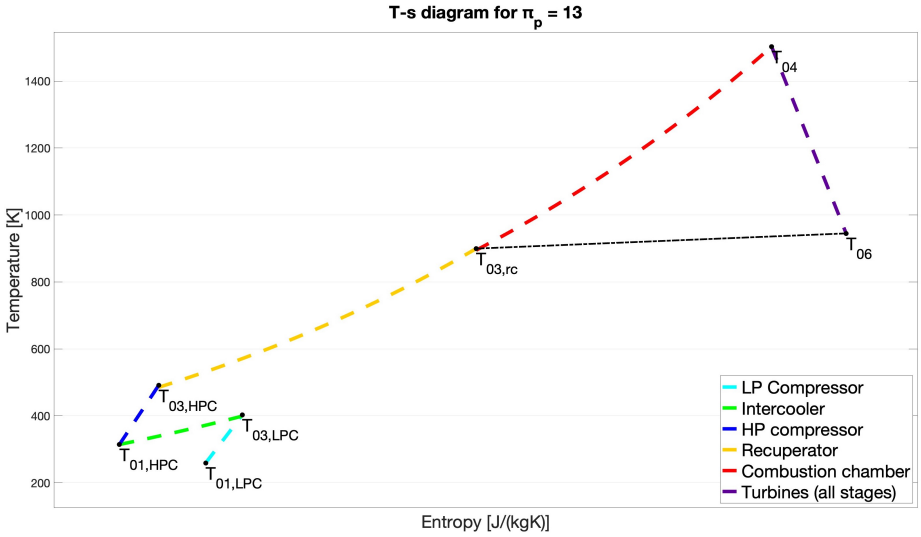

Figure 2.17: T-s diagram

External conditions	
External Temperature T_a	255.65 K
External Pressure P_a	54.02 kPa
Flight Mach number M_a	0.272
Air mass flow $\dot{m}$	0.289 kg/s
Air intake	
Efficiency η_d	0.98
Inlet total temperature T_0	259.48 K
Inlet total pressure P_0	56.881 kPa
Exit total temperature T_{01}	259.48 K
Exit total pressure P_{01}	56.822 kPa
Low-pressure compressor	
Stage pressure ratio π_c'	3.606
Polytropic efficiency η_p	0.839
Isentropic efficiency η_s	0.807
Power $P_{c,LPC}$	41385 W
Inlet total temperature $T_{01,LPC}$	259.48 K
Inlet total pressure $P_{01,LPC}$	56.822 kPa
Exit total temperature $T_{03,LPC}$	403.01 K
Exit total pressure $P_{03,LPC}$	204.876 kPa
Intercooler	
Pressure drop δp_{ic}	0.03
Efficiency ε_{ic}	0.6
Inlet total temperature $T_{03,LPC}$	403.01 K
Inlet total pressure $P_{03,LPC}$	204.876 kPa
Exit total temperature $T_{01,HPC}$	314.59 K
Exit total pressure $P_{01,HPC}$	198.723 kPa
High-pressure compressor	
Stage pressure ratio π_c'	3.606
Polytropic efficiency η_p	0.829
Isentropic efficiency η_s	0.796
Power $P_{c,HPC}$	50910 W
Inlet total temperature $T_{01,HPC}$	314.59 K
Inlet total pressure $P_{01,HPC}$	198.723 kPa
Exit total temperature $T_{03,LPC}$	491.15 K
Exit total pressure $P_{03,LPC}$	716.531 kPa
Recuperator	
Pressure drop δp_{ic}	0.04
Efficiency ε_{ic}	0.9
Inlet total temperature $T_{03,HPC}$	491.15 K
Inlet total pressure $P_{03,HPC}$	716.531 kPa
Exit total temperature $T_{03,rc}$	899.74 K
Exit total pressure $P_{03,rc}$	687.870 kPa

Combustion chamber	
Pressure drop f_c	0.02
Combustion efficiency ν_c	0.98
Inlet total temperature $T_{03,rc}$	899.74 K
Inlet total pressure $P_{03,rc}$	687.870 kPa
Exit total temperature T_{04}	1503 K
Exit total pressure P_{04}	674.112 kPa
Gas mass flow $\dot{m}_t$	0.296 kg/s
$\dot{m}_{fuel}/\dot{m}$	0.024
Turbines (all stages)	
Expansion ratio P_{06}/P_{04}	0.086
Polytropic efficiency η_p	0.894
Isentropic efficiency η_s^{tt}	0.917
Power P_t	235353 W
Inlet total temperature T_{04}	1503 K
Inlet total pressure P_{04}	674.112 kPa
Exit total temperature T_{06}	945.14 K
Exit total pressure P_{06}	57.741 kPa
Nozzle	
Efficiency η_n	0.98
Inlet temperature T_{06}	945.14 K
Inlet pressure P_{06}	57.741 kPa
Exit temperature T_7	930.98 K
External Pressure P_a	54.02 kPa
Exit velocity V_{exit}	192 m/s
Nozzle thrust $Thrust_{nozzle}$	31.55 N
Nozzle thrust power P_{nozzle}	4340 W
Total thrust $Thrust$	1366 N
Thrust power P_W	119 kW
Net power P_N	143 kW
Power imparted to the airflow (fans+engine) P_J	133 kW
Thermal power $\dot{m}_{fuel}H_u$	349 kW
Thermal efficiency (of the whole system) ε_t^{sys}	38.2 %
Thermal efficiency (of the engine unit) ε_t^{unit}	42.2 %
Propulsive efficiency ε_p	89.3 %
Overall efficiency ε_o	34.1 %
Specific fuel consumption SFC	188.281 g/kWh
Specific power SP	461.447 kJ/kg
Total weight W_{tot}	198 kg
Fuel weight W_{fuel}	127 kg

Table 2: Thermodynamic cycle initial results

3 Compressors

Since the cycle with an intercooler and a recuperator was demonstrated to be the most advantageous in terms of efficiency, weight, and fuel consumption, it is necessary to use two compressors.
Let's assume the following cycle parameters:

- Total pressure ratio: $\pi_p = 13$
- Air mass flow: $\dot{m} = 0.2892\,kg/s$
- Low-pressure compressor inlet total temperature: $T_{01,LPC} = 259.48\,K$
- Low-pressure compressor inlet total pressure: $P_{01,LPC} = 56.82\,kPa$
- Intercooler efficiency: $\varepsilon_{ic} = 0.6$
- Pressure drop across the intercooler: $\delta p_{ic} = 0.03$

The pressure ratio has been chosen so that the overall efficiency is maximized. Because of the small air mass flow and to be able to achieve the aforementioned pressure ratio without employing several stages, the compressors will be assumed to be centrifugal[30].

	mass flow [kg/s]
Predominantly centrifugal	< 1.5
Centrifugal or axial depending upon requirements	1.5–10
Predominantly axial	> 10

Now, it is necessary to determine the efficiency of each compressor and, once that is done, check whether it is better to mount them both on the same shaft or have them on different ones. Usually, a setup with just one shaft would be less bulky and complex, allowing the compressors to stay closer; however, because of the presence of the intercooler, the two compressors must stay farther apart anyway, making the complexity loss when using a single shaft less relevant. Therefore, the decision will be based on efficiency.

3.1 Efficiency estimation

Generally speaking, loss of efficiency in a compressor is the sum of the aerodynamic and parasitic losses.
Aerodynamic losses may include, but are not limited to:

- friction losses on the wetted boundaries for the different components;
- incidence losses on all blade rows;

- blade loading losses, due to the blade-to-blade pressure gradients that cause secondary flows;
- losses due to the hub-to-tip pressure gradients and their associated secondary flows;
- losses caused by a poor inlet flow distribution;
- blade clearance losses caused by the leakage flow of open impellers due to the passage of flow through the tip gap;
- recirculation losses generated by the reverse flow at the impeller tip at low flow rates, and any flow recirculation at the trailing edge;
- mixing losses, to account for the mixing of blade wakes and regions of separated flow
- volute or return channel losses downstream of the diffuser.

Parasitic losses usually include three components:

- disc friction losses due to the skin friction on the impeller backplate and shroud, if present;
- losses caused by leakage from the seals over the shroud of a shrouded stage;
- losses related to recirculation of the flow at the inlet or outlet of the impeller, which generally occurs only at part-load conditions;

These three components are not independent of each other because they all depend on the fluid flow patterns in the impeller side spaces, which depend on the swirl and mass flow of the leakage entering these domains. The Reynolds number and the roughness also play a role.
There are four approaches to determining stage efficiency and losses:

- measurement by testing in a suitable test rig, either at full scale or as a scale model;
- 3D CFD simulations with RANS equations;
- loss estimate for each individual contribution through the use of 1D mean-line loss models or 2D compressor model
- correlations based only on global parameters representing the duty of the compressor

Since the first two methods are too resource-intensive for preliminary design, they are not taken into consideration. Between the second two, the last one strikes the balance between the oversimple and the too sophisticated during the preliminary design phase and will be used here.

3.1.1 Non-dimensional analysis

Numerical correlations to estimate the performance of compressors are based on experimental data obtained from state-of-the-art machines; this is done by similarity.
There are three conditions required for two machines to be considered similar:

- geometrical similarity: two machines are geometrically similar if they differ only through scaling in size with a certain scaling factor (in radial compressors and turbines, the impeller diameter is often used as the reference scale);
- fluid dynamic similarity: two machines can be considered to share fluid dynamic similarity if the kinematic motion of the fluid and the dynamic forces acting on the blades are similar in non-dimensional terms;
- thermodynamic similarity: two machines must have similar changes in gas conditions (ratios of temperatures, pressures, and densities) to be considered thermodynamically similar.

The usefulness of non-dimensional parameters lies in the fact that they allow the performance to be defined in a way that is nearly independent of the fluid, the absolute dimensions of the machine, and the inlet conditions; they also make it possible to convert the measured overall performance (efficiency, pressure rise, and flow ratio) of a certain machine at a particular speed to other conditions (such as a different speed, different fluid, different inlet conditions) or to a geometrically similar machine of a different size. Therefore, similarity allows the designer to use data from real machines and generalize them to create dimensionless performance curves which can be used for the preliminary design of new machines.
There are two common choices of non-dimensional parameters to evaluate turbomachinery:

- flow coefficient and work coefficient
- specific speed and specific diameter

which are defined as follows.
Flow coefficient
The flow coefficient can be interpreted as a dimensionless mass flow and is the ratio between the actual mass flow and that which would occur if the total flow were to pass through the flow channels with annulus area A, at a velocity equivalent to the reference blade speed u. The flow coefficient is defined as

$$\phi = \frac{\dot{m}}{\rho A u} = \frac{\dot{V}}{A u} = \frac{c_m}{u} \tag{3.1.1}$$

Where

- ρ: local density

- $\dot{V}$: local volumetric flow
- c_m: local meridional velocity
- u: local blade speed

This local flow coefficient is often used to characterize the flow at a particular location within an impeller. The problem with this definition is that the local conditions are not known a priori; this is why the *global flow coefficient* is defined, which is the ratio between the real mass flow and the mass flow which would occur if the total flow were to pass through a virtual area A with the velocity of the tip blade speed and the density of the inlet total conditions. Since it is based on the inlet total conditions and a virtual area, it requires no detailed information about the local density or flow area. Two definitions of the virtual area are possible: $A = D_2^2$ or $A = \frac{\pi}{4} D_2^2$.
If the first definition is in use, then

$$\phi_{01} = \frac{\dot{m}}{\rho_{01} A u_2} = \frac{\dot{m}}{\rho_{01} D_2^2 u_2} = \frac{\dot{V}_{01}}{D_2^2 u_2} \tag{3.1.2}$$

When $A = \frac{\pi}{4} D_2^2$, the flow coefficient becomes

$$\phi_M = \frac{4}{\pi} \frac{\dot{V}_{01}}{u_2 D_2} = \frac{4}{\pi} \phi_{01}$$

where

- D_2: impeller diameter
- u_2: impeller tip speed
- ρ_{01}: inlet total density

Work coefficient
The non-dimensional work input coefficient, which characterizes the dynamic effects of the impeller rotational speed on the total enthalpy rise across a compressor, is defined as

$$\lambda = \frac{\Delta h}{u_2^2} \tag{3.1.3}$$

where Δh is the total-to-total enthalpy rise across a compressor.
Since a real compressor does not work in isentropic conditions, it is also useful to define:

- Isentropic head rise coefficient: this coefficient is defined analogously to equation 3.1.3 but is based on the ideal enthalpy rise

$$\psi_s = \frac{\Delta h_s}{u_2^2} = \eta_s \lambda \tag{3.1.4}$$

  where η_s is the compressor total-to-total isentropic efficiency.

- Polytropic head rise coefficient: this is similar to the isentropic head rise coefficient but is defined referring to the aerodynamic work $\int \nu dp$:

$$\psi_p = \frac{\int \nu dp}{u_2^2} = \eta_p \lambda \tag{3.1.5}$$

  where η_p is the compressor total-to-total polytropic efficiency.

Specific speed and specific diameter
The specific speed and specific diameter represent a non-dimensional speed and a non-dimensional size of the impeller for a given pressure rise and volume flow rate. They are defined, respectively, as follows:

$$\omega_s = \omega \frac{\dot{V}_{01}^{1/2}}{\Delta h_s^{3/4}} \tag{3.1.6}$$

$$D_s = D_2 \frac{\Delta h_s^{1/4}}{\dot{V}_{01}^{1/2}} \tag{3.1.7}$$

where ω is the rotational speed in rad/s.
The main use of specific speed is to check if a radial compressor can be built for a specific duty or whether another type of compressor is needed. All single-stage centrifugal compressors have a specific speed between about 0.3 and 2.0.
It is possible to write ω_s and D_s in terms of the global flow coefficient and the isentropic work coefficient.
Since

$$u_2 = \omega D_2/2$$
$$\dot{V}_{01} = \phi_{01} u_2 D_2^2 = \phi_{01} \omega D_2^3/2$$
$$\Delta h_s = \psi_s u_2^2 = \psi_s \omega^2 D_2^2/4$$

the specific speed and specific diameter can be written as

$$\omega_s = \omega \frac{\dot{V}_{01}^{1/2}}{\Delta h_s^{3/4}} = \omega \frac{(\phi_{01} \omega D_2^3/2)^{1/2}}{(\psi_s \omega^2 D_2^2/4)^{3/4}} = 2 \frac{\phi_{01}^{1/2}}{\psi_s^{3/4}} \tag{3.1.8}$$

$$D_s = D_2 \frac{\Delta h_s^{1/4}}{\dot{V}_{01}^{1/2}} = D_2 \frac{(\psi_s \omega^2 D_2^2/4)^{1/4}}{(\phi_{01} \omega D_2^3/2)^{1/2}} = \frac{\psi_s^{1/4}}{\phi_{01}^{1/2}} \tag{3.1.9}$$

The Cordier diagram and its usefulness

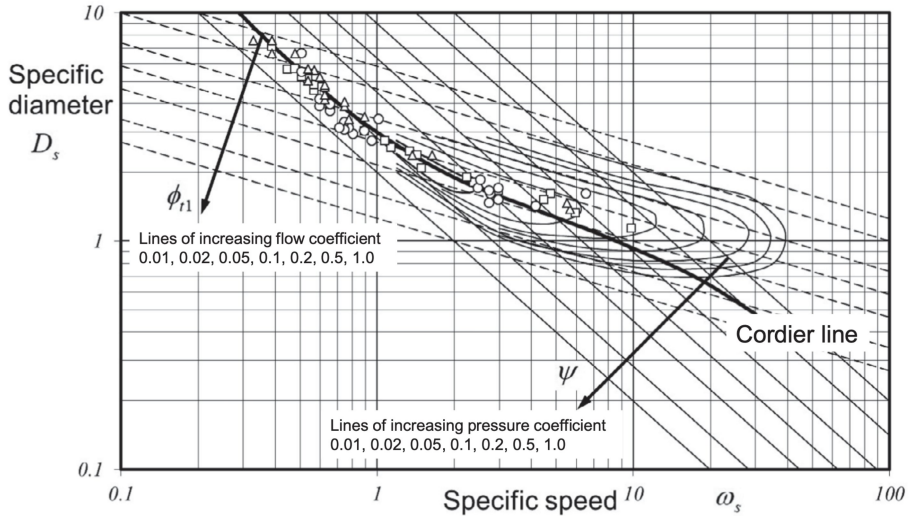

Figure 3.1: A Cordier diagram in the form recommended by Balje (1981).

In the Cordier(1953) diagram, shown in Figure 3.1, the specific diameter of a range of machines at the best operating point is plotted versus the specific speed. It is important to notice that there is no condition of similarity between the different points in the Cordier diagram. Since the condition of maximum efficiency is imposed, the graph shows only the best efficiency points of machines with different geometries; therefore, a change in specific speed implies a change in machine geometry instead of a change in operating point. Generally speaking, the following machines are used in the following ranges:

- radial machines with a radial inlet and a radial outlet: $\omega_s < 0.5$
- radial machines with a more axial inlet and a radial outlet: $0.5 < \omega_s < 1.5$
- mixed flow machines with a diagonal outlet: $1.0 < \omega_s < 2.0$
- axial machines: $\omega_s > 2.0$

In Figure 3.1, lines of constant flow and work coefficient are present, which become straight lines in the log-log graph. These lines can be determined by rearranging equations 3.1.8 and 3.1.9:

$$\ln D_s + \ln \omega_s = \ln \frac{2}{\psi_s^{1/2}} \tag{3.1.10}$$

$$3 \ln D_s + \ln \omega_s = \ln \frac{2}{\phi_{01}} \tag{3.1.11}$$

At first glance, the Cordier diagram looks well suited for preliminary design: from the specific speed, it determines the optimum specific diameter and head coefficient and, finally, the efficiency level and the shape of the machine. However, it can be argued that there is no benefit in using the quite obscure specific speed over the simpler flow coefficient.
For starters, it is not harder to classify turbocompressors in terms of flow coefficient instead of specific speed: just as a low specific speed on the Cordier diagram implies a high specific diameter, so a low flow coefficient implies a high work coefficient compared to that of an axial or mixed flow compressor. However, the great advantage of the flow coefficient is that it is linearly dependent on the volume flow. The flow coefficient is also linearly coupled to the work coefficient through the Euler equation, which makes it useful for evaluating off-design performance.
Also, an issue with the Cordier diagram is that it is always plotted on a log-log scale, which makes it more difficult to discern between different design points.
Finally, if the rotational speed (in radians per second) is not known a priori, there is no advantage in using the specific speed instead of the much simpler global flow coefficient for purely radial and mixed flow machines. Furthermore, in most applications, a rule-of-thumb value for the tip speed is usually known, either from the required tip speed Mach number or mechanical considerations, so the flow coefficient is often much more useful as it includes the tip speed and not the rotational speed.
That being said, a correlation based on the flow coefficient instead of the specific speed will be used.

Aungier's correlation

There are several correlations of this kind, such as those of Rodgers (1980), Casey and Marty (1985), Aungier (1995), and Robinson et al. (2011). For this work, the choice fell on Aungier's correlations, which are as follows.

$$\phi_M = \frac{4}{\pi}\frac{\dot{V}_{01}}{u_2 D_2} = \frac{4}{\pi}\phi_{01}$$

For shrouded stages:

$$\lambda = 0.62 - (\phi_M/0.4)^{0.3} + 0.0014/\phi_M$$

$$\psi_p^{vd} = 0.51 + \phi_M - 7.6\phi_M^2 - 0.00025/\phi_M$$

$$\eta_p^{vd} = \lambda/\psi_p^{vd}$$

$$\eta_p^{vld} = \eta_p^{vd} - 0.017/[0.04 + 5\phi_M + (\eta_p^{vd})^3]$$

For open impellers:

$$\lambda = 0.68 - (\phi_M/0.37)^3 + 0.002/\phi_M$$

$$\psi_p^{vd} = 0.59 + 0.7\phi_M - 7.5\phi_M^2 - 0.00025/\phi_M$$

$$\eta_p^{vd} = \psi_p^{vd}/\lambda$$
$$\eta_p^{vld} = \eta_p^{vd} - 0.017/[0.04 + 5\phi_M + \eta_{vd}^3]$$
$$\psi_p^{vld} = \eta_p^{vld}\lambda$$

where *vd* stands for vaned diffuser, *vld* for vaneless diffuser and η_p is the total-to-total polytropic efficiency. Going forward, a vaned diffuser is assumed.

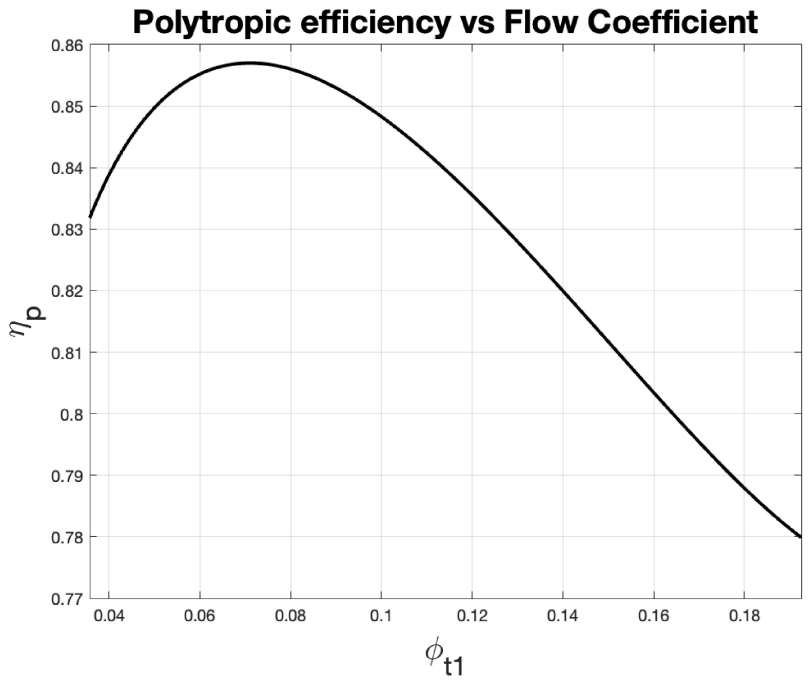

Figure 3.2: Polytropic efficiency versus flow coefficient

Aungier's correlations, similar to all the other compressor correlations, are best suited for medium-sized impellers ($200\,mm < D_2 < 450\,mm$). For smaller machines, the results obtained by this method are too optimistic and need to be adjusted. This point will be elaborated on in paragraph 3.2.1. Reynolds number, roughness, and clearance also play a role.
The curve in Figure 3.2 is based on experimental testing and shows that the best total-to-total polytropic efficiency is equal to $\eta_p = 0.857$ at a flow coefficient of $\phi_{01} = 0.071$. Of course, this is just an approximation. High levels of efficiency are generally obtained for flow coefficients in the range $0.07 \leq \phi_{01} \leq 0.10$ for medium-sized machines; for smaller devices, the optimum value is found at lower flow coefficients.

3.2 Preliminary Design

The first step is to assume a value of the flow coefficient ϕ_{01} to get a first estimate of the polytropic efficiency η_p^i (where the apex ^{i} implies that it has not been corrected for size, see section 3.2.1) and of the work input coefficient λ through Aungier's correlations. Let's define the tip speed Mach number as

$$M_{u2} = \frac{u_2}{\sqrt{\gamma R T_{01}}} \tag{3.2.1}$$

where the speed of sound is based on the inlet total conditions. It is possible to demonstrate that M_{u2} is equal to

$$M_{u2}^2 = \frac{{\pi'_c}^{\frac{(\gamma-1)}{\eta_p^i \gamma}} - 1}{(\gamma-1)\lambda} \tag{3.2.2}$$

where ${\pi'}_c$ is the stage pressure ratio which, since both compressors perform the same pressure ratio, is equal to

$$\pi'_c = \sqrt{\pi_c} \tag{3.2.3}$$

Since the pressure ratio is known and η_p and λ can be found through Aungier's equations, the impeller tip speed can be calculated. The diameter of the impeller is then given by the definition of the global flow coefficient (equation 3.1.2) as

$$D_2 = \sqrt{\frac{\dot{m}}{\rho_{01} u_2 \phi_{01}}} \tag{3.2.4}$$

The rotational speed is then computed from the diameter and the tip speed as

$$\omega = 2\frac{u_2}{D_2} \tag{3.2.5}$$

A first estimate of the isentropic efficiency can also be obtained as

$$\eta_s^i = \frac{{\pi_c}'^{\frac{\gamma-1}{\gamma}} - 1}{{\pi_c}'^{\frac{\gamma-1}{\gamma\eta_p}} - 1} \tag{3.2.6}$$

which makes it possible to find the isentropic head rise coefficient with equation 3.1.4 (which is repeated here for readability)

$$\psi_s = \frac{\Delta h_s}{u_2^2} = \eta_s \lambda \tag{3.2.7}$$

The knowledge of ϕ_{01} and ψ_s allows for the computation of ω_s and D_s through equations 3.1.8 and 3.1.9.

3.2.1 Correction for size

As said in paragraph 3.1.1, it is necessary to correct the estimation of the polytropic efficiency to take into consideration the smaller size of the impeller, which is due to the small air mass flow ratio. There are different ways to perform this correction and most of them are based on Reynolds' number. The chosen one for this work is the following[22]:

$$\Delta\eta_p = (1 - \eta_p^i)\left(\left(\frac{1.5 \cdot 10^7}{R_e}\right)^{0.2} - 1\right) \tag{3.2.8}$$

where R_e is defined as

$$R_e = \frac{u_2 D_2}{\nu_1} \tag{3.2.9}$$

where ν_1 is the cinematic viscosity at the impeller inlet which is

$$\nu_1 = \frac{\mu}{\rho_1} \tag{3.2.10}$$

It is, therefore, necessary to find the inlet total conditions.
Let's start by finding the relative Mach number at the tip of the impeller eye. Rusch and Casey (2013) provide several equations for the geometry and Mach numbers of compact stages designed with a minimum relative Mach number at the impeller eye M_{w1}; however, these equations are provided in the form of diagrams and equations that have to be solved iteratively. By analyzing these equations, an approximate empirical equation for M_{u2} as a function of ϕ_{01} and M_{w1} can be found:

$$M_{u2} = \frac{M_{w1}(3.2\phi_{01}/k)^{0.36}}{(3.2\phi_{01}/k)^{0.36} + 0.15M_{w1}(0.45 + \phi_{01}/k)} \tag{3.2.11}$$

which, for stages designed for maximum compactness, can be rearranged to provide a direct equation to calculate M_{w1} as a function of M_{u2} and ϕ_{01}

$$M_{w1} = \frac{M_{u2}(3.2\phi_{01}/k)^{0.36}}{1 - 0.15M_{u2}(0.45 + \phi_{01}/k)} \tag{3.2.12}$$

where k is the impeller inlet blockage factor and is defined as

$$k = 1 - \left(\frac{D_{h1}}{D_{t1}}\right)^2 \tag{3.2.13}$$

in which

- D_{h1}: impeller eye hub diameter
- D_{t1}: impeller eye tip diameter

Let's assume an inlet blockage factor of $k = 0.9$; from equation 3.2.12, it is possible to compute the value of the impeller inlet relative Mach number at the tip.
When designing compact stages, it is also important to select the optimum inlet flow angle at the tip β_{t1}, which is the one that gives the maximum flow per unit area. According to Rusch and Casey (2013), assuming no inlet swirl, the optimum β_{t1} is given by

$$\cos\beta_{t1} = \frac{\sqrt{3+\gamma M_{w1}^2 + 2M_{w1}} - \sqrt{3+\gamma M_{w1}^2 - 2M_{w1}}}{2M_{w1}} \tag{3.2.14}$$

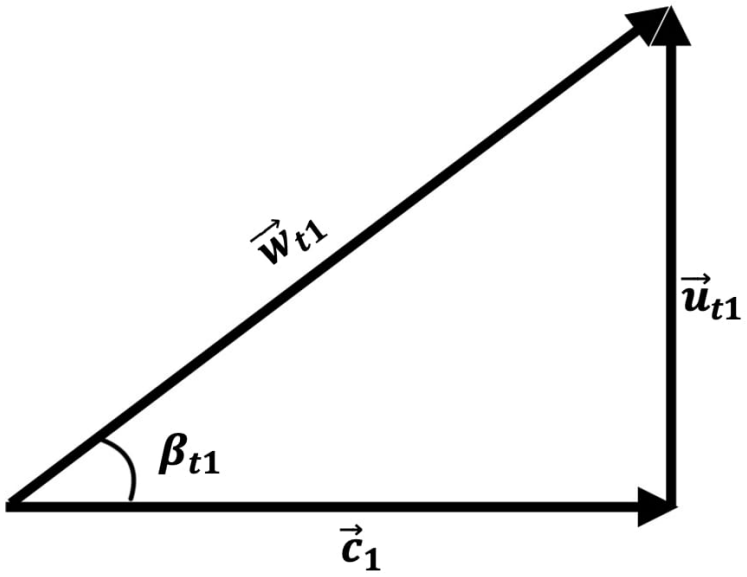

Figure 3.3: Velocity triangle at the tip of the impeller eye with no inlet swirl

To compute the impeller inlet tip diameter, let's write the rotational speed as

$$\omega = 2\frac{u_2}{D_2} = 2\frac{u_{t1}}{D_{t1}} \tag{3.2.15}$$

then, by looking at the velocity triangle of Figure 3.3 and rearranging 3.2.15

$$\frac{D_{t1}}{D_2} = \frac{u_{t1}}{u_2} = \frac{w_{t1}\sin\beta_{t1}}{u_2} = \frac{M_{w1}\sin\beta_{t1}\sqrt{\gamma R T_1}}{M_{u2}\sqrt{\gamma R T_{01}}} = \frac{M_{w1}\sin\beta_{t1}}{M_{u2}}\sqrt{\frac{T_1}{T_{01}}}$$

which means that the tip diameter is equal to

$$D_{t1} = D_2 \frac{M_{w1}}{M_{u2}} \sin \beta_{t1} \left[1 + \frac{\gamma - 1}{2} M_{w1}^2 \cos^2 \beta_{t1} \right]^{-1/2} \tag{3.2.16}$$

and u_{t1} is immediately found as

$$u_{t1} = \frac{D_{t1}}{2} \omega \tag{3.2.17}$$

Then, the inlet absolute velocity c_1, assuming zero inlet swirl, is

$$c_1 = \frac{u_{t1}}{\tan \beta_{t1}} \tag{3.2.18}$$

which allows for the computation of:

- inlet static temperature:

$$T_1 = T_{01} - \frac{c_1^2}{2c_p} \tag{3.2.19}$$

- inlet static pressure:

$$P_1 = P_{01} \left(\frac{T_1}{T_{01}} \right)^{\frac{\gamma}{\gamma - 1}} \tag{3.2.20}$$

- inlet static density:

$$\rho_1 = \frac{P_1}{R T_1} \tag{3.2.21}$$

Through the continuity equation, it is then possible to find a new value of the inlet blockage factor k as

$$A_1 = \frac{\dot{m}}{\rho_1 c_1} \tag{3.2.22}$$

$$D_{h1} = \sqrt{D_{t1}^2 - \frac{4}{\pi} A_1} \tag{3.2.23}$$

$$k = 1 - \left(\frac{D_{h1}}{D_{t1}} \right)^2 \tag{3.2.24}$$

which should be similar to the value assumed at the beginning and, if it is not, it is possible to iterate.
To compute the Reynolds number, dynamic viscosity must be estimated. There are different ways to do that; here, Sutherland's law has been used[7]:

$$\mu = \mu_{ref} \left(\frac{T_1}{T_{ref}} \right)^{3/2} \frac{T_{ref} + S}{T_1 + S} \tag{3.2.25}$$

where:

- $\mu_{ref} = 17.16 * 10^{-6} kgm^{-1}s^{-1}$
- $T_{ref} = 273.15K$
- $S = 110.4K$

It is now possible to find R_e with equation 3.2.9 and apply equation 3.2.8 to get the new value of the polytropic efficiency η_p

$$\eta_p = \eta_p^i - \Delta\eta_p \tag{3.2.26}$$

and the new value of the isentropic efficiency η_s

$$\eta_s^i = \frac{\pi'_c{}^{\frac{\gamma-1}{\gamma}} - 1}{\pi'_c{}^{\frac{\gamma-1}{\gamma\eta_p}} - 1} \tag{3.2.27}$$

Note: equation 3.2.8 tends to zero as R_e tends to $1.5 \cdot 10^7$ (which is used as reference); therefore, the larger the machine (which means larger R_e), the less it is penalized by the correction.
It is now possible to find the exit parameters as

- exit total pressure:
$$P_{03} = \pi'_c P_{01} \tag{3.2.28}$$
- exit total temperature:
$$T_{03} = T_{01} + \frac{1}{\eta_s}(T_{03s} - T_{01}) \tag{3.2.29}$$

where T_{03s} is the ideal exit total temperature and is equal to

$$T_{03s} = T_{01}\pi'_c{}^{\frac{\gamma-1}{\gamma}} \tag{3.2.30}$$

and the power used by the compressor is equal to

$$P_c = \dot{m}c_p(T_{03} - T_{01}) \tag{3.2.31}$$

3.2.2 Before and after correction

Since the global flow coefficient ϕ_{01} is only dependent on the inlet total conditions, the geometry, and the tip speed, it does not change after the correction. Similarly, the work coefficient λ can be shown from Euler's equation to only depend on velocity triangles:

$$\Delta h = u_2 c_{u2} - u_1 c_{u1} \tag{3.2.32}$$

$$\lambda = \frac{u_2 c_{u2} - u_1 c_{u1}}{u_2^2} = \frac{c_{u2}}{u_2} - \left(\frac{u_1}{u_2}\right)\left(\frac{c_{u1}}{u_2}\right) \tag{3.2.33}$$

where c_{u1} and c_{u2} are the tangential components of the absolute velocity at the impeller inlet and impeller outlet, respectively. With zero inlet swirl, $c_{u1} = 0$ and equation 3.2.33 becomes

$$\lambda = \frac{c_{u2}}{u_2} \tag{3.2.34}$$

which means that, since the velocity triangles stay constant, λ also does not change.
Remembering that $\psi_s = \lambda\eta_s$, if η_s changes, ψ_s also changes; hence, remembering its definition (see equation 3.1.4) and assuming that u_2 stays the same, one can deduce that the isentropic enthalpy rise Δh_s changes. Moreover, Δh_s can be written as

$$\Delta h_s = c_p T_{01} \left[\pi_c'^{\frac{\gamma-1}{\gamma}} - 1 \right] \tag{3.2.35}$$

which implies, since the inlet total conditions are constant, that the pressure ratio diminishes. Since the purpose is to obtain a set pressure ratio, it would be necessary to find a machine that can reach the target pressure ratio after the correction. Nevertheless, this would require an iterative process that would be computationally costly and which would not be accurate anyway, since to get a high level of accuracy a CFD analysis is required. Therefore, for the purpose of the preliminary design, it is acceptable to assume that the pressure ratio remains unchanged. For the same reason, the specific speed and specific diameter will be approximated to stay unchanged after correction, even though, since they depend on ψ_s, they do not.

3.3 Configuration comparison

As mentioned at the beginning of the chapter, because of the presence of the intercooler, two compressors are required and it is possible to mount them either on a single shaft or on two different ones. Now that a method to estimate the performance of a single radial compressor stage has been described, it is possible to evaluate which setup has the best combined isentropic efficiency.
Knowing the inlet total conditions for the low-pressure compressor, the pressure ratio, and the mass flow, it is possible to estimate the low-pressure compressor performances as a function of its global flow coefficient; then, the inlet total conditions of the high-pressure compressor, which occur after the intercooler, can be found as

$$T_{01,HPC} = T_{03,LPC} - \varepsilon_{ic}(T_{03,LPC} - T_a) \tag{3.3.1}$$

$$P_{01,HPC} = P_{03,LPC}(1 - \delta p_{ic}) \tag{3.3.2}$$

where T_a is the external air temperature.
For a given global flow coefficient of the LPC, the performance evaluation of the HPC depends on whether a single or double shaft is used.

3.3.1 One shaft

If both compressors share the same shaft, they both have to rotate at the same speed. Hence, for a given global flow coefficient of the low-pressure compressor, the shaft speed of both compressors is set.
Since the global flow coefficient of the high-pressure compressor is necessary to evaluate its performance, it must be found by solving the following system of equations in the unknowns $\eta_{p,HPC}$, $\phi_{01,HPC}$, λ_{HPC}, $D_{2,HPC}$, $M_{u2,HPC}$, and $u_{2,HPC}$:

$$\begin{cases} (\eta^i_{p,HPC}, \lambda_{HPC}) = f(\phi_{01,HPC}) \\ M^2_{u2,HPC} = \frac{\pi'^{\frac{(\gamma-1)}{\eta^i_{p,HPC}\gamma}}_p - 1}{(\gamma-1)\lambda_{HPC}} \\ u_{2,HPC} = M_{u2,HPC}\sqrt{\gamma R T_{01,HPC}} \\ D_{2,HPC} = 2\frac{u_{2,HPC}}{\omega} \\ \phi_{01} = \frac{\dot{m}}{\rho_{01,HPC} D^2_{2,HPC} u_{2,HPC}} \end{cases} \tag{3.3.3}$$

Where the first equation represents Aungier's correlation.
From here, it is possible to use equations from 3.2.6 to 3.2.31 to compute everything else.

3.3.2 Two shafts

In this case, the global flow coefficients of the two compressors have to be set independently of each other and the analysis for both compressors is the same and is described in paragraphs 3.2.
With two shafts, it is also necessary to use at least two turbines; hence, it is possible to have the generator run by the high-pressure turbine, the low-pressure turbine, a free turbine, or to use two generators, one for the high-pressure turbine and one for the low-pressure one. This topic has been expanded upon in the next chapter.
The possible schemes are described in the following images.

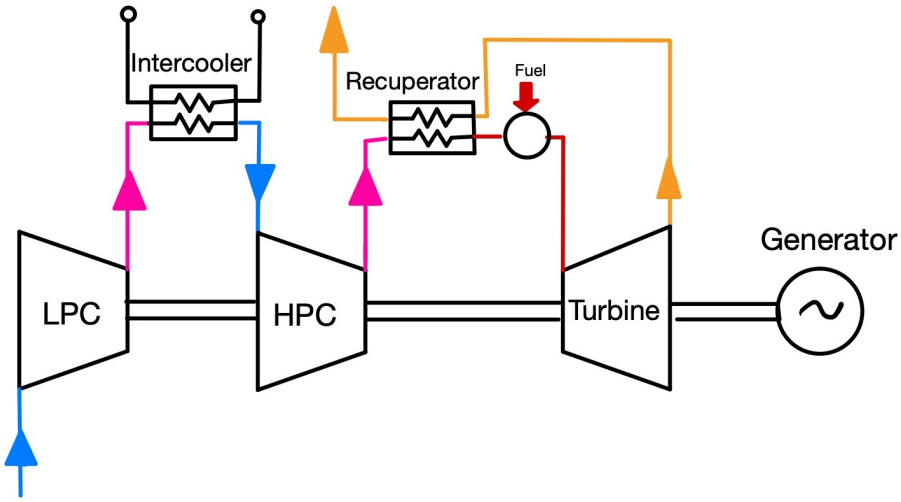

Figure 3.4: 1 shaft setup

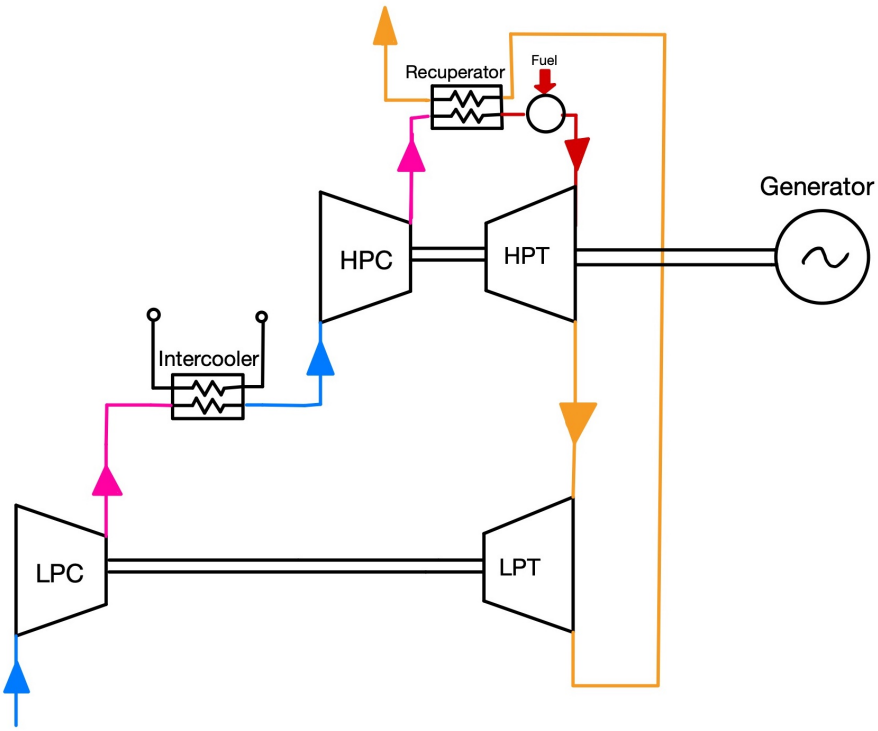

Figure 3.5: 2 shafts setup with the generator run by HPT

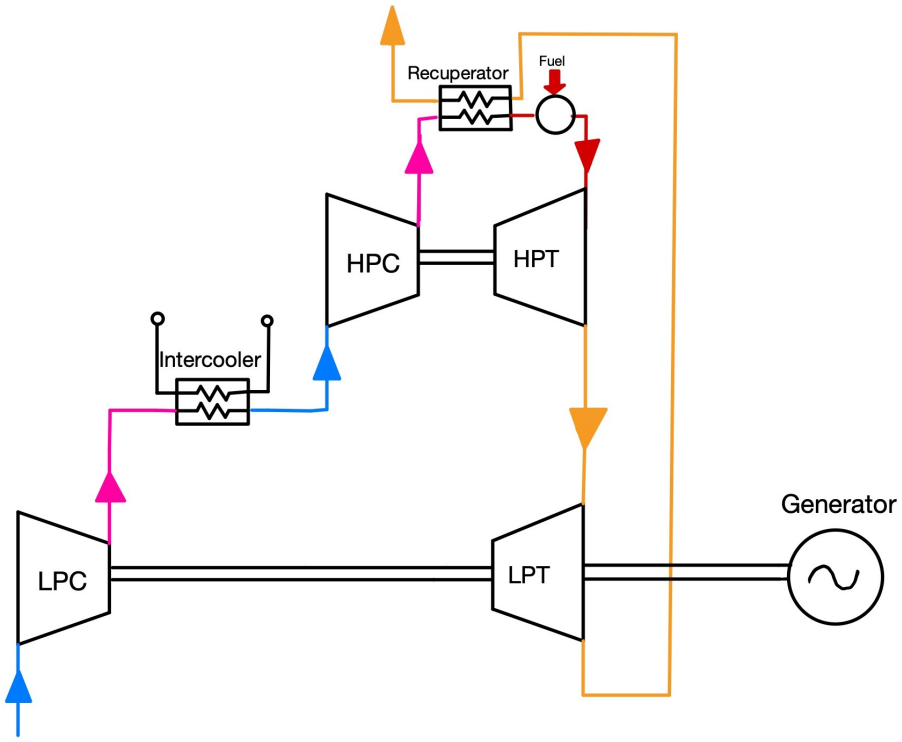

Figure 3.6: 2 shafts setup with the generator run by LPT

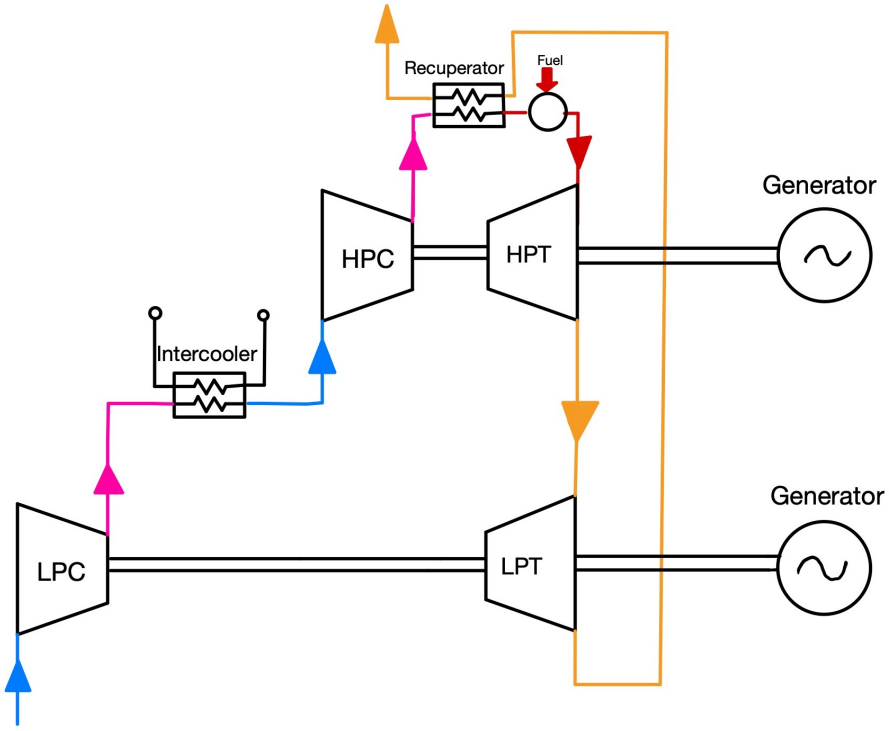

Figure 3.7: 2 shafts setup with 2 generators

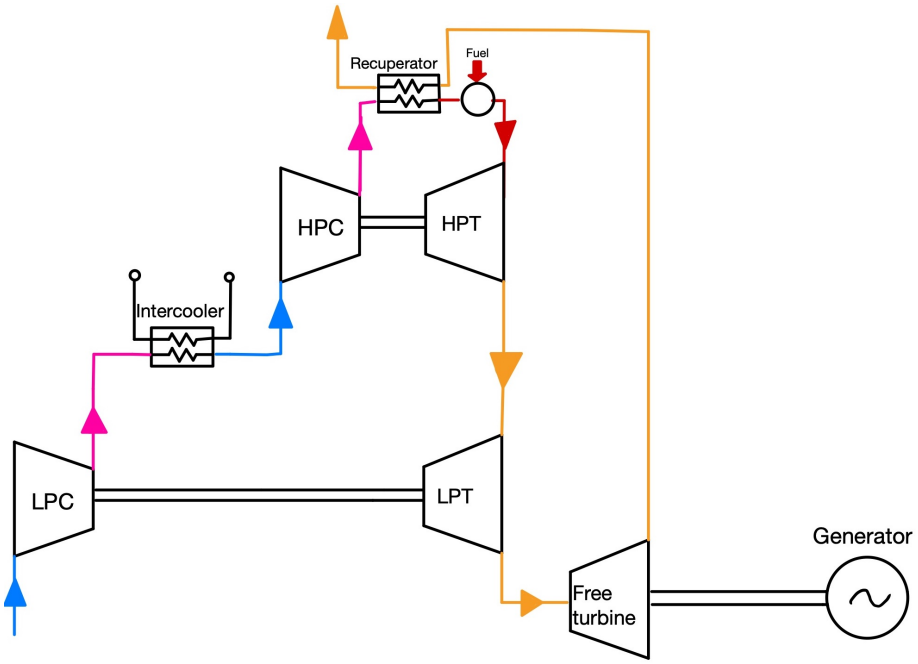

Figure 3.8: 2 shafts setup with free turbine

3.3.3 Results

In each of the following tables, the performances when the combined isentropic efficiency is maximized are shown. The combined isentropic efficiency is defined as

$$\eta_{s,combined} = \frac{\Delta T_{s,LPC} + \Delta T_{s,HPC}}{\Delta T_{LPC} + \Delta T_{HPC}} \tag{3.3.4}$$

where

$$\Delta T_{s,LPC} = T_{03s,LPC} - T_{01s,LPC} \tag{3.3.5}$$

$$\Delta T_{s,HPC} = T_{03ss,HPC} - T_{01s,HPC} \tag{3.3.6}$$

and

$$T_{01s,HPC} = T_{03s,LPC} - \varepsilon_{ic}(T_{03s,LPC} - T_a) \tag{3.3.7}$$

$$T_{03ss,HPC} = T_{01s,HPC}{\pi'}_c^{\frac{\gamma-1}{\gamma}} \tag{3.3.8}$$

Mass flow $\dot{m}$	0.2892 kg/s	
Stage pressure ratio π_c'	3.61	
	Without correction	**With correction**
Low Pressure Compressor		
Polytropic efficiency η_p	0.831	0.765
Isentropic efficiency η_s	0.798	0.720
Global flow coefficient ϕ_{01}	0.126	0.102
Work coefficient λ	0.611	0.652
Specific speed ω_s	1.215	1.023
Specific diameter D_s	2.356	2.678
Inlet total temperature T_{01}	259.484 K	259.484 K
Inlet total pressure P_{01}	56822.436 Pa	56822.436 Pa
Exit total temperature T_{03}	404.590 K	420.315 K
Exit total pressure P_{03}	204876.205 Pa	204876.205 Pa
Power P_c	41841 W	46375 W
Temperature rise ΔT	145.106 K	160.831 K
Rotational speed ω	12369 rad/s 118118 rpm	10408 rad/s 99385 rpm
High Pressure Compressor		
Polytropic efficiency η_p	0.842	0.773
Isentropic efficiency η_s	0.812	0.729
Global flow coefficient ϕ_{01}	0.042	0.029
Work coefficient λ	0.714	0.733
Specific speed ω_s	0.619	0.518
Specific diameter D_s	4.245	5.098
Inlet total temperature T_{01}	315.226 K	321.516 K
Inlet total pressure P_{01}	198729.919 Pa	198729.919 Pa
Exit total temperature T_{03}	488.676 K	518.360 K
Exit total pressure P_{03}	716530.913 Pa	716530.913 Pa
Power P_c W	50014 W	56759 W
Temperature rise ΔT	173.451 K	196.844 K
Rotational speed ω	12369 rad/s 118118 rpm	10408 rad/s 99385 rpm
Combined isentropic efficiency	0.789	0.703

Table 3: Results with maximum combined isentropic efficiency with single shaft

Mass flow $\dot{m}$	0.2892 kg/s	
Stage pressure ratio π_c'	3.61	
	Without correction	**With correction**
Low Pressure Compressor		
Polytropic efficiency η_p	0.857	0.790
Isentropic efficiency η_s	0.829	0.749
Global flow coefficient ϕ_{01}	0.071	0.063
Work coefficient λ	0.688	0.695
Specific speed ω_s	0.812	0.758
Specific diameter D_s	3.264	3.477
Inlet total temperature T_{01}	259.484 K	259.484 K
Inlet total pressure P_{01}	56822.436 Pa	56822.436 Pa
Exit total temperature T_{03}	399.196 K	414.147 K
Exit total pressure P_{03}	204876.205 Pa	204876.205 Pa
Power P_c	40285 W	44596 W
Temperature rise ΔT	139.712 K	154.663 K
Rotational speed ω	8260 rad/s 78875 rpm	7718 rad/s 73701 rpm
High Pressure Compressor		
Polytropic efficiency η_p	0.857	0.806
Isentropic efficiency η_s	0.829	0.769
Global flow coefficient ϕ_{01}	0.071	0.063
Work coefficient λ	0.688	0.695
Specific speed ω_s	0.812	0.758
Specific diameter D_s	3.264	3.477
Inlet total temperature T_{01}	313.068 K	319.049 K
Inlet total pressure P_{01}	198729.919 Pa	198729.919 Pa
Exit total temperature T_{03}	481.632 K	504.325 K
Exit total pressure P_{03}	716530.913 Pa	716530.913 Pa
Power P_c	48604 W	53423 W
Temperature rise ΔT	168.564 K	185.276 K
Rotational speed ω	16189 rad/s 154594 rpm	15199 rad/s 145139 rpm
Combined isentropic efficiency	0.815	0.740

Table 4: Results with maximum combined isentropic efficiency with two shafts

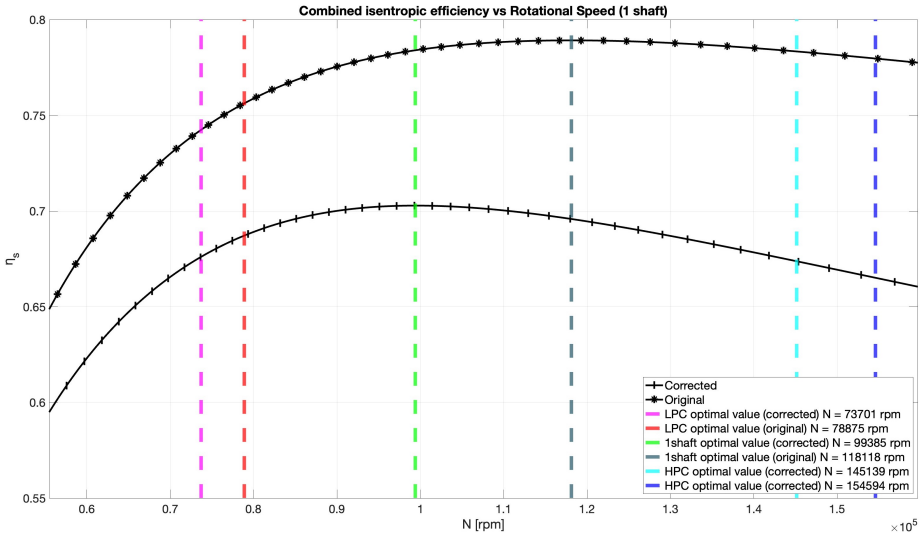

Figure 3.9: Combined isentropic efficiency versus shaft speed with a single shaft

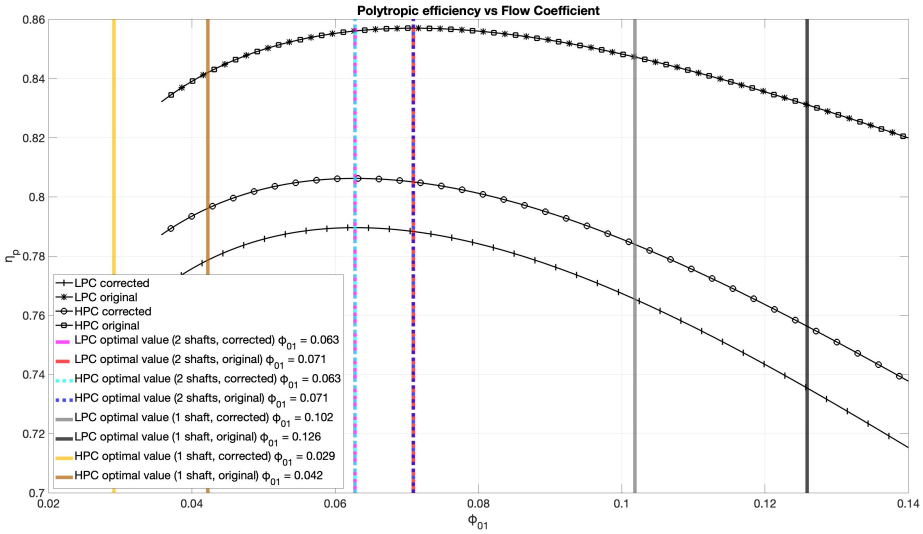

Figure 3.10: Polytropic efficiency versus global flow coefficient

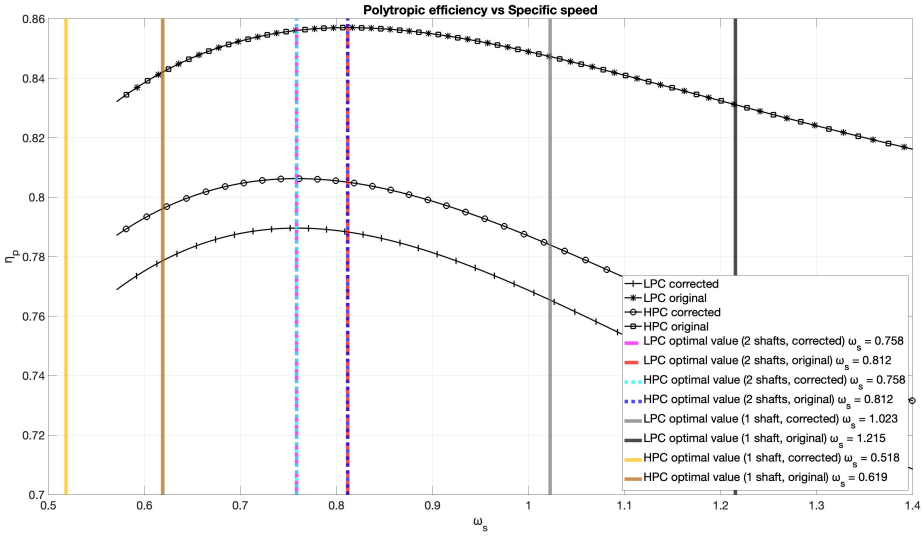

Figure 3.11: Polytropic efficiency versus specific speed

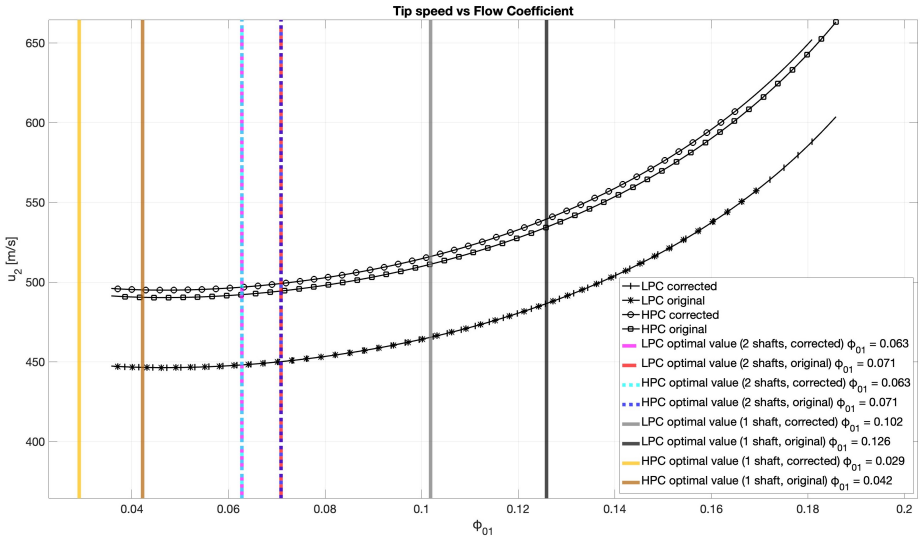

Figure 3.12: Tip speed versus global flow coefficient

From Figure 3.9, it is apparent how the optimal rotational speed with a single shaft is located between the optimal values of the two compressors, which means that it is a compromise between them. Another thing to notice is that, in each case, the optimal speed when the correction for size is employed is always slower than when the correction is not used.
In Figure 3.10, one can see how, without correction for size, the polytropic efficiency curve is the same for both compressors since it only depends on the global flow coefficient[3]. However, when the correction is applied, the polytropic efficiency changes between the two; in particular, the low-pressure compressor appears more penalized than the high-pressure compressor. The reason is seen in Figure 3.13: the Reynolds number is higher for the high-pressure compressor and stages with higher Reynolds number are less penalized by equation 3.2.8. The reason for higher R_e is the higher inlet total density due to the compression process in the previous stage and the higher tip speed u_2 due to the higher inlet temperature (see equation 3.2.1) (see Figure 3.12).

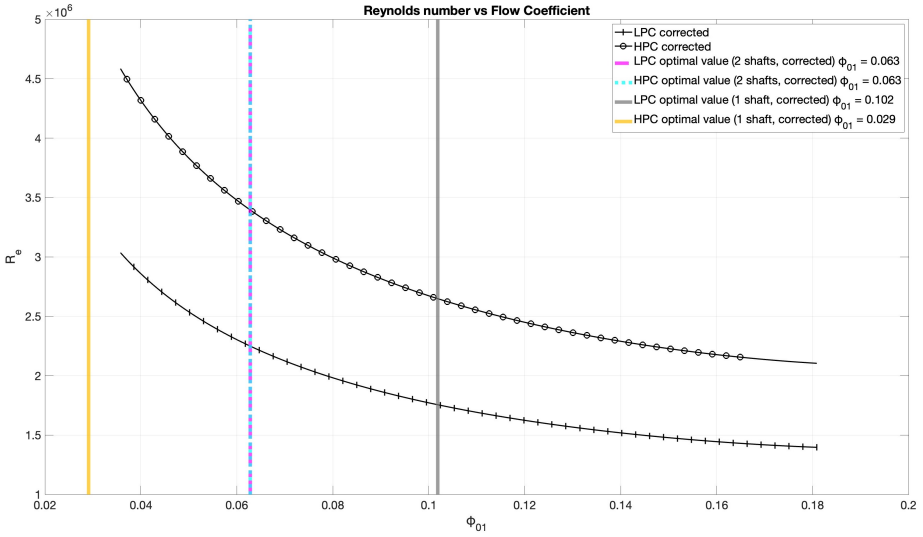

Figure 3.13: Reynolds number versus global flow coefficient

Observation: When comparing the impeller diameter between the two compressors in Figure 3.14, the HPC has a larger diameter than the LPC. This, in theory, should account for a smaller penalization when correcting the estimate of η_p. Size and Reynolds number are both relevant factors when evaluating changes in performance, and not all size-related penalties are directly linked to Reynolds-related effects (for example, those related to relative clearance). With the correction used in this chapter, only Reynolds-related effects are accounted for. This is a limitation of this methodology, which highlights the fact that

[3]This is an approximation

this is a preliminary analysis and, for more detailed data, experiments or CFD simulations need to be carried out.
It is also noticeable that, from Figures 3.9, 3.10, and 3.11, the difference between the corrected efficiency and the original one is quite drastic and it is certainly a conservative estimate.

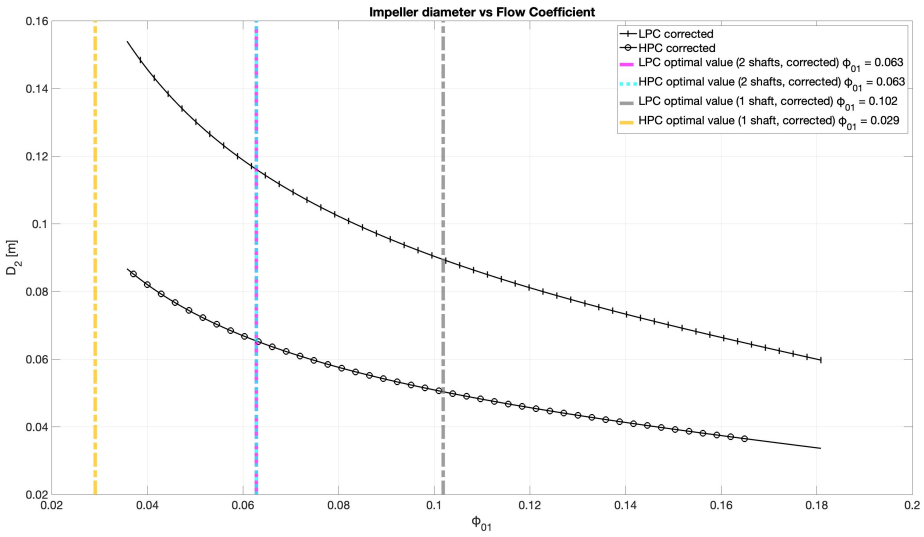

Figure 3.14: Impeller diameter versus global flow coefficient

By comparing Tables 3 and 4, it is evident that using two shafts is beneficial to the combined isentropic efficiency and, therefore, is the setup that will be assumed going forward. Indeed, when looking at Table 3, in the case of a single shaft, both compressors have a flow coefficient that is very far from the theoretical optimal value of ≈ 0.07. The low-pressure one has a $\phi_{01} = 0.102$, which is considerably high. High flow coefficient stages, with $\phi_{01} > 0.1$, have lower efficiencies because of the high velocities and high Mach numbers that occur particularly at the tip of the inducer (see Figure 3.15). Conversely, the flow coefficient of the high-pressure compressor at $\phi_{01} = 0.029$ is considerably too low, which causes lower efficiency because of narrow channels with small hydraulic diameters and proportionally more friction loss on the end-walls than the blades, leading to higher overall frictional losses. Instead, in the case with two shafts, the flow coefficients are both equal to 0.063, which is much closer to 0.07 (see Table 4).

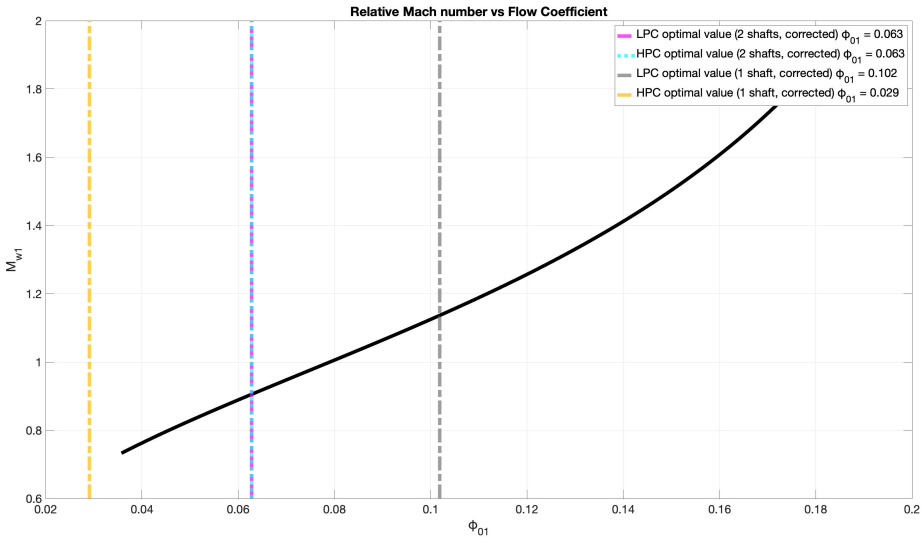

Figure 3.15: Relative Mach number versus global flow coefficient

Moreover, from Figure 3.12, it appears that, with two shafts, the tip speed is 448.02 m/s for the LPC and 496.78 m/s for the HPC, which makes using forged aluminum a viable option without incurring in structural problems instead of going for the more expensive titanium. When opting for a single shaft, while the HPC tip speed is only marginally affected, the LPC tip speed goes up to 514.37 m/s, which is at the upper boundary of the range that forged aluminum can endure and might require the use of titanium. For reference, the typical values for the maximum tip speeds based on the impeller material are reported here:

- Open impellers in cast aluminum: 200–300 m/s,
- Open impellers in forged aluminum: 450–560 m/s
- Open impellers in titanium alloys: 500–700 m/s
- Open impellers in steel: 350–500 m/s
- Shrouded impellers in steel: 280–340 m/s

4 Turbines

As it was done for compressors in the section 3, turbines' performance will be evaluated. Here are the initial parameters:

- Net power: $P_N = 143.059\,kW$
- High-pressure turbine inlet total temperature: $T_{04,HPT} = 1503\,K$
- Low-pressure turbine inlet total pressure: $P_{04,HPT} = 674.112\,kPa$
- Gas mass flow: $\dot{m}_t = 0.296\,kg/s$
- Low-pressure compressor power: $P_{c,LPC} = 44596\,W$
- High-pressure compressor power: $P_{c,HPC} = 53423\,W$
- High-pressure turbine shaft speed: $\omega_{HPT} = 15199\,rad/s = 145139\,rpm$
- Low-pressure turbine shaft speed: $\omega_{HPT} = 7718\,rad/s = 73701\,rpm$

where the shaft speeds are the same as the compressors'.
Firstly, let's see whether axial or radial turbines are better suited for the application; this can be evaluated by using the parameter called *flow capacity*, which is defined as

$$C = \frac{\dot{m}_t\sqrt{T_{01,HPT}}}{P_{01,HPT}} = 0.0170\frac{kg\sqrt{K}}{s\cdot kPa} \tag{4.0.1}$$

which is low enough to be suited for radial turbines[30].

	capacity $[\frac{kg\sqrt{K}}{s\cdot kPa}]$
Predominantly radial	< 0.05
radial or axial depending upon requirements	0.05–0.1
Predominantly axial	> 0.1

As mentioned in section 3.3.2, one must decide whether it is more appropriate to have the net power generated by only one turbine, by two of them, or if it is better to have it produced by a free turbine. This will be cleared in the following paragraphs.

4.1 Preliminary stage design

As for the compressors, the efficiency of each turbine is evaluated based on non-dimensional parameters. The difference here is that the specific speed will be used instead of the flow coefficient since this is the most available method in radial turbines' literature[3]. The definition of specific speed used here is the one given by Baljie:

$$\omega_s = \omega\frac{\sqrt{\frac{\dot{m}_t}{\rho_{06}}}}{(\Delta h_s^{ts})^{0.75}} \tag{4.1.1}$$

Where

- ω: rotational speed in rad/s
- ρ_{06}: rotor exit total density
- Δh_s^{ts}: enthalpy drop caused by the isentropic expansion from the stage inlet total conditions to the rotor exit static pressure P_6

The specific speed is linked to the total-to-static efficiency by the following equation:

$$\eta_s^{ts} = 0.87 - 1.07(\omega_s - 0.55)^2 - 0.5(\omega_s - 0.55)^3 \tag{4.1.2}$$

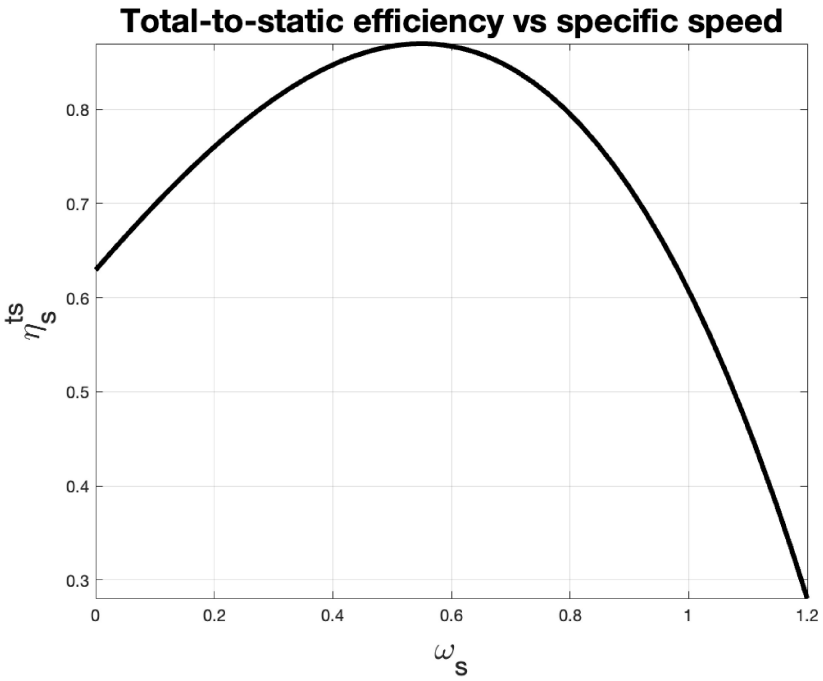

Figure 4.1: Total-to-static efficiency versus specific speed

As a general rule, the preferred range for specific speed is 0.45 to 0.75.
In many applications, the designer knows the static pressure at the exit P_6 from the beginning; since this is not the case here, an iterative method has been developed.
It starts by assuming a value for the specific speed, let's say $\omega_s = 0.6$. The corresponding total-to-static efficiency is found with equation 4.1.2.

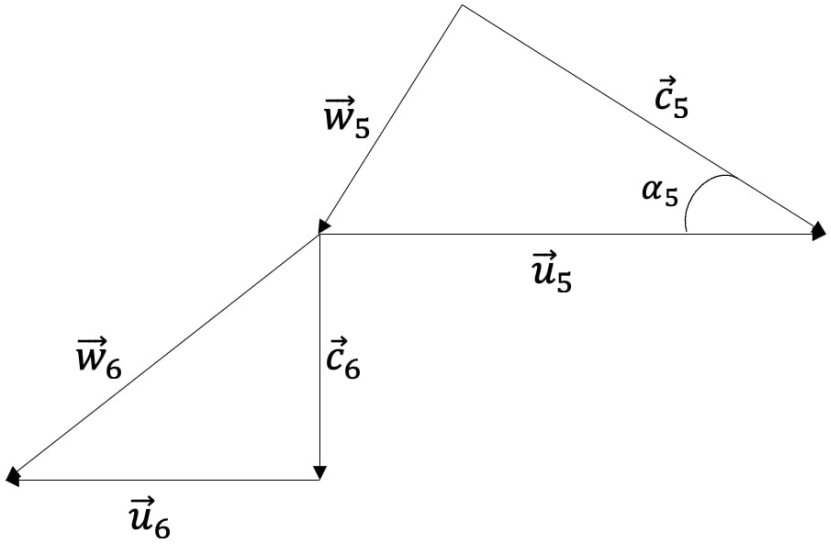

Figure 4.2: Velocity triangles in a radial inflow turbine

The ideal total-to-static enthalpy drop can be computed as

$$\Delta h_s^{ts} = \frac{\Delta h}{\eta_s^{ts}} \tag{4.1.3}$$

where Δh is the actual total-to-total enthalpy drop and is equal to

$$\Delta h = \frac{P_t}{\dot{m}_t} \tag{4.1.4}$$

where P_t is the total power generated by the turbine.
The ideal exit static temperature is then found as

$$T_{6s} = T_{04} - \frac{\Delta h_s^{ts}}{c_{p,t}} \tag{4.1.5}$$

and the exit static pressure is

$$P_6 = P_{04}\left(\frac{T_{6s}}{T_{04}}\right)^{\frac{\gamma_t}{\gamma_t - 1}} \tag{4.1.6}$$

where γ_t and $c_{p,t}$ are the isentropic exponent of the gas and the specific heat capacity, respectively. The rotor inlet absolute flow angle (see Figure 4.2) can

be approximated according to Rohlik as

$$\alpha_5 = 10.8 + 14.2\omega_s^2 \tag{4.1.7}$$

where α_5 is expressed in degrees.
Then, the optimum number of blades can be estimated as

$$Z = 12 + 0.03(33 - \alpha_5)^2 \tag{4.1.8}$$

The slip factor is defined as the ratio between the tangential component of the absolute velocity at the rotor inlet and the rotor tip speed:

$$\sigma = \frac{c_{u5}}{u_5} \tag{4.1.9}$$

The slip factor can be found, knowing the number of blades, through the Stanitz formula:

$$\sigma = 1 - \frac{0.63\pi}{Z} \tag{4.1.10}$$

Let's define the total-to-static velocity ratio as

$$\nu_s = \frac{c_{0s}}{u_5} \tag{4.1.11}$$

where c_{0s} is the discharge spouting velocity:

$$c_{0s} = \sqrt{2\Delta h_s^{ts}} \tag{4.1.12}$$

The total-to-static velocity ratio can be demonstrated to be equal to

$$\nu_s = \frac{1}{\sqrt{2}}\sqrt{\frac{\eta_s^{ts}}{\sigma}} \tag{4.1.13}$$

Once ν_s is computed, it is possible to compute the rotor tip speed,

$$u_5 = \nu_s\sqrt{2\Delta h_s^{ts}} \tag{4.1.14}$$

the rotor diameter,

$$D_5 = 2\frac{u_5}{\omega} \tag{4.1.15}$$

and, by using the definition of slip factor, the tangential component of the absolute velocity at the rotor inlet

$$c_{u5} = u_5\sigma \tag{4.1.16}$$

The meridional component of c_5 can be found by using the inlet absolute flow angle:

$$c_{m5} = c_{u5}\tan\alpha_5 \tag{4.1.17}$$

The exit total temperature is found as

$$T_{06} = T_{04} - \frac{\Delta h}{c_{p,t}} \tag{4.1.18}$$

and the static exit temperature is

$$T_6 = T_{06} - \frac{c_6^2}{2c_{p,t}} \tag{4.1.19}$$

in which, by assuming zero exit swirl, the exit absolute velocity is equal to its meridional component:

$$c_6 = c_{m6} \tag{4.1.20}$$

where c_{m6}, according to El-Sayed(2017)[25], can be approximated to be equal to the meridional velocity at the rotor inlet c_{m5}:

$$c_{m6} = c_{m5} \tag{4.1.21}$$

It is then possible to find the exit total pressure

$$P_{06} = P_6 \left(\frac{T_{06}}{T_6} \right)^{\frac{\gamma_t}{\gamma_t - 1}} \tag{4.1.22}$$

exit total density,

$$\rho_{06} = \frac{P_{06}}{R_t T_{06}} \tag{4.1.23}$$

exit Mach number,

$$M_6 = \frac{c_6}{\sqrt{\gamma_r R_t T_6}} \tag{4.1.24}$$

and exit static density

$$\rho_6 = \frac{P_6}{R_t T_6} \tag{4.1.25}$$

At this point, the new value of ω_s can be computed with equation 4.1.1. If it is not equal to the one assumed at the beginning, it is possible to iterate until convergence.
The exit hub diameter is set to be equal to

$$D_{h6} = 0.185 D_5 \tag{4.1.26}$$

and the tip diameter is found as

$$D_{t6} = 2\sqrt{\frac{A_6}{\pi} + \left(\frac{D_{h6}}{2} \right)^2} \tag{4.1.27}$$

where the exit area A_6 is equal to

$$A_6 = \frac{\dot{m}_t}{\rho_6 c_{m6}} \tag{4.1.28}$$

It is now possible to find the isentropic total-to-total efficiency as

$$\eta_s^{tt} = \frac{T_{04} - T_{06}}{T_{04} - T_{06s}} \tag{4.1.29}$$

where T_{06s} is the ideal exit total temperature and is equal to

$$T_{06s} = T_{04}\left(\frac{P_{06}}{P_{04}}\right)^{\frac{\gamma_t - 1}{\gamma_t}} \tag{4.1.30}$$

The specific diameter can also be computed:

$$D_s = D_5 \frac{(\Delta h_s^{ts})^{0.25}}{\sqrt{\frac{\dot{m}_t}{\rho_{06}}}} \tag{4.1.31}$$

and the degree of reaction is found as

$$R = \frac{h_5 - h_6}{\Delta h} \tag{4.1.32}$$

where h_5 and h_6 are the rotor inlet and rotor exit static enthalpy, respectively:

$$h_5 = c_{p,t}T_{05} - \frac{1}{2}(c_{m5}^2 + c_{u5}^2) \tag{4.1.33}$$

$$h_6 = c_{p,t}T_{06} - \frac{1}{2}c_6^2 \tag{4.1.34}$$

in which the rotor inlet total temperature can be assumed to be equal to T_{04}:

$$T_{05} = T_{04} \tag{4.1.35}$$

4.2 Turbines setup

4.2.1 Two turbines

The first option is to use two radial turbines. In this case, it is possible to either use a single generator and have only one of them produce the net power (and the other is just for running the respective compressor) or two generators so that both turbines contribute to the production of the net power (See Figures 3.5, 3.6, and 3.7).
Let's define the parameter $\xi \in [0, 1]$ as the ratio between the net power generated by the high-pressure turbine and the total net power:

$$\xi = \frac{P_{N,HPT}}{P_N} \tag{4.2.1}$$

Hence, the total power produced by each turbine is:

- HPT: $P_{t,HPT} = P_{c,HPC} + \xi P_N$
- LPT: $P_{t,LPT} = P_{c,LPC} + (1 - \xi)P_N$

The inlet conditions of the high-pressure turbine and the net power are known from the thermodynamic cycle analysis, while the shaft speeds and the power consumed by each compressor are known from the compressors analysis of the previous chapter. It is, therefore, possible to apply the procedure in section 4.1 at first to the high-pressure turbine, and then use its exit conditions to apply the same procedure to the low-pressure turbine.

4.2.2 Free turbine

In this case, all of the net power is produced by a third radial turbine that is not running any compressor (hence the name *free turbine*)(see Figure 3.8). The other two are just used to run their respective compressor. The procedure in section 4.1 is still valid for each stage and the rotational speed of the free turbine is chosen to maximize its total-to-total isentropic efficiency.

4.2.3 Results

The different setups are compared based on their combined total-to-total efficiency.
With two turbines, the combined total-to-total isentropic efficiency is defined as

$$\eta^{tt}_{s,combined} = \frac{T_{04,HPT} - T_{06,LPT}}{T_{04,HPT} - T_{06ss,LPT}} \tag{4.2.2}$$

where $T_{06ss,LPT}$ is the ideal exit total temperature of the low-pressure turbine assuming isentropic expansion through both turbines:

$$T_{06ss,LPT} = T_{06s,HPT}\left(\frac{P_{06,LPT}}{P_{06,HPT}}\right)^{\frac{\gamma_t - 1}{\gamma_t}} \tag{4.2.3}$$

With a free turbine, the combined total-to-total efficiency is

$$\eta^{tt}_{s,combined} = \frac{T_{04,HPT} - T_{06,free}}{T_{04,HPT} - T_{06sss,free}} \tag{4.2.4}$$

where $T_{06sss,free}$ is the ideal exit total temperature of the free turbine assuming isentropic expansion through all turbines:

$$T_{06sss,free} = T_{06ss,LPT}\left(\frac{P_{06,free}}{P_{06,LPT}}\right)^{\frac{\gamma_t - 1}{\gamma_t}} \tag{4.2.5}$$

The results are as follows.

Mass flow $\dot{m}_t$	0.296 kg/s
Net Power P_N	143.059 kW
High-pressure Turbine	
Polytropic efficiency η_p	0.882
Isentropic efficiency (total-to-total) η_s^{tt}	0.895
Isentropic efficiency (total-to-static) η_s^{ts}	0.868
Specific speed ω_s	0.590
Specific diameter D_s	3.321
Inlet total temperature T_{04}	1503 K
Inlet total pressure P_{04}	674112.283 Pa
Exit total temperature T_{06}	1194.833 K
Exit total pressure P_{06}	196814.978 Pa
Expansion ratio $\frac{P_{06}}{P_{04}}$	0.292
Power P_t	130011 W
Temperature drop ΔT	308.167 K
Rotational speed ω	15199 rad/s 145139 rpm
Degree of reaction r	0.547
% of P_N	53.54 %
Low-pressure Turbine	
Polytropic efficiency η_p	0.881
Isentropic efficiency (total-to-total) η_s^{tt}	0.896
Isentropic efficiency (total-to-static) η_s^{ts}	0.869
Specific speed ω_s	0.581
Specific diameter D_s	3.371
Inlet total temperature T_{04}	1194.833 K
Inlet total pressure P_{04}	196814.978 Pa
Exit total temperature T_{06}	931.566 K
Exit total pressure P_{06}	51687.201 Pa
Expansion ratio $\frac{P_{06}}{P_{04}}$	0.263
Power P_t	111068 W
Temperature drop ΔT	263.267 K
Rotational speed ω	7718 rad/s 73701 rpm
Degree of reaction r	0.547
% of P_N	46.46%
Combined isentropic efficiency	0.908

Table 5: Results with maximum combined isentropic efficiency with two generators

Mass flow $\dot{m}_t$	0.296 kg/s
Net Power P_N	143.059 kW
High-pressure Turbine	
Polytropic efficiency η_p	0.872
Isentropic efficiency (total-to-total) η_s^{tt}	0.894
Isentropic efficiency (total-to-static) η_s^{ts}	0.868
Specific speed ω_s	0.596
Specific diameter D_s	3.288
Inlet total temperature T_{04}	1503 K
Inlet total pressure P_{04}	674112.283 Pa
Exit total temperature T_{06}	1037.273 K
Exit total pressure P_{06}	90019.742 Pa
Expansion ratio $\frac{P_{06}}{P_{04}}$	0.134
Power P_t	196483 W
Temperature drop ΔT	465.727 K
Rotational speed ω	15199 rad/s 145139 rpm
Degree of reaction r	0.547
% of P_N	100 %
Low-pressure Turbine	
Polytropic efficiency η_p	0.617
Isentropic efficiency (total-to-total) η_s^{tt}	0.638
Isentropic efficiency (total-to-static) η_s^{ts}	0.604
Specific speed ω_s	1.003
Specific diameter D_s	1.673
Inlet total temperature T_{04}	1037.273 K
Inlet total pressure P_{04}	90019.742 Pa
Exit total temperature T_{06}	931.566 K
Exit total pressure P_{06}	39478.878 Pa
Expansion ratio $\frac{P_{06}}{P_{04}}$	0.439
Power P_t	44596 W
Temperature drop ΔT	105.707 K
Rotational speed ω	7718 rad/s 73701 rpm
Degree of reaction r	0.571
% of P_N	0 %
Combined isentropic efficiency	0.843

Table 6: Results with the generator run by the HPT

Mass flow $\dot{m}_t$	0.296 kg/s
Net Power P_N	143.059 kW
High-pressure Turbine	
Polytropic efficiency η_p	0.824
Isentropic efficiency (total-to-total) η_s^{tt}	0.832
Isentropic efficiency (total-to-static) η_s^{ts}	0.794
Specific speed ω_s	0.802
Specific diameter D_s	2.362
Inlet total temperature T_{04}	1503 K
Inlet total pressure P_{04}	674112.283 Pa
Exit total temperature T_{06}	1376.369 K
Exit total pressure P_{06}	406544.883 Pa
Expansion ratio $\frac{P_{06}}{P_{04}}$	0.603
Power P_t	53423 W
Temperature drop ΔT	126.631 K
Rotational speed ω	15199 rad/s 145139 rpm
Degree of reaction r	0.558
% of P_N	0 %
Low-pressure Turbine	
Polytropic efficiency η_p	0.839
Isentropic efficiency (total-to-total) η_s^{tt}	0.869
Isentropic efficiency (total-to-static) η_s^{ts}	0.851
Specific speed ω_s	0.414
Specific diameter D_s	4.657
Inlet total temperature T_{04}	1376.369 K
Inlet total pressure P_{04}	406544.883 Pa
Exit total temperature T_{06}	931.566 K
Exit total pressure P_{06}	44954.540 Pa
Expansion ratio $\frac{P_{06}}{P_{04}}$	0.111
Power P_t	187655 W
Temperature drop ΔT	444.803 K
Rotational speed ω	7718 rad/s 73701 rpm
Degree of reaction r	0.542
% of P_N	100 %
Combined isentropic efficiency	0.873

Table 7: Results with the generator run by the LPT

Mass flow $\dot{m}_t$	0.296 kg/s
Net Power P_N	143.059 kW
High-pressure Turbine	
Polytropic efficiency η_p	0.824
Isentropic efficiency (total-to-total) η_s^{tt}	0.832
Isentropic efficiency (total-to-static) η_s^{ts}	0.794
Specific speed ω_s	0.802
Specific diameter D_s	2.362
Inlet total temperature T_{04}	1503 K
Inlet total pressure P_{04}	674112.283 Pa
Exit total temperature T_{06}	1376.369 K
Exit total pressure P_{06}	406544.883 Pa
Expansion ratio $\frac{P_{06}}{P_{04}}$	0.603
Power P_t	53423 W
Temperature drop ΔT	126.631 K
Rotational speed ω	15199 rad/s 145139 rpm
Degree of reaction r	0.558
% of P_N	0 %
Low-pressure Turbine	
Polytropic efficiency η_p	0.892
Isentropic efficiency (total-to-total) η_s^{tt}	0.896
Isentropic efficiency (total-to-static) η_s^{ts}	0.868
Specific speed ω_s	0.592
Specific diameter D_s	3.306
Inlet total temperature T_{04}	1376.369 K
Inlet total pressure P_{04}	406544.883 Pa
Exit total temperature T_{06}	1270.662 K
Exit total pressure P_{06}	265971.063 Pa
Expansion ratio $\frac{P_{06}}{P_{04}}$	0.654
Power P_t	44596 W
Temperature drop ΔT	105.707 K
Rotational speed ω	7718 rad/s 73701 rpm
Degree of reaction r	0.547
% of P_N	0 %

Free Turbine	
Polytropic efficiency η_p	0.877
Isentropic efficiency (total-to-total) η_s^{tt}	0.895
Isentropic efficiency (total-to-static) η_s^{ts}	0.869
Specific speed ω_s	0.575
Specific diameter D_s	3.408
Inlet total temperature T_{04}	1270.662 K
Inlet total pressure P_{04}	265971.063 Pa
Exit total temperature T_{06}	931.566 K
Exit total pressure P_{06}	49788.975 Pa
Expansion ratio $\frac{P_{06}}{P_{04}}$	0.187
Power P_t	143059 W
Temperature drop ΔT	339.096 K
Rotational speed ω	9057 rad/s 86489 rpm
Degree of reaction r	0.547
% of P_N	100 %
Combined isentropic efficiency	0.898

Table 8: Results with maximum combined isentropic efficiency with free turbine

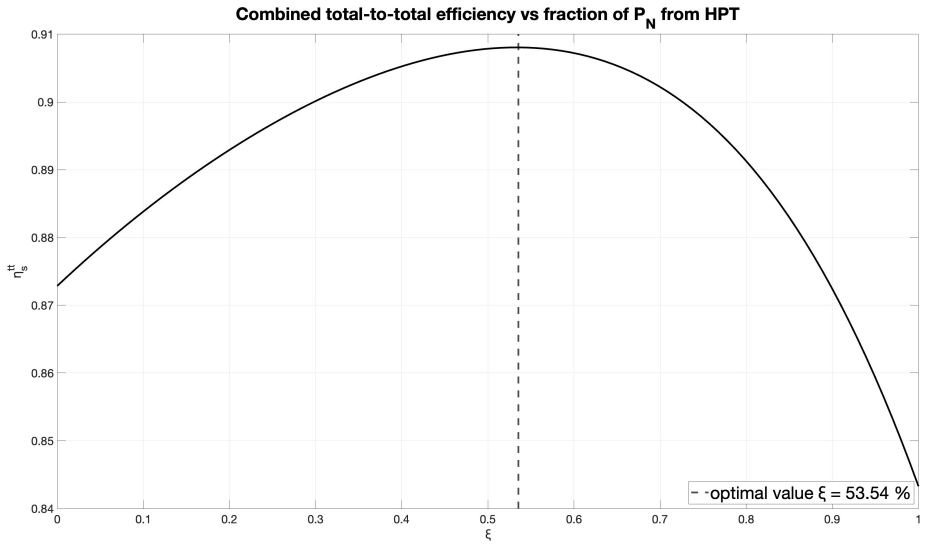

Figure 4.3: Combined total-to-total isentropic efficiency versus the fraction of P_N from HPT

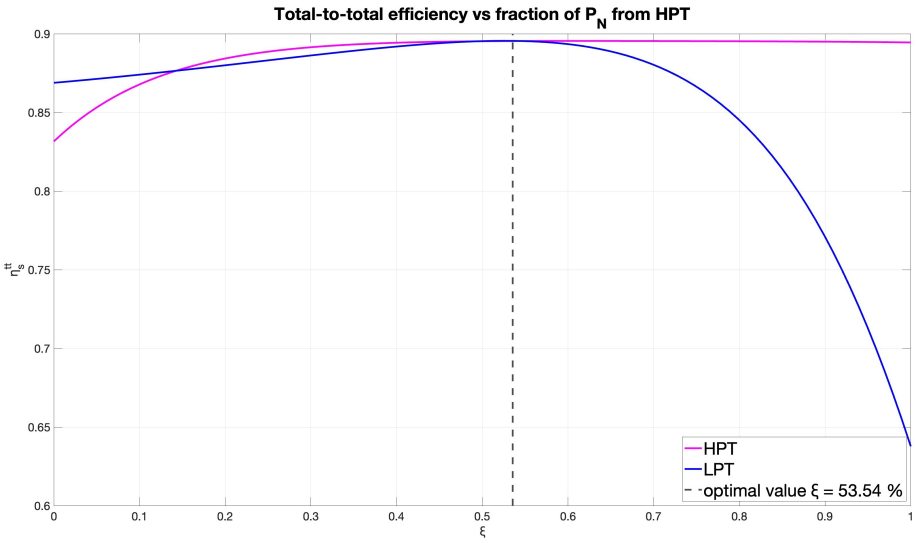

Figure 4.4: Total-to-total isentropic efficiency versus the fraction of P_N from HPT

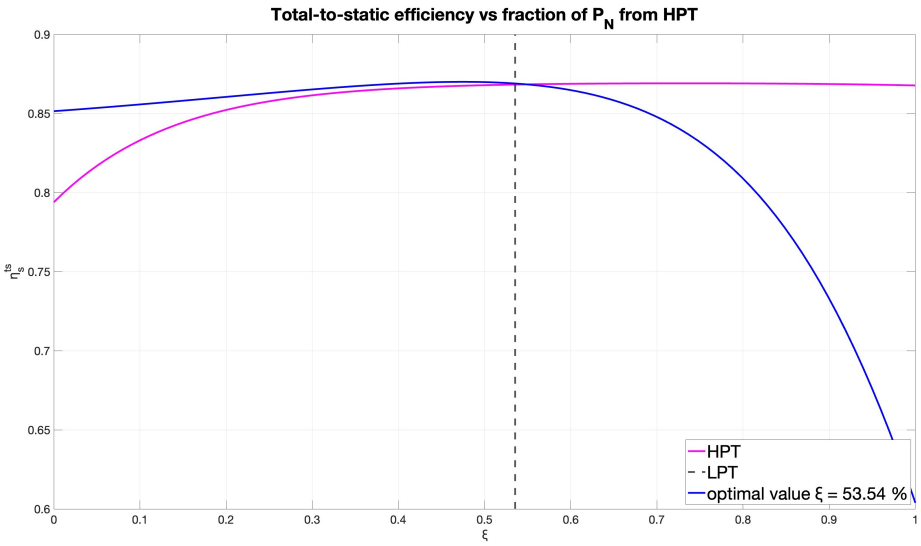

Figure 4.5: Total-to-static isentropic efficiency versus the fraction of P_N from HPT

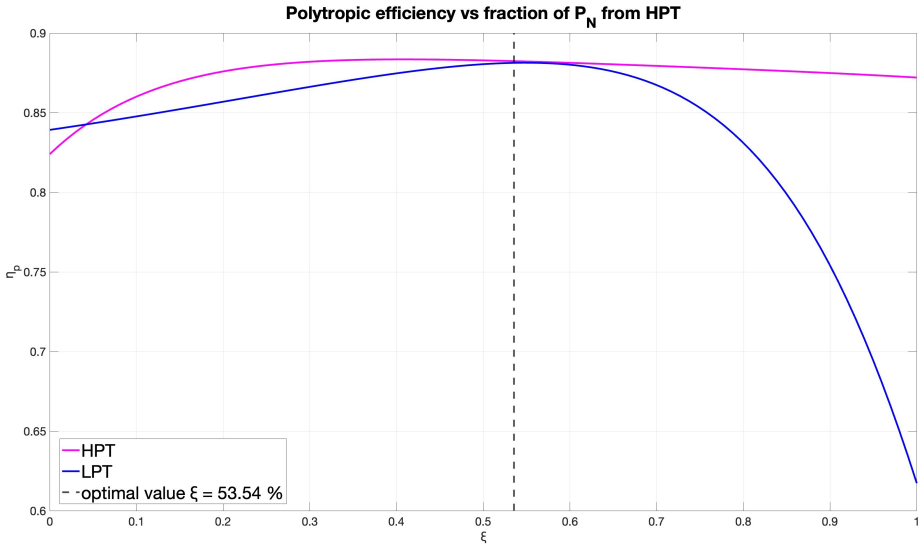

Figure 4.6: Polytropic efficiency versus the fraction of P_N from HPT

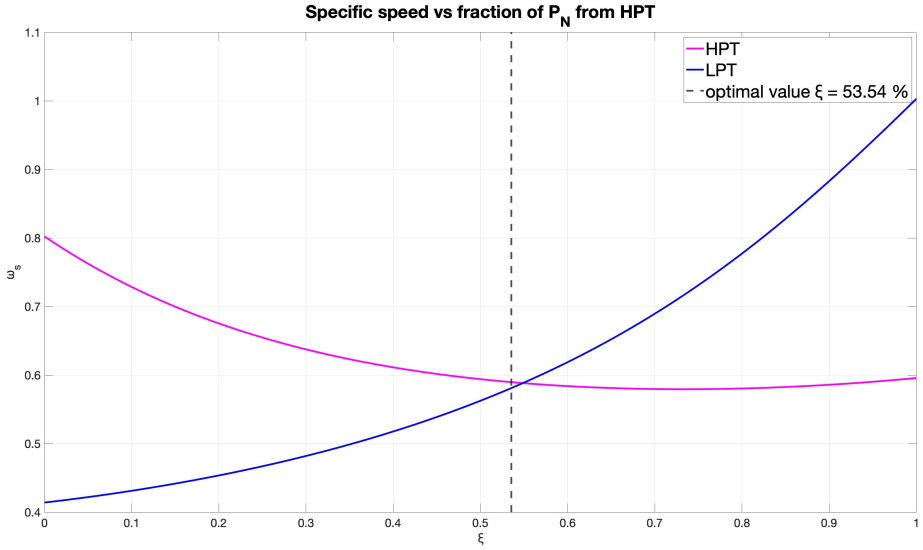

Figure 4.7: Specific speed versus the fraction of P_N from HPT

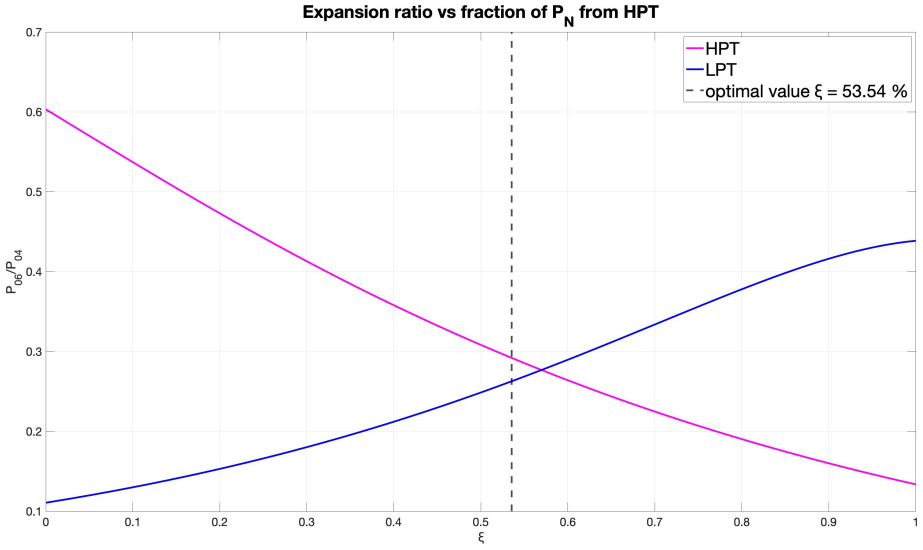

Figure 4.8: Expansion ratio versus the fraction of P_N from HPT

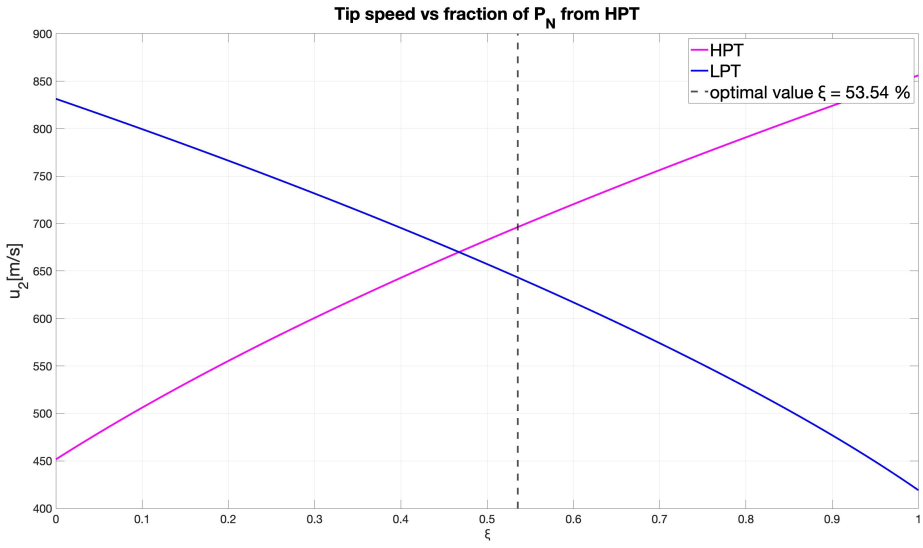

Figure 4.9: Tip speed versus the fraction of P_N from HPT

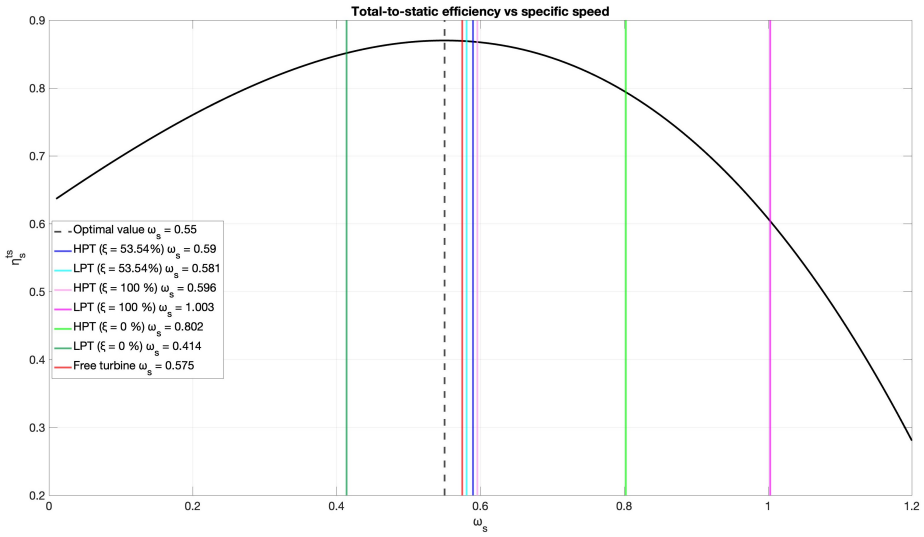

Figure 4.10: Total-to-static efficiency versus specific speed for all cases

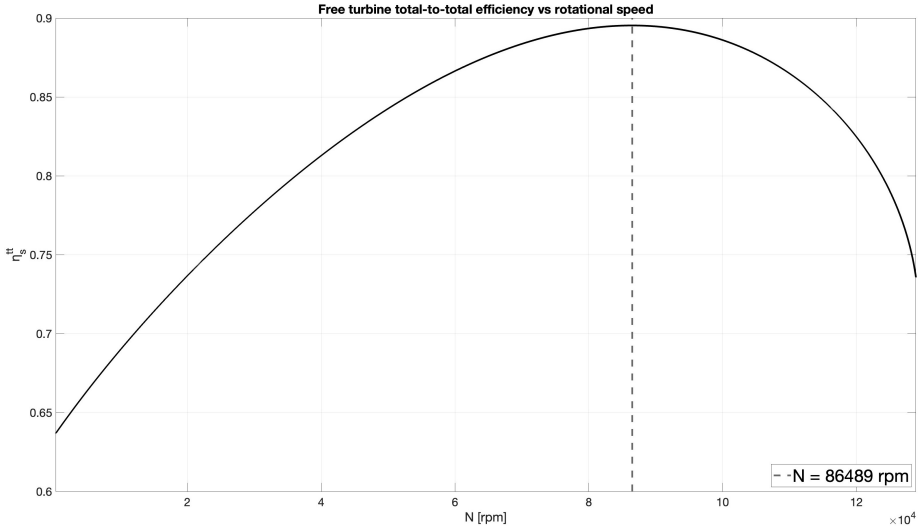

Figure 4.11: Total-to-total efficiency versus shaft speed [Free turbine]

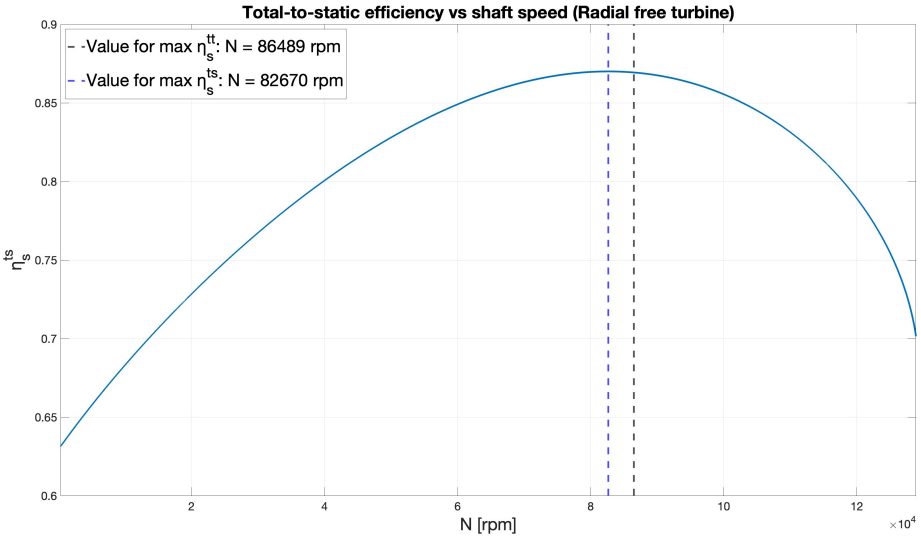

Figure 4.12: Total-to-static efficiency versus shaft speed [Free turbine]

By comparing Tables 5, 6, 7 and 8, and Figure 4.3, it appears that the best option in terms of combined efficiency is to use two generators, specifically with $\xi = 53.54\%$.
When looking at Figures 4.4, 4.5 and 4.6, each turbine functions the worst when it is doing the least amount of work: the worst efficiency for the LPT is obtained when all of the net power is generated by the HPT and vice versa. It should be noted that, for the low-pressure turbine, by varying ξ, its inlet conditions also change, which is not the case for the other turbine. That is why it shows more drastic variations of efficiency with ξ (see Figures 4.4, 4.5, and 4.6).
It is also noticeable how, in Figure 4.7, the optimum point is close to where the specific speeds are equal. This is reasonable since the maximum total-to-static efficiency, from equation 4.1.2, only depends on specific speed (Note: this is an approximation for preliminary design purposes, the reality is more complex than this). In this case, since the optimization was done for the total-to-total efficiency, the two values of specific speed are close but not equal.
In Figure 4.10, the same graph of Figure 4.1 is presented but with the specific speeds of each turbine in each configuration highlighted. It is clear that when having two generators with $\xi = 53.54\%$, both specific speeds are closer to the optimal one than in every other case.
Another advantage of opting for sharing the net power between the two turbines is that, since the work is shared, neither turbine reaches extremely high tip speeds. From Figure 4.9, it is seen that if a single generator were employed, the tip speed would reach over 800 m/s for the turbine that is providing the net power. Especially with small radial turbines that do not have a cooling system, the tip speed must be kept reasonably low to avoid structural problems.
For the same reason stated for the specific speed, the tip speeds of the two

turbines are close to each other at the optimum point.
Finally, another advantage of having two generators is being able to use them to start each turbine independently.
All that being said, the setup with two generators is the one chosen here.

4.2.4 Evaluating Rotor Design

Let's compare the rotor sizing results obtained for the setup with two generators and $\xi = 53.54\%$ with some guidelines provided by the literature.
Baljie[68] recommends the following limits for the meridional velocity at the exit and the tip radius:

$$0.2 \leq \frac{c_{m6}}{u_5} \leq 0.4 \tag{4.2.6}$$

$$\frac{D_{t6}}{D_5} \leq 0.78 \tag{4.2.7}$$

Wood[95] recommends limiting the ratio of meridional velocities by

$$1 \leq \frac{C_{m6}}{C_{m5}} \leq 1.5 \tag{4.2.8}$$

The degree of reaction should preferably belong to the range

$$0.45 \leq R \leq 0.65 \tag{4.2.9}$$

The obtained results are shown in Table 9.

	High-pressure Turbine	**Low-pressure Turbine**
$\frac{c_{m6}}{c_{u_5}}$	0.255	0.253
$\frac{D_{t6}}{D_5}$	0.716	0.710
$\frac{c_{m6}}{c_{m5}}$	1	1
R	0.547	0.547

Table 9: Rotor design evaluation

From Table 9, it is seen that all parameters fall into the preferred ranges, as expected.

4.3 Insertion in the thermodynamic cycle

As will be elaborated upon in section 5, the thermodynamic cycle needs to be updated to ensure that the requirement to produce 100 kW of thrust power is met.
In section 4, the net power was assumed as an initial parameter; however, the net power generated is not known before the completion of the thermodynamic cycle, which means after the turbines analysis.

What is known, from the initial parameters, is the fraction of pressure drop that is done by the exit nozzle instead of the turbines, which is defined as

$$\delta p_n = \frac{P_{06,LPT} - P_a}{P_{04,HPT} - P_a} \tag{4.3.1}$$

and is equal to

$$\delta p_n = 0.006$$

It is possible to use an iterative method to find the turbines' performance without knowing the net power and it works as follows:

1. Input parameters:
   - Power consumed by each compressor (from the compressors' analysis): $P_{c,HPC}$ and $P_{c,LPC}$
   - Shaft speeds (from the compressors' analysis): $\omega_{HPT} = \omega_{HPC}$ and $\omega_{LPT} = \omega_{LPC}$
   - High-pressure turbine inlet total temperature: $T_{04,HPT} = 1503\,K$
   - High-pressure turbine inlet total pressure: $P_{04,HPT}$
   - Gas mass flow: $\dot{m}_t$
   - Flight altitude: $h = 5000\,m$
   - Fraction of pressure drop done by the exit nozzle: $\delta p_n = 0.006$
2. A value of the fraction ξ of net power generated by the HPT is assumed (and the procedure is repeated for every value of $\xi \in [0, 1]$ to find the one that maximizes the combined total-to-total efficiency; to save on computational cost, it is possible to restrict the range in $\approx [0.48, 0.56]$)
3. A value of the combined total-to-total efficiency as defined by equation 4.2.2 is assumed (for example, $\eta^{tt}_{s,combined} = 0.8$)
4. A first estimate of the LPT exit temperature values is:
   - Ideal exit total temperature:

$$T_{06s,LPT} = T_{04,HPT}\left(\frac{P_{06,LPT}}{P_{04,HPT}}\right)^{\frac{\gamma_t - 1}{\gamma_t}}$$

   - Exit total temperature:

$$T_{06,LPT} = T_{04,HPT} - \eta^{tt}_{s,combined}(T_{04,HPT} - T_{06s,LPT})$$

5. The LPT exit total pressure is found as

$$P_{06,LPT} = P_{04,HPT} - (P_{04,HPT} - P_a)(1 - \delta p_n)$$

6. The net power can be computed as

$$P_N = \dot{m}_t c_{p,t}(T_{04,HPT} - T_{06,LPT}) - (P_{c,HPC} + P_{c,LPC})$$

7. And the total power generated by each turbine is

   - HPT: $P_{t,HPT} = P_{c,HPC} + \xi P_N$
   - LPT: $P_{t,LPT} = P_{c,LPC} + (1 - \xi)P_N$

8. The procedure at section 4.1 is applied to the HPT to find

   - HPT exit total temperature: $T_{06,HPT}$
   - HPT exit total pressure: $P_{06,HPT}$
   - HPT ideal exit total temperature: $T_{06s,HPT}$

9. The HPT exit values are used as input to apply the procedure at section 4.1 to the LPT and find

   - LPT exit total temperature: $T_{06,LPT}$
   - LPT exit total pressure: $P_{06,LPT}$

10. The LPT ideal exit total temperature, assuming isentropic expansion through both turbines, is

$$T_{06ss,LPT} = T_{06s,HPT}\left(\frac{P_{06,LPT}}{P_{06,HPT}}\right)^{\frac{\gamma_t - 1}{\gamma_t}}$$

11. Finally, the new value of $\eta^{tt}_{s,combined}$ is found as

$$\eta_{s,combined} = \frac{T_{04,HPT} - T_{06,LPT}}{T_{04,HPT} - T_{06ss,LPT}}$$

12. If the value is not equal to the one assumed at step 3, iterate until convergence.

5 Updated thermodynamic cycle

The thermodynamic cycle can be updated to include what was done in sections 3 and 4 and to meet the requirement to produce 100 kW of thrust power.
The air mass flow to get the required thrust power is dependent on the net power (see section 5.0.1). From the last two chapters, it can be seen that compressors and turbines efficiencies are dependent on the mass flow; on the other hand, the net power is dependent on the efficiencies, meaning that the mass flow necessary to reach the required thrust power is dependent on compressors and turbines efficiencies. Hence, an iterative method must be employed to take everything into consideration and, for each value of the pressure ratio π_c, it goes as follows:

1. Initial parameters:
   - LPC inlet total temperature: $T_{01,LPC} = 259.48\,K$
   - LPC inlet total pressure: $P_{01,LPC} = 56.82\,kPa$
   - HPT inlet total temperature. $T_{04,HPT} = 1503\,K$
   - Intercooler efficiency: $\varepsilon_{ic} = 0.6$
   - Pressure drop across the intercooler: $\delta p_{ic} = 0.03$
   - Combustion efficiency: $\nu_c = 0.98$
   - Pressure drop across the combustion chamber: $f_c = 0.98$
   - Recuperator efficiency: $\varepsilon_{rc} = 0.9$
   - Pressure drop across the recuperator: $\delta p_{rc} = 0.04$
   - Nozzle efficiency: $\eta_n = 0.98$
2. An initial value of the mass flow is assumed
3. Apply the procedure described in section 3.2 to the low-pressure compressor to obtain
   - LPC exit total temperature: $T_{03,LPC}$
   - LPC exit total pressure: $P_{03,LPC}$
   - LPC polytropic efficiency: $\eta_{p,LPC}$
   - LPC isentropic efficiency: $\eta_{s,LPC}$
   - LPC power: $P_{c,LPC}$
   - LPC shaft speed: ω_{LPC}

   An iterative method is used to find the flow coefficient that maximizes the polytropic efficiency
4. Use the LPC exit values as input for the intercooler to find the HPC inlet values:
   - HPC inlet total temperature:

$$T_{01,HPC} = T_{03,LPC} - \varepsilon_{ic}(T_{03,LPC} - T_a)$$

- HPC inlet total pressure:

$$P_{01,HPC} = P_{03,LPC}(1 - \delta p_{ic})$$

5. Apply the procedure described in section 3.2 to the high-pressure compressor to obtain

   - HPC exit total temperature: $T_{03,HPC}$
   - HPC exit total pressure: $P_{03,HPC}$
   - HPC polytropic efficiency: $\eta_{p,HPC}$
   - HPC isentropic efficiency: $\eta_{s,HPC}$
   - HPC power: $P_{c,HPC}$
   - HPC shaft speed: ω_{HPC}

   An iterative method is used to find the flow coefficient that maximizes the polytropic efficiency

6. Use the HPC exit values as input for the combustion chamber to find:

   - HPT inlet total pressure:

$$P_{04,HPT} = f_c P_{03,LPC}$$

   - hot gas mass flow:

$$\dot{m}_t = \dot{m}(1 + f)$$

   where

$$f = \frac{c_{p,t} T_{04,HPT} - c_p T_{03,LPC}}{\nu_{comb} H_u - c_{p,t} T_{04,HPT}}$$

7. Use the procedure at section 4.3 to find:

   - LPT exit total temperature: $T_{06,LPT}$
   - LPT exit total pressure: $P_{06,LPT}$

8. If $T_{06,LPT} > T_{03,HPC}$, find the exit values after the recuperator:

   - recuperator exit total temperature:

$$T_{03,rc} = T_{03,HPC} - \varepsilon_{rc}(T_{03,HPC} - T_{06,LPT})$$

   - recuperator exit total pressure:

$$P_{03,rc} = (1 - \delta p_{rc}) P_{03,HPC}$$

9. Use the recuperator's exit values as input for the combustion chamber to find:

   - HPT inlet total pressure: $P_{04,HPT} = f_c P_{03,rc}$

- hot gas mass flow:

$$\dot{m}_t = \dot{m}(1+f)$$

where

$$f = \frac{c_{p,t}T_{04,HPT} - c_p T_{03,rc}}{\nu_c H_u - c_{p,t}T_{04,HPT}}$$

10. Repeat step 7 (Note: The exit temperature $T_{06,LPT}$ may not be exactly equal to the one found before at step 7, iterate from step 8 to 10 for convergence)

11. Compute the net power as:

$$P_N = \dot{m}_t c_{p,t}(T_{04,HPT} - T_{06,LPT}) - (P_{c,LPC} + P_{c,HPC})$$

12. Find the nozzle exit speed as:

$$V_{exit} = \sqrt{2c_{p,t}(T_{06,LPT} - T_7)}$$

where

- Nozzle exit ideal static temperature:

$$T_{7s} = T_{06,LPT}\left(\frac{P_a}{P_{06,LPT}}\right)^{\frac{\gamma_t - 1}{\gamma_t}}$$

- Nozzle exit static temperature:

$$T_7 = T_{06,LPT} - \eta_n(T_{06,LPT} - T_{7s})$$

13. Find the new value of the mass flow with the procedure in section 5.0.1

14. If the new value of the mass flow is different from the one assumed at the beginning, iterate until convergence.

5.0.1 Air mass flow

Fulfilling the requirement of reaching 100 kW of thrust power depends on the value of the engine air mass flow. For this paragraph, let's call $\dot{m}$ the mass flow assumed at step 2, and $\dot{m}'$ the mass flow for which, with the compressors and turbines efficiencies of the current iteration, the thrust power is the required one.
The total thrust is the sum of the contributions from the fans and the nozzle

$$Thrust = n_{fan}Thrust_{fan} + Thrust_{nozzle} \tag{5.0.1}$$

and, as derived from the requirements, is equal to 1147 N.
The contribution from the nozzle is equal to

$$Thrust_{nozzle} = \dot{m}'\left[(1+f)V_{exit} - V_{cruise}\right] \tag{5.0.2}$$

Where V_{exit} is found at step 12.
When it comes to the fans, their performance is evaluated according to actuator disk theory. It is important to remember that the procedure changes depending on whether or not the fans are ducted. The reference plane chosen here does have ducted fans; however, to not lose generality, both the cases with ducted and unducted fans are examined[10].

Unducted fans

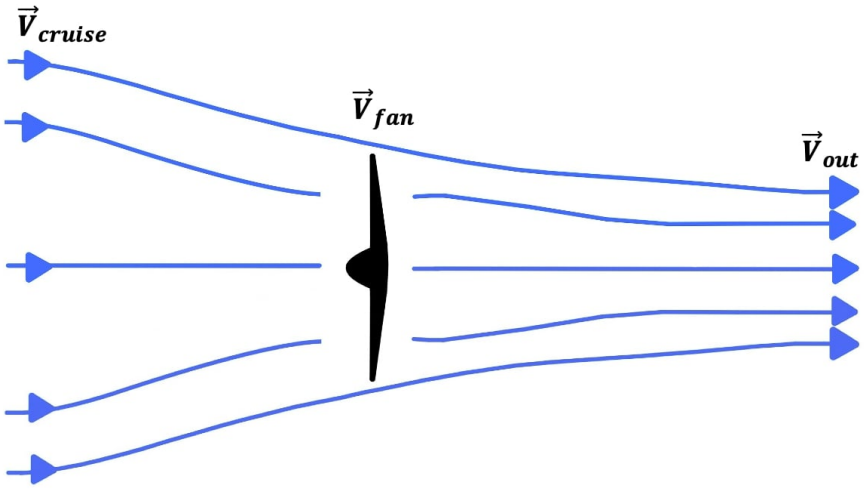

Figure 5.1: Scheme for an unducted fan

The thrust generated by a single fan is equal to

$$Thrust_{fan} = \dot{m}_{fan}(V_{out} - V_{cruise}) \tag{5.0.3}$$

where

$$\dot{m}_{fan} = \rho_a A_{fan} V_{fan} \tag{5.0.4}$$

and

$$A_{fan} = \frac{\pi}{4} d_{fan}^2 = 0.4465 m^2 \tag{5.0.5}$$

and ρ_a is the external air density.
By combining equations 5.0.1, 5.0.2, 5.0.3 and 5.0.4, the total thrust can be written as

$$Thrust = n_{fan}\rho_a A_{fan} V_{fan}(V_{out} - V_{cruise}) + \dot{m}' \left[(1+f)V_{exit} - V_{cruise}\right] \tag{5.0.6}$$

The power imparted to the air by a single fan, given the net power found at the current iteration, can be found as

$$P_{fan} = \eta_{fan} \frac{P_N}{n_{fan}} \tag{5.0.7}$$

where P_N is found at step 11.
Since the net power P_N is directly proportional to the air mass flow passing through the engine and P_{fan} is directly proportional to P_N (see equation 5.0.7), P_{fan} is directly proportional to the air mass flow passing through the engine. Therefore, the power imparted to the airflow by a single fan to reach the required thrust power is

$$P_{fan} \frac{\dot{m}'}{\dot{m}}$$

which is equal to the change in kinetic energy of the flow as it passes through the fan

$$P_{fan} \frac{\dot{m}'}{\dot{m}} = \frac{1}{2} \dot{m}' (V_{out}^2 - V_{cruise}^2) = \dot{m}' \frac{V_{out} + V_{cruise}}{2} (V_{out} - V_{cruise}) \tag{5.0.8}$$

thus, from equation 5.0.8, the velocity at the fan is shown to be equal to

$$V_{fan} = \frac{V_{out} + V_{cruise}}{2} \tag{5.0.9}$$

By combining equations 5.0.8, 5.0.9 and 5.0.4, the following equation is obtained:

$$P_{fan} \frac{\dot{m}'}{\dot{m}} = 2 A_{fan} \rho_a V_{fan}^2 (V_{fan} - V_{cruise}) \tag{5.0.10}$$

Hence, equations 5.0.6, 5.0.9, and 5.0.10 form a system of three equations with three unknowns, which are V_{fan}, V_{out}, and most importantly, $\dot{m}'$.

$$\begin{cases} Thrust = n_{fan} \rho_a A_{fan} V_{fan} (V_{out} - V_{cruise}) + \dot{m}' \left[(1+f) V_{exit} - V_{cruise} \right] \\ V_{fan} = \frac{V_{out} + V_{cruise}}{2} \\ P_{fan} \frac{\dot{m}'}{\dot{m}} = 2 A_{fan} \rho_a V_{fan}^2 (V_{fan} - V_{cruise}) \end{cases} \tag{5.0.11}$$

By solving the system, $\dot{m}'$ can be found.

Ducted fans

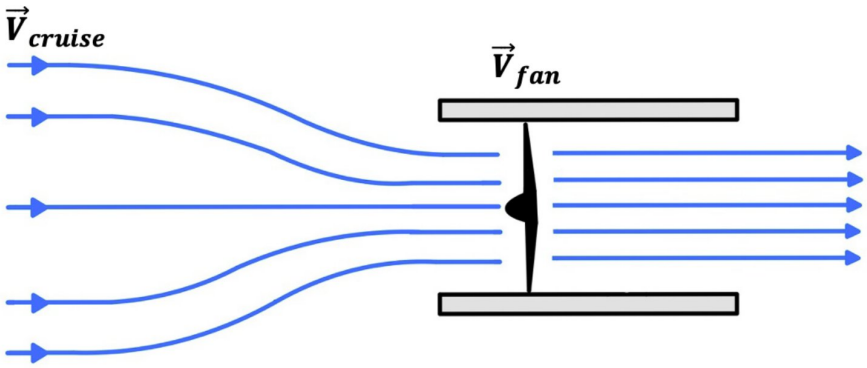

Figure 5.2: Scheme for a ducted fan

The procedure is analogous to the one for unducted fans; the difference is that

$$V_{out} = V_{fan}$$

hence, equation 5.0.6 becomes

$$Thrust = n_{fan}\rho_a A_{fan} V_{fan}(V_{fan} - V_{cruise}) + \dot{m}'\left[(1+f)V_{exit} - V_{cruise}\right] \tag{5.0.12}$$

and, from equation 5.0.8

$$P_{fan}\frac{\dot{m}'}{\dot{m}} = \frac{1}{2}A_{fan}\rho_a V_{fan}(V_{fan}^2 - V_{cruise}^2) \tag{5.0.13}$$

Since $V_{out} = V_{fan}$, there are only two unknown variables; therefore, the system of equations composed of equation 5.0.12 and equation 5.0.13 can be solved for the unknowns $\dot{m}'$ and V_{fan}.

$$\begin{cases} Thrust = n_{fan}\rho_a A_{fan} V_{fan}(V_{fan} - V_{cruise}) + \dot{m}'\left[(1+f)V_{exit} - V_{cruise}\right] \\ P_{fan}\frac{\dot{m}'}{\dot{m}} = \frac{1}{2}A_{fan}\rho_a V_{fan}(V_{fan}^2 - V_{cruise}^2) \end{cases} \tag{5.0.14}$$

5.1 Final results

The final results are shown here.

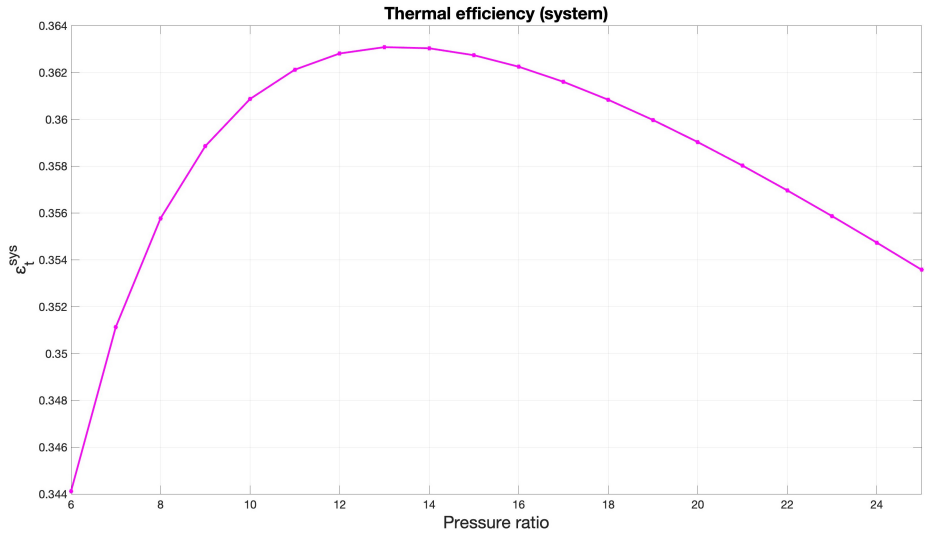

Figure 5.3: Thermal efficiency (of the whole system) versus pressure ratio

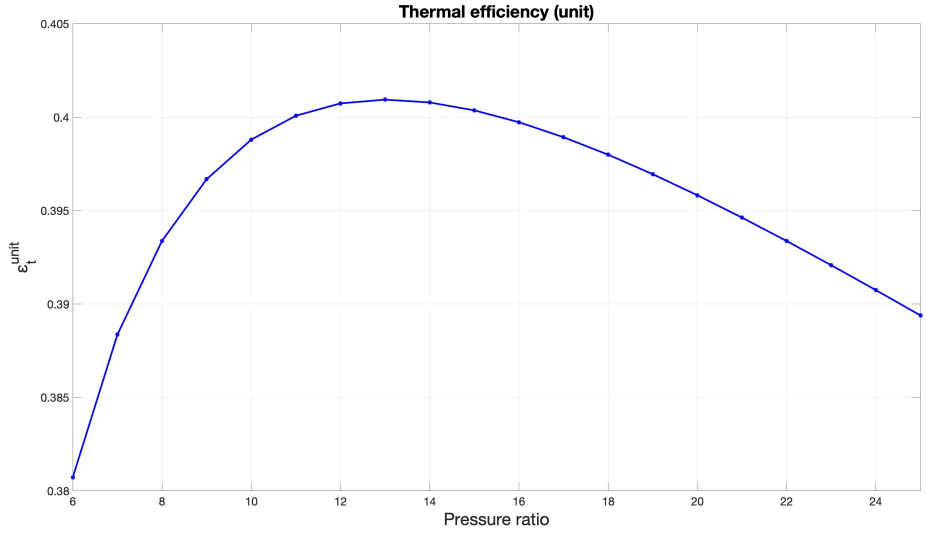

Figure 5.4: Thermal efficiency (of the engine unit) versus pressure ratio

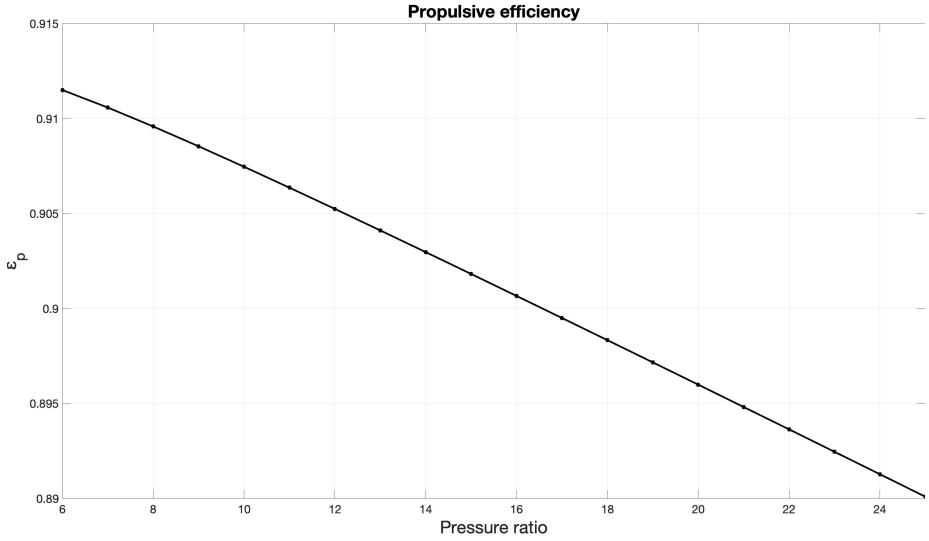

Figure 5.5: Propulsive efficiency versus pressure ratio[4]

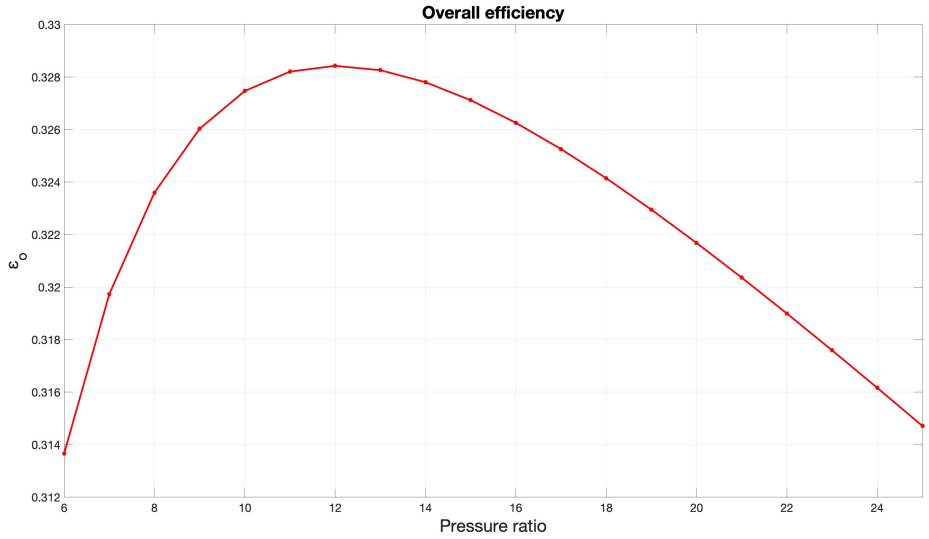

Figure 5.6: Overall efficiency versus pressure ratio

[4]Note: Because the thrust power is set as constant, if there was no exit nozzle the propulsive efficiency would be constant as well. Since the power contribution from the nozzle is present but small, ε_p does change but its variations are contained.

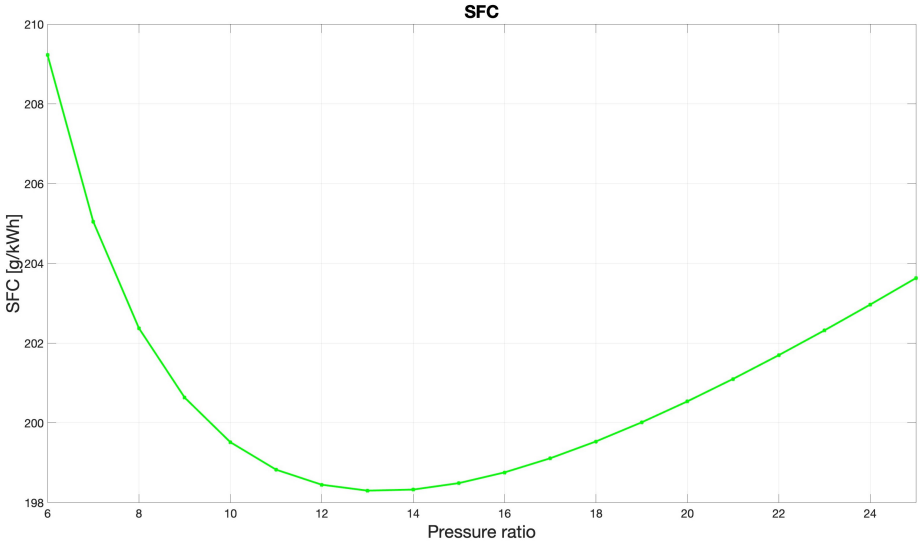

Figure 5.7: Specific fuel consumption versus pressure ratio

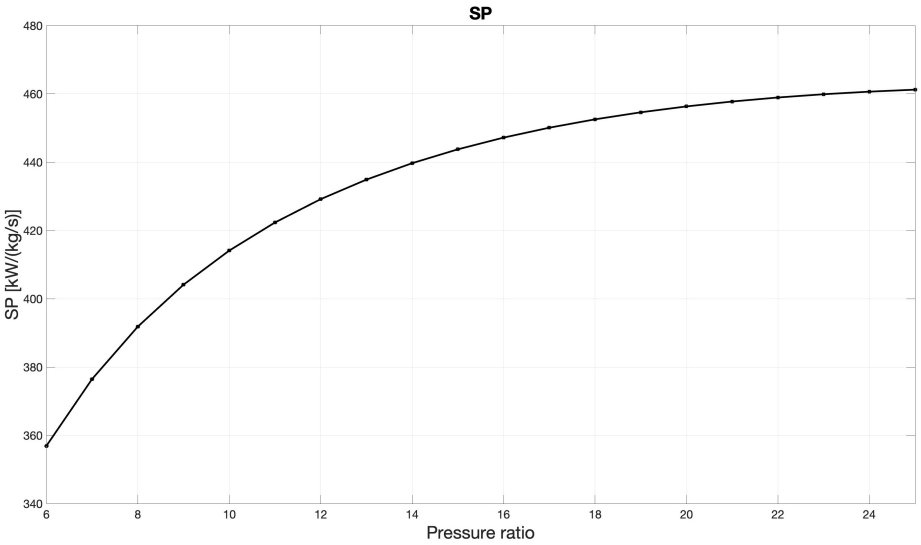

Figure 5.8: Specific power versus pressure ratio

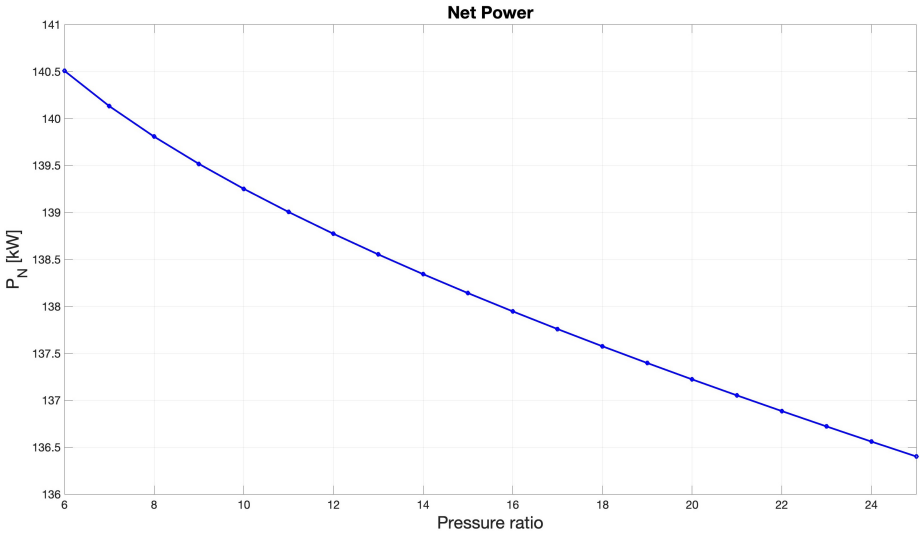

Figure 5.9: Net power versus pressure ratio

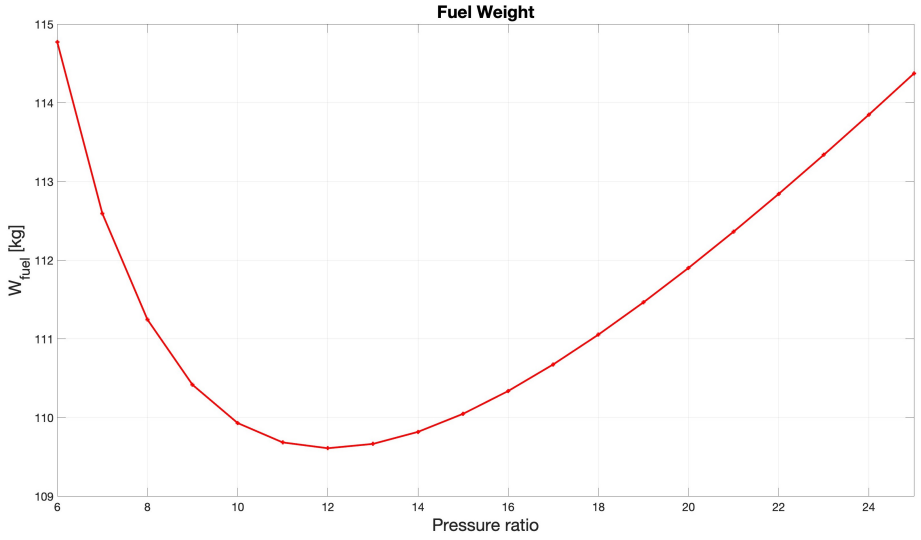

Figure 5.10: Fuel weight versus pressure ratio

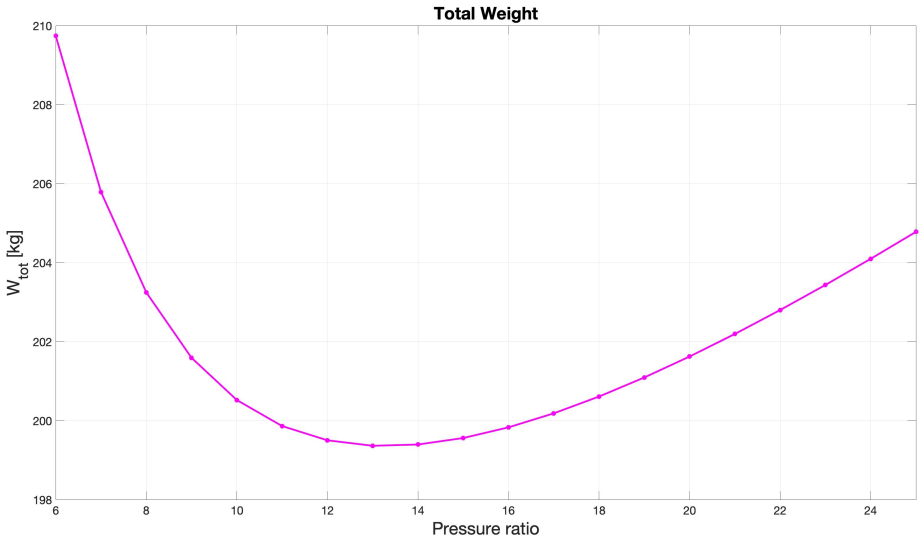

Figure 5.11: Total weight versus pressure ratio

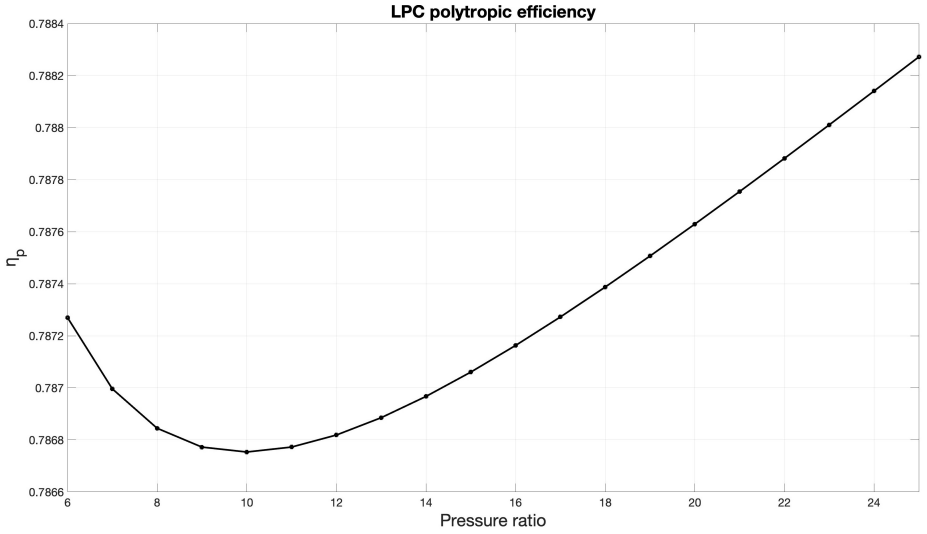

Figure 5.12: LPC polytropic efficiency versus pressure ratio

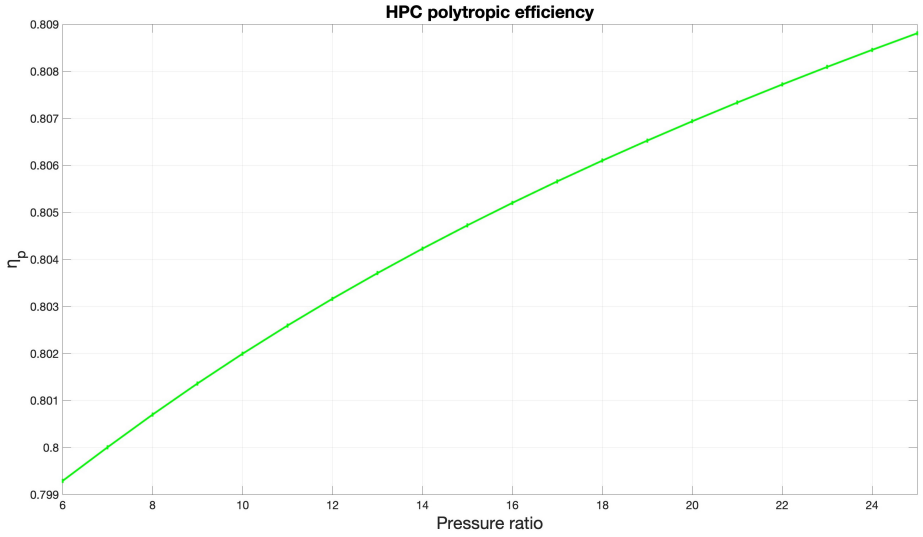

Figure 5.13: HPC polytropic efficiency versus pressure ratio

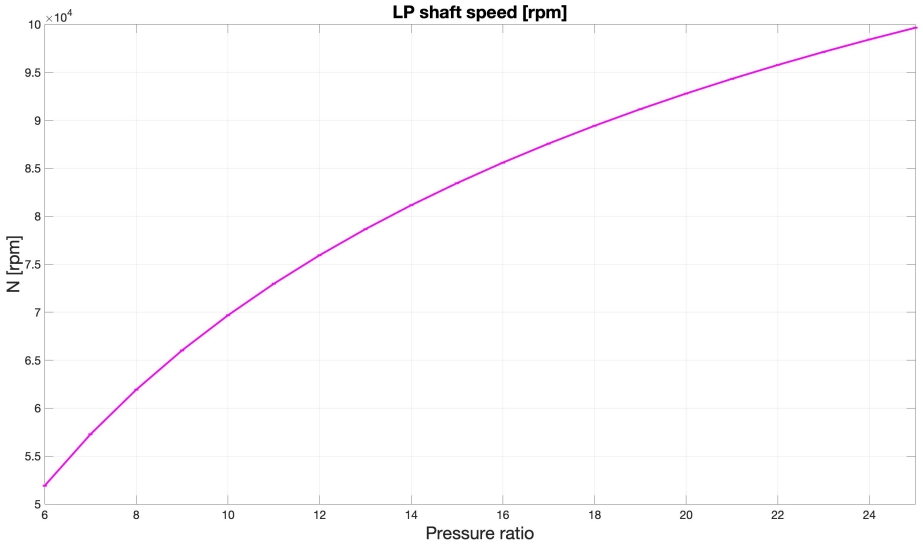

Figure 5.14: LP shaft speed versus pressure ratio

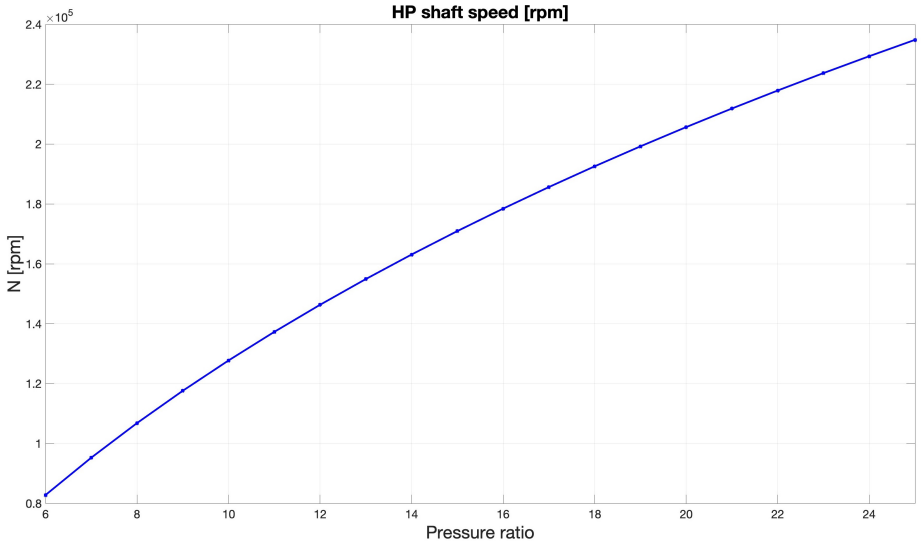

Figure 5.15: HP shaft speed versus pressure ratio

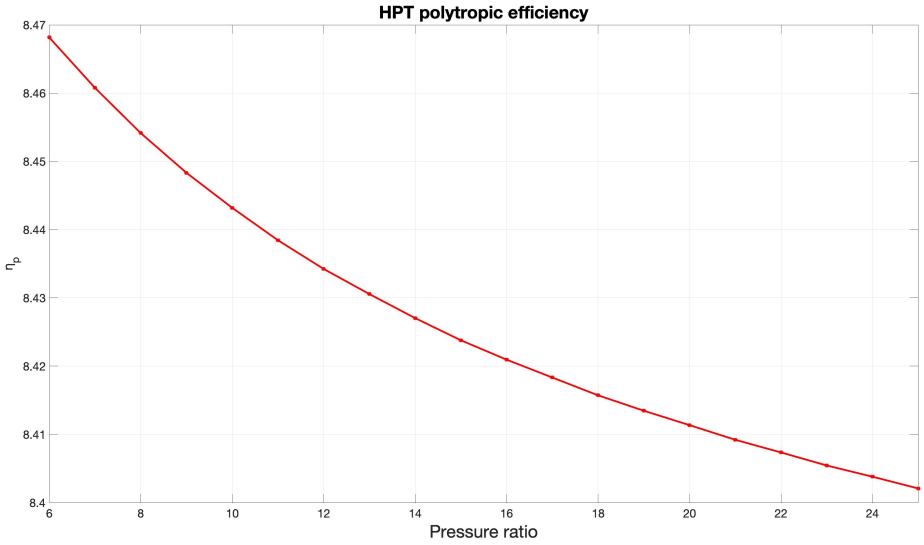

Figure 5.16: HPT polytropic efficiency versus pressure ratio

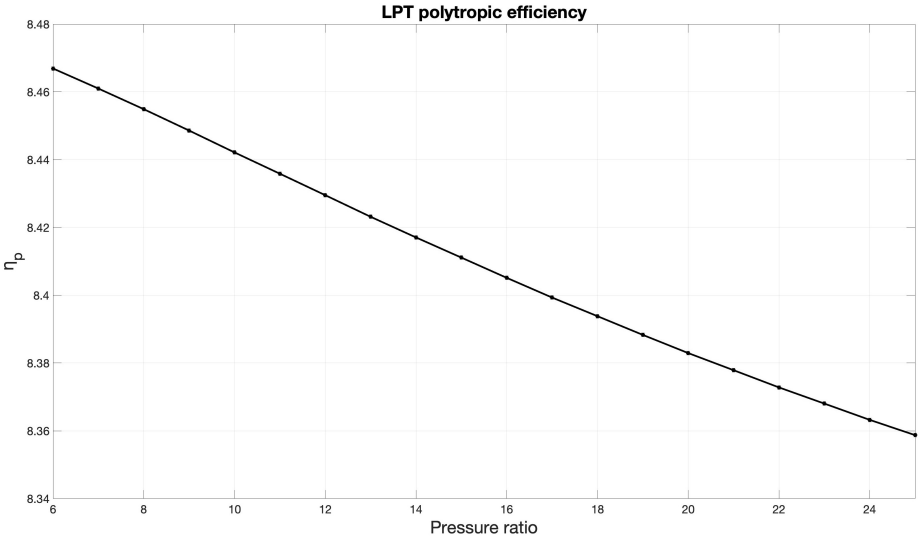

Figure 5.17: LPT polytropic efficiency versus pressure ratio

The maximum overall efficiency is obtained at the pressure ratio $\pi_c = 12$ and is $\varepsilon = 32.8\%$, this is the final setup.
The T-s diagram with $\pi_c = 12$ is shown in Figure 5.18.

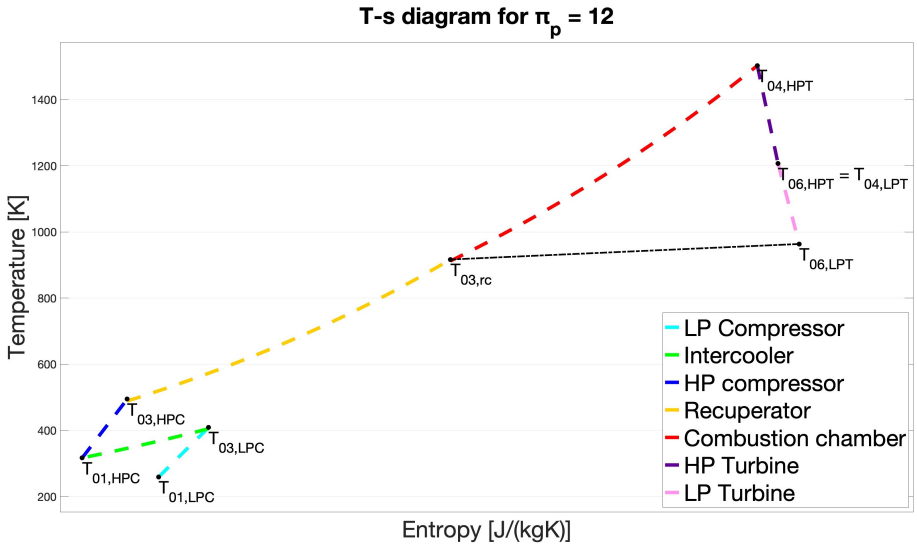

Figure 5.18: T-s diagram

External conditions	
External Temperature T_a	255.65 K
External Pressure P_a	54.02 kPa
Flight Mach number M_a	0.272
Air mass flow $\dot{m}$	0.257 kg/s
Air intake	
Efficiency η_d	0.98
Inlet total temperature T_0	259.48 K
Inlet total pressure P_0	56.881 kPa
Exit total temperature T_{01}	259.48 K
Exit total pressure P_{01}	56.822 kPa
Low-pressure compressor	
Stage pressure ratio π_c'	3.464
Polytropic efficiency η_p	0.787
Isentropic efficiency η_s	0.747
Power $P_{c,LPC}$	38321 W
Inlet total temperature $T_{01,LPC}$	259.48 K
Inlet total pressure $P_{01,LPC}$	56.822 kPa
Exit total temperature $T_{03,LPC}$	408.80 K
Exit total pressure $P_{03,LPC}$	196.839 kPa
Intercooler	
Pressure drop δp_{ic}	0.03
Efficiency ε_{ic}	0.6
Inlet total temperature $T_{03,LPC}$	408.80 K
Inlet total pressure $P_{03,LPC}$	196.839 kPa
Exit total temperature $T_{01,HPC}$	316.91 K
Exit total pressure $P_{01,HPC}$	190.934 kPa
High-pressure compressor	
Stage pressure ratio π_c'	3.464
Polytropic efficiency η_p	0.803
Isentropic efficiency η_s	0.766
Power $P_{c,HPC}$	45622 W
Inlet total temperature $T_{01,HPC}$	316.91 K
Inlet total pressure $P_{01,HPC}$	190.934 kPa
Exit total temperature $T_{03,LPC}$	494.68 K
Exit total pressure $P_{03,LPC}$	661.413 kPa
Recuperator	
Pressure drop δp_{ic}	0.04
Efficiency ε_{ic}	0.9
Inlet total temperature $T_{03,HPC}$	494.68 K
Inlet total pressure $P_{03,HPC}$	661.413 kPa
Exit total temperature $T_{03,rc}$	916.81 K
Exit total pressure $P_{03,rc}$	634.957 kPa

Combustion chamber	
Pressure drop f_c	0.02
Combustion efficiency ν_c	0.98
Inlet total temperature $T_{03,rc}$	916.81 K
Inlet total pressure $P_{03,rc}$	634.957 kPa
Exit total temperature $T_{04,HPT}$	1503 K
Exit total pressure $P_{04,HPT}$	622.257 kPa
Gas mass flow $\dot{m}_t$	0.263 kg/s
$\dot{m}_{fuel}/\dot{m}$	0.024
High-pressure turbine	
Expansion ratio $P_{06,HPT}/P_{04,HPT}$	0.308
Polytropic efficiency η_p	0.883
Isentropic efficiency η_s^{tt}	0.896
Power $P_{t,HPT}$	111193 W
Inlet total temperature $T_{04,HPT}$	1503 K
Inlet total pressure $P_{04,HPT}$	622.257 kPa
Exit total temperature $T_{06,HPT}$	1206.73 K
Exit total pressure $P_{06,HPT}$	191.824 kPa
% of net power ξ	55.35 %
Low-pressure turbine	
Expansion ratio $P_{06,LPT}/P_{04,LPT}$	0.299
Polytropic efficiency η_p	0.883
Isentropic efficiency η_s^{tt}	0.895
Power $P_{t,LPT}$	91208 W
Inlet total temperature $T_{04,LPT}$	1206.73 K
Inlet total pressure $P_{04,LPT}$	191.824 kPa
Exit total temperature $T_{06,LPT}$	963.72 K
Exit total pressure $P_{06,LPT}$	57.429 kPa
% of net power ξ	44.65 %
Nozzle	
Efficiency η_n	0.98
Inlet temperature $T_{06,LPT}$	963.72 K
Inlet pressure $P_{06,LPT}$	57.429 kPa
Exit temperature T_7	950.50 K
External Pressure P_a	54.02 kPa
Exit velocity V_{exit}	185.58 m/s
Nozzle thrust $Thrust_{nozzle}$	26.46 N
Nozzle thrust power P_{nozzle}	3559 W

Total thrust $Thrust$	1147 N
Thrust power P_W	100 kW
Net power P_N	118 kW
Power imparted to the airflow (engine+fans) P_J	110 kW
Thermal power $\dot{m}_{fuel} H_u$	304 kW
Thermal efficiency (of the whole system) ε_t^{sys}	36.3 %
Thermal efficiency (of the engine unit) ε_t^{unit}	40.1 %
Propulsive efficiency ε_p	90.5%
Overall efficiency ε_o	32.8 %
Specific fuel consumption SFC	194.452 g/kWh
Specific power SP	429.172 kJ/kg
Total weight W_{tot}	176 kg
Fuel weight W_{fuel}	110 kg

Table 10: Thermodynamic cycle final results

Mass flow $\dot{m}$	0.257 kg/s
Stage pressure ratio π_c'	3.464
Low-pressure Compressor	
Polytropic efficiency η_p	0.787
Isentropic efficiency η_s	0.747
Global flow coefficient ϕ_{01}	0.063
Work coefficient λ	0.695
Specific speed ω_s	0.758
Specific diameter D_s	3.475
Inlet total temperature T_{01}	259.484 K
Inlet total pressure P_{01}	56822.436 Pa
Exit total temperature T_{03}	408.80 K
Exit total pressure P_{03}	196838.69 Pa
Power P_c	38321 W
Temperature rise ΔT	149.32 K
Rotational speed ω	7952 rad/s 75934 rpm
High-pressure Compressor	
Polytropic efficiency η_p	0.803
Isentropic efficiency η_s	0.766
Global flow coefficient ϕ_{01}	0.063
Work coefficient λ	0.695
Specific speed ω_s	0.758
Specific diameter D_s	3.475
Inlet total temperature T_{01}	316.91 K
Inlet total pressure P_{01}	190933.53 Pa
Exit total temperature T_{03}	494.68 K
Exit total pressure P_{03}	661413.15 Pa
Power P_c W	45622 W
Temperature rise ΔT	177.77 K
Rotational speed ω	15323 rad/s 146328 rpm
Combined isentropic efficiency	0.738

Table 11: Compressors' final results

Mass flow $\dot{m}_t$	0.263 kg/s
Net Power P_N	118.458 kW
High-pressure Turbine	
Polytropic efficiency η_p	0.883
Isentropic efficiency (total-to-total) η_s^{tt}	0.895
Isentropic efficiency (total-to-static) η_s^{ts}	0.868
Specific speed ω_s	0.588
Specific diameter D_s	3.331
Inlet total temperature T_{04}	1503 K
Inlet total pressure P_{04}	622257.49 Pa
Exit total temperature T_{06}	1206.73 K
Exit total pressure P_{06}	191823.95 Pa
Expansion ratio $\frac{P_{06}}{P_{04}}$	0.308
Power P_t	111193 W
Temperature drop ΔT	296.25 K
Rotational speed ω	15323 rad/s 146328 rpm
Degree of reaction r	0.547
% of P_N	55.35 %
Low-pressure Turbine	
Polytropic efficiency η_p	0.883
Isentropic efficiency (total-to-total) η_s^{tt}	0.896
Isentropic efficiency (total-to-static) η_s^{ts}	0.869
Specific speed ω_s	0.578
Specific diameter D_s	3.385
Inlet total temperature T_{04}	1206.75 K
Inlet total pressure P_{04}	191823.95 Pa
Exit total temperature T_{06}	963.72 K
Exit total pressure P_{06}	57428.97 Pa
Expansion ratio $\frac{P_{06}}{P_{04}}$	0.299
Power P_t	91208 W
Temperature drop ΔT	243.02 K
Rotational speed ω	7952 rad/s 75934 rpm
Degree of reaction r	0.547
% of P_N	44.65 %
Combined isentropic efficiency	0.907

Table 12: Turbines' final results

Note: It is preferable to avoid having the static pressure at the exit of the last turbine stage lower than the external air pressure. Otherwise, the exit nozzle would have to act as a diffuser to decelerate the flow, which is detrimental to this application. In this case, the turbine exit static pressure is

$$P_{6,LPT} = 55.062\,kPa > 54.020\,kPa = P_a$$

as expected.

6 Conclusions

While fully electric aircraft propulsion offers several environmental and functional advantages compared to traditional gas turbines, it is still not feasible for most applications due to the low specific energy of batteries, which for now limits it to small-scale applications with short range. To still reduce carbon emissions and retain, at least to a certain extent, some of the other benefits of electric propulsion such as noise reduction, efficiency, and scalability, the preliminary design of a hybrid setup with a microturbine generating the power to drive an electric motor was produced in this work.

Starting from the hypothesis established from a previous work that it is convenient to use an intercooled-recuperated thermodynamic cycle, mathematical methods based on non-dimensional analysis were developed to estimate compressors' and turbines' performances. It was proven that, for applications with size and power output that are comparable to the one proposed here, the optimal setup is to use two centrifugal compressors and two radial turbines, with the low-pressure compressor and turbine on one shaft and the high-pressure compressor and turbine on another one, with each turbine driving its own generator.

The final architecture of the system is composed of a microturbine engine running two electrical generators which are powering the electric motors that are driving the fans; in turn, the final arrangement of the engine is comprised of two radial compressors, that are each driven by a radial turbine, an intercooler, a recuperator, and a combustion chamber (in addition to an air intake and an exit nozzle).

While such a design approach has the advantage of simplicity and allows for a quick overview of the performance of the system, which makes it convenient for preliminary design, its results must not be taken as final: simulations and tests are still necessary for detailed results. In particular, as mentioned in section 3, this method tends to be pessimistic when it comes to compressors' performance evaluation. A suggestion for future research is to improve the scaling of efficiency estimation with size to get more accurate results.

References

[1] Emmanuel Ocbazghi Abby Narishkin and Steve Cameron. *Why electric planes haven't taken off yet*. URL: https://www.businessinsider.com/electric-planes-future-of-aviation-problems-regulations-2020-3?r=US&IR=T. (accessed: 12.02.2023).

[2] ATAG. *Facts and Figures*. URL: https://www.atag.org/facts-figures.html. (accessed: 04.01.2023).

[3] Ronald H. Aungier. *Turbine Aerodynamics, Axial-Flow and Radial-Inflow Turbine Design and Analysis*. ASME PRESS, 2005.

[4] Patrick Bernard. *Three battery technologies that could power the future*. URL: https://www.saftbatteries.com/media-resources/our-stories/three-battery-technologies-could-power-future. (accessed: 12.02.2023).

[5] Jeremy Bogaisky. *With Toyota's Help, This Secretive Entrepreneur May Finally Give Us Flying Cars*. URL: https://www.forbes.com/sites/jeremybogaisky/2020/11/23/joby-toyota-flying-cars/. (accessed: 12.02.2023).

[6] Keith Button. *Flying on electrons*. American Institute of Aeronautics and Astronautics, 2016.

[7] Michael Casey and Chris Robinson. *Radial Flow Turbocompressors Design, Analysis, and Applications*. Cambridge University Press, 2021.

[8] Michael Ciaglo. *U.S. Implementing 1st-Ever Airplane Emission Rules; Critics Say They're Ineffective*. URL: https://www.npr.org/2020/12/28/950863508/u-s-implementing-1st-ever-airplane-emission-rules-critics-say-theyre-ineffective. (accessed: 04.01.2023).

[9] European Commission. *Reducing emissions from aviation*. URL: https://climate.ec.europa.eu/eu-action/transport-emissions/reducing-emissions-aviation_en. (accessed: 04.01.2023).

[10] I. A. Waitz E. M. Greitzer Z. S. Spakovszky. *Performance of Propellers*. URL: https://web.mit.edu/16.unified/www/FALL/thermodynamics/notes/node86.html. (accessed: 08.02.2023).

[11] EASA. *Overview of Aviation Sector*. URL: https://www.easa.europa.eu/eco/eaer/topics/overview-of-aviation-sector. (accessed: 04.01.2023).

[12] Influit Energy. *Comparing Electric Cars and Their Batteries*. URL: https://www.influitenergy.com/post/comparing-electric-cars-and-their-batteries. (accessed: 12.02.2023).

[13] Kyle Field. *BloombergNEF: Lithium-Ion Battery Cell Densities Have Almost Tripled Since 2010*. URL: https://cleantechnica.com/2020/02/19/bloombergnef-lithium-ion-battery-cell-densities-have-almost-tripled-since-2010/. (accessed: 12.02.2023).

[14] Steve Fox. *Cockpit of the First All-Electric Propulsion Aircraft*. URL: https://www.nasa.gov/image-feature/cockpit-of-the-first-all-electric-propulsion-aircraft. (accessed: 12.02.2023).

[15] Peter Garrison. *The Electric Airplane*. URL: https://www.smithsonianmag.com/air-space-magazine/the-electric-airplane-34986164/. (accessed: 12.02.2023).

[16] Bill Gates. *How to Avoid a Climate Disaster: The Solutions We Have and the Breakthroughs We Need*. Alfred A. Knopf, 2021.

[17] P. Grosz. "Helicopter pioneers of World War I". In: *Air Enthusiast* 6 (1978), pp. 154–159.

[18] Ye Xie Al Savvarisal Antonios Tsourdos Dan Zhang Jason Gu. "Review of hybrid electric powered aircraft its conceptual design and energy management methodologies". In: *Chinese Journal of Aeronautics* 34.4 (2021), pp. 432–450. DOI: https://doi.org/10.1016/j.cja.2020.07.017.

[19] ICAO. *Future of Aviation*. URL: https://www.icao.int/Meetings/FutureOfAviation/Pages/default.aspx. (accessed: 04.01.2023).

[20] Fred Lambert. *Tesla Model Y is now the best-selling car in all of Europe*. URL: https://electrek.co/2022/12/29/tesla-model-y-is-now-the-best-selling-car-in-all-of-europe/. (accessed: 12.02.2023).

[21] Juliette Oriot. *Trois liaisons aériennes interdites en France: est-ce vraiment une avancée pour le climat? (French)*. URL: https://www.ouest-france.fr/leditiondusoir/2022-12-07/trois-liaisons-aeriennes-interdites-en-france-est-ce-vraiment-une-avancee-pour-le-climat-154b134c-a830-4d79-b884-25ba83db65f0. (accessed: 04.01.2023).

[22] C. Rodgers. "The Efficiencies of Single-Stage Centrifugal Compressors for Aircraft Applications". In: *International Gas Turbine and Aeroengine Congress and Exposition* (1991).

[23] Federico De Rossi. *Design of an Advanced Microturbine Generator for Light Electric Aircrafts*. Università Degli Studi Di Padova, 2022.

[24] Samsung. *The Composition of EV Batteries: Cells? Modules? Packs? Let's Understand Properly!* URL: https://www.samsungsdi.com/column/all/detail/54344.html. (accessed: 12.02.2023).

[25] Ahmed F. El-Sayed. *Aircraft Propulsion and Gas Turbine Engines, Second Edition*. CRC PRESS, 2017.

[26] Bryan Swopes. *8 October 1883*. URL: https://www.thisdayinaviation.com/tag/tissandier-electric-airship/. (accessed: 12.02.2023).

[27] Terega. *What is the difference between biogas and biomethane?* URL: https://www.terega.fr/en/lab/what-is-the-difference-between-biogas-and-biomethane. (accessed: 12.02.2023).

[28] Gaston Tissandier. *La Navigation aérienne(French)*. Hachette, 1886.

[29] Dries Verstraete. *Climate explained: why don't we have electric aircraft?* URL: https://theconversation.com/climate-explained-why-dont-we-have-electric-aircraft-123910. (accessed: 05.01.2023).

[30] Philip P. Walsh and Paul Fletcher. *Gas Turbine Performance*. Blackwell Science, 2004.

[31] Graham Warwick. *NASA's Electric-Propulsion Wing Test Helps Shape Next X-Plane*. URL: https://aviationweek.com/aerospace/nasas-electric-propulsion-wing-test-helps-shape-next-x-plane. (accessed: 12.02.2023).

[32] Graham Warwick. *What Are The Advantages And Challenges Of Electric-Powered Airliners?* URL: https://aviationweek.com/aerospace/aircraft-propulsion/what-are-advantages-challenges-electric-powered-airliners. (accessed: 12.02.2023).